INTEGRATED PHYSICS-ORIENTED STATISTICAL MODELING, SIMULATION AND OPTIMIZATION

J.W. Bandler, R.M. Biernacki, Q. Cai,
S.H. Chen, S. Ye and Q.J. Zhang

SOS-92-3-R

February 1992

INTEGRATED PHYSICS-ORIENTED STATISTICAL MODELING, SIMULATION AND OPTIMIZATION

John W. Bandler, Fellow, IEEE, Radoslaw M. Biernacki, Senior Member, IEEE,
Qian Cai, Student Member, IEEE, Shao Hua Chen, Member, IEEE,
Shen Ye, Member, IEEE and Qi-Jun Zhang, Member, IEEE

Abstract

We contribute herein to the effective utilization of physics-, geometry- and process-related parameters for yield-driven microwave device modeling and circuit design. We address physics-based modeling of MESFETs from the point of view of efficient simulation, accurate behaviour prediction and robust parameter extraction. We present a novel integration of a large-signal physics-based model into the harmonic balance equations for simulation of nonlinear circuits, involving an efficient Newton update. We exploit this integration in gradient-based FAST (*F*easible *A*djoint *S*ensitivity *T*echnique) circuit optimization. For the purpose of yield-driven circuit design we present a relevant physics-based statistical modeling methodology. Our statistical implementations use models originated by Ladbrooke and Khatibzadeh and Trew. We embed these physics-based device models in the yield optimization process for MMICs using appropriate multidimensional statistical distributions. Quadratic approximation of responses and gradients suitable for yield optimization is discussed. We verify our theoretical contributions and exemplify our computational results using built-in and user-programmable modeling capabilities of the CAE systems OSA90/hope and HarPE. In this context, we report on results of device modeling using a field-theoretic nonlinear device simulator.

J.W. Bandler, R.M. Biernacki, Q. Cai and S.H. Chen are with the Simulation Optimization Systems Research Laboratory, Department of Electrical and Computer Engineering, McMaster University, Hamilton, Canada L8S 4L7. J.W. Bandler, R.M. Biernacki and S.H. Chen are also with and S. Ye is with Optimization Systems Associates Inc., P.O. Box 8083, Dundas, Ontario, Canada L9H 5E7. Q.J. Zhang is with the Department of Electronics, Carleton University, Ottawa, Canada K1S 5B6.

This work was supported in part by Optimization Systems Associates Inc., by the Natural Sciences and Engineering Research Council of Canada under Grants OGP0042444, OGP0007239, and STR0040923 and by the National Research Council of Canada through its IRAP-M program.

I. INTRODUCTION

We believe that microwave computer-aided engineering (CAE) technology must address physics-based circuit optimization, directly linking geometrical, material and process-related parameters, or simply, physical parameters, with system performance and production yield. Field theory, circuit theory and system theory need to be integrated into hierarchically structured computer-aided design (CAD) systems for linear, nonlinear and statistical microwave circuit simulation and design.

For active microwave circuit design the effectiveness of modern CAD methods relies heavily on accurate device models. Approaches to device modeling have been developed and a variety of models have been implemented into circuit simulators for such purposes as small- and large-signal circuit design. Generally, the methods for device modeling can be classified into two categories: equivalent circuit-based models (ECMs) and physics-based models (PBMs).

ECM modeling assumes an equivalent circuit to simulate the external behaviour of the device under consideration. Such models consist of a number of linear and nonlinear circuit elements connected in a predefined manner. To approximate device characteristics, empirical equations are devised *a priori* for those nonlinear circuit elements. Various FET ECMs, including small-signal and nonlinear large-signal (e.g., Curtice and Ettenberg, Materka and Kacprzak, Statz *et al.*) models [1-5], have been widely used in microwave CAD. To properly utilize these models, devices must be characterized through an accurate parameter extraction process where the ECM parameter values are determined from DC, S-parameter and/or large-signal measurement data (e.g., Bandler *et al.* [6-7]). ECMs enjoy high computational efficiency and are relatively easy to implement into circuit simulators. They have been the foundation of pre-MMIC (monolithic microwave integrated circuits) CAD and continue to dominate today's microwave simulators. However, there is no obvious relationship between ECM parameters and device physical parameters. Also, since the model parameters are usually identified after device fabrication, they have limited extrapolative or statistically meaningful forecasting abilities. This opens the door to PBM modeling.

PBMs address the fundamental device equations and characterize device behaviour in terms of physical parameters such as gate length, channel thickness, doping profile, etc. Circuit design can then be considered at the device parameter level. In other words, the design variables can directly include device geometrical, material and process-related parameters [8]. Therefore, PBMs should be very effective in terms of predictability and first-time success in the design of microwave integrated circuits (MICs) and MMICs.

Efficient microwave nonlinear circuit analysis has been a subject of serious research for a long time. Its importance has resurged with the development of MICs and MMICs, where nonlinear active devices are components critical to performance. Simulation of nonlinear circuits is much more complicated than that of linear circuits. It can be carried out in the time domain, frequency domain, and mixed frequency/time domains, as reviewed by Gilmore and Steer in [9].

Time-domain methods try to solve the circuit equations entirely in the time domain using numerical methods. There are three major time-domain simulation techniques [9]: direct methods [10-15], associated discrete circuit model approaches [10,16] and shooting methods [17-22]. Frequency-domain methods, recently reviewed by Steer, Chang and Rhyne [23], attempt to analyze nonlinear circuits entirely in the frequency domain. Functional expansions enable the frequency components of the output spectrum to be calculated directly from the input spectrum. Frequency-domain methods such as power series expansion analysis [24-27], Volterra series analysis [28-33] and spectral balance analysis [34-36], have been used successfully for the analysis of microwave nonlinear circuits [37-44].

Mixed frequency/time-domain methods include the harmonic balance (HB) technique [45-51] which was significantly advanced by Nakhla and Vlach, Kundert and Sangiovanni-Vincentelli, Rizzoli *et al.*, and several other authors. The HB technique was recently reviewed by Gilmore and Steer [9,52]. The HB technique is an efficient tool for the simulation of steady-state responses of nonlinear microwave circuits [53-58]. The waveform balance (or sample balance) technique is another mixed frequency/time-domain method and can be considered a dual to the HB method. It was, for

example, used by Hwang *et al.* for nonlinear modeling and verification of MMIC amplifiers [59].

Nonlinear circuit optimization requires efficient nonlinear circuit simulation. It has become feasible because of the efficiency of the HB method. Optimization employing the HB method has been applied to large-signal FET model parameter extraction [7], nonlinear circuit design [60-62] and nonlinear circuit yield optimization [63], although most of the developments have been based on ECMs. Active and passive elements are explicitly represented through their equivalent circuit models. Direct treatment of the effects of device physical parameters on the overall MMIC circuit performance has been studied by a number of researchers [8,64-71]. One of the most significant benefits of PBMs over ECMs is the opportunity of directly optimizing controllable/designable physical parameters of the passive and active devices for low noise, high power, high yield, etc.

Statistical device modeling is a prerequisite for accurate yield-driven or cost-driven circuit analysis and optimization [72,73]. The model statistics originate from random variations of geometrical, material and process-related parameter values during manufacturing. Those random variations result in complicated distributions and correlations of device responses. The aim of statistical device modeling is to provide tools for generating random device outcomes which can reproduce the actual distribution of the device responses. Statistical modeling has been extensively studied for passive devices, bipolar junction transistors (BJT), metal-oxide semiconductor (MOS) and complementary metal-oxide semiconductor (CMOS) circuits for more than a decade [74-82]. Statistical modeling techniques have also been applied to microwave devices [73,83-86].

With the rapid progress of GaAs fabrication technology, MMICs are becoming increasingly practical [87]. During the past two decades, hybrid microwave integrated circuits (HMICs) have been used in the microwave industry, where active and passive discrete components such as transistors, thin- or thick-film capacitors, inductors and resistors are connected on a dielectric substrate. In MMICs, all the active and passive components are fabricated on a common semi-insulating substrate. Post-production tuning of MMICs is restricted, and device replacement is not possible. In the production of MMICs, circuits are manufactured in batches rather than individually. The cost of

manufacturing is directly affected by yield. Therefore, yield analysis and optimization, which take into account the manufacturing tolerances, model uncertainties, variations in the process parameters, environmental uncertainties, etc., have become widely accepted as indispensable components of the MMIC design methodology.

Pioneering work on yield optimization was carried out in the early 1970s by a number researchers (e.g., Karafin, Pinel and Roberts, Bandler [88-92]) and was advanced subsequently during the last two decades [93-118]. Yield optimization of nonlinear microwave circuits with statistically characterized devices has been reported in the literature, e.g., [63, 119, 120]. Purviance and Meehan [121] recently reviewed statistical analysis and design of microwave circuits. Many approaches developed for yield optimization are restricted to circuits employing ECMs. Statistics are then applied to the equivalent circuit elements such as capacitances, inductances or resistances. There is doubt as to whether such an approach is capable of reflecting the actual statistical behaviour of the physical parameters. In MMICs, a change of one device physical parameter may result in correlated changes in all elements of the equivalent circuit model. Furthermore, the resulting correlations may be very complicated and quite difficult to describe. Therefore, conventional design methods at the circuit level are of limited value for yield optimization of MMICs. PBMs, on the other hand, are more likely to provide reliable statistical behaviour because of the physical nature of the model. Consequently, meaningful results of yield optimization should be attainable [122-123].

State-of-the-art microwave circuit analysis and design requires comprehensive general-purpose CAD software to integrate device modeling, steady-state and transient circuit simulation, sensitivity analysis, statistical modeling and analysis, performance- and yield-driven design optimization, as well as physics-based and process-oriented circuit design within the same framework. Different aspects of a CAD system, such as technology optimization, cell design, software modularity and adaptability, have been discussed [124-126]. The open architecture of the software systems OSA90/hope [127] and HarPE [128] are designed to address these challenges. These two systems are used to carry out the calculations presented in this paper and implement our new theoretical

contributions.

In Section II, we present PBM modeling of MESFETs. Nonlinear circuit analysis using PBMs integrated with the HB method is addressed in Section III. Circuit design exploiting gradient optimizers is discussed in Section IV. Sections V and VI are devoted, respectively, to statistical modeling and yield optimization using PBMs. Section VII describes how an external simulator, such as a two-dimensional (2D) field-based MESFET simulator, can be integrated with OSA90/hope.

II. PHYSICS-BASED MESFET MODELING

The fundamental device equations for PBMs may be solved either numerically or analytically. Numerical models typically employ finite-difference or finite-element techniques [129-134]. They are potentially the most accurate and play an important role in understanding device physics. However, they are slow and have been hitherto regarded as cumbersome.

Analytical PBM modeling can be traced back to the early pioneering work of Shockley [135] in 1952. He invented the JFET and developed a detailed analysis based on three major assumptions: constant carrier mobility, gradual channel approximation and abrupt transition between the depletion region and the conducting channel [71]. His model was applicable to long gate devices operating in a non-saturated mode, and therefore is not suitable for modern high-frequency transistors. The Shockley model was subsequently improved by including velocity saturation effects and nonuniform doping profiles in the channel [136-141]. All these models are based on one-dimensional or quasi one-dimensional analysis and are suitable for DC and small-signal AC operation. They are restricted to devices with large ratios of gate-length to channel thickness. These restrictions were lifted for large-signal analytical models proposed in [142-145]. Large-signal analytical models try to solve the device equations with a minimum number of simplifying assumptions. These models offer a reasonable compromise between model accuracy and simulation efficiency. They are quite promising for circuit design and optimization.

A. Basic Device Equations [144]

Following Khatibzadeh and Trew's approach [144], the device model is formulated for the active, or "intrinsic", region, i.e., the channel directly under the gate electrode, as shown in Fig. 1. All other regions of the device are modeled phenomenologically using external or "extrinsic" linear elements. How to derive the values of these extrinsic elements in terms of physical parameters is not yet well established. Usually, their values are assumed according to practical knowledge or obtained through parameter extraction from measurements.

The basic device equations in the active region are

$$\nabla^2\psi = -\frac{q}{\varepsilon}\left[N(y) - n(x, y)\right] \tag{1}$$

$$\boldsymbol{J} = -qn\boldsymbol{v} + qD\nabla n \tag{2}$$

$$\nabla\cdot\boldsymbol{J} = q\frac{\partial n}{\partial t} \tag{3}$$

and

$$\boldsymbol{J}_t = \boldsymbol{J} + \varepsilon\frac{\partial \boldsymbol{E}}{\partial t} \tag{4}$$

where

$$\boldsymbol{E} = -\nabla\psi \tag{5}$$

is the electric field, ψ the electrostatic potential, q the electron charge, ε the permittivity of the active layer material, N the donor concentration in the channel, n the free-electron density, $\boldsymbol{v}$ the electron velocity, $\boldsymbol{J}$ the conduction (drift + diffusion) current density, D the diffusion coefficient, and $\boldsymbol{J}_t$ the total (conduction + displacement) current density. It is assumed that $\boldsymbol{v}$ and $\boldsymbol{E}$ are codirectional, i.e.,

$$\boldsymbol{v} = -\mu(E)\boldsymbol{E} \tag{6}$$

where E is the magnitude of $\boldsymbol{E}$ and $\mu(E)$ is the field-dependent mobility. Among the basic device equations, (1) is Poisson's equation, and (3) is the current continuity equation. They contribute to a "drift-diffusion" PBM which characterizes the behaviour of the FET devices.

The active region is divided into three parts: a depletion region under the gate Schottky barrier where $n = 0$, a free channel region where $n = N_d$ (N_d is the doping density) and a transition region

where n varies smoothly from zero to N_d as indicated by Yamaguchi and Kodera [142] and Madjar and Rosenbaum [143]. The free electron density in the transition region may be expressed as [142–144]

$$n(x, y) = N(y)\left[1 + \gamma(x - L_1)\right] T(d(x), y) \tag{7}$$

where γ and L_1 are the parameters to be determined from the boundary and bias conditions, and the transition function $T(d(x), y)$ can be defined as [144]

$$T(d(x), y) = 1 - \frac{1}{1 + \exp\left[\dfrac{y - d(x)}{\lambda}\right]}. \tag{8}$$

$d(x)$ is considered in [144] as an "effective depletion-layer width" and λ is a model parameter allowed to vary. Function (8) increases from almost 0 to almost 1 within the range of $y - d(x)$ from -3λ to 3λ, so according to [142,143] λ should be of the order of the Debye length λ_D. Alternatively, adapting the sinusoidal expression proposed in [142,143] to the notation of Fig. 1 and allowing λ to vary, the transition function can be defined as

$$T(d(x), y) = \begin{cases} \dfrac{1}{2} + \dfrac{1}{2}\sin\left[\pi\dfrac{y - d(x)}{6\lambda}\right] & \text{if } d(x) - 3\lambda < y < d(x) + 3\lambda \\ 0 & \text{if } y \le d(x) - 3\lambda \\ 1 & \text{if } y \ge d(x) + 3\lambda. \end{cases} \tag{9}$$

Equation (7) with (8) or (9) eliminates the assumption of abrupt transition between the depletion region and the conducting channel.

B. Dependence of Electron Velocity on Electric Field

In [143,144], the dependence of the electron drift velocity v on the electric field E is modeled either by a piecewise linear or a quadratic function, both shown in Fig. 2. This neglects the negative differential mobility of GaAs, exemplified by a typical v–E curve, also shown in Fig. 2. An equation with a step function was used by Chang and Day [145] to approximate the negative differential mobility, though the calculated and measured mobilities did not match well.

A good fit to the measured v-E data can be achieved using the Snowden formula [133]

$$\mu(E) = \frac{300\mu_0}{T}\left[\frac{1 + \dfrac{8.5\times10^4 E^3}{\mu_0 E_0^4(1 - 5.3\times10^{-4}T)}}{1 + \left(\dfrac{E}{E_0}\right)^4}\right] \tag{10}$$

where

$$\mu_0 = \frac{0.8}{1 + \sqrt{N\times10^{-23}}}$$

is the doping-dependent low field mobility. Incorporating the functional form of (10) into (6) we express the v-E curve as

$$v = v_s \frac{\dfrac{E}{E_1} + \left(\dfrac{E}{E_0}\right)^\beta}{1 + \left(\dfrac{E}{E_0}\right)^\beta} \tag{11}$$

where v_s (the saturation velocity), E_0 (the characteristic field), E_1 and β are fitting parameters. Equations (10) and (11) can be reconciled if

$$\beta = 4$$

$$E_1 = \frac{v_{s0}}{\mu_0}$$

$$v_{s0} = \frac{T}{300}v_s = \frac{8.5\times10^4}{1 - 5.3\times10^{-4}T}.$$

When T = 300°K we have $v_s = v_{s0} = \mu_0 E_1$ (as shown in Fig. 2). Thus E_1 is defined similarly to the critical field E_c (see Fig. 2) introduced in [143,144]. However, while E_1 denotes the intersection of $v = v_s$ and the line tangent at the origin to the v-E curve, E_c corresponds to the maximum velocity. Therefore, μ_0 is, in general, interpreted differently in the two definitions.

As in [133], in our implementation β is fixed as $\beta = 4$. In Fig. 3 we show the v-E curve calculated by (11) with $v_s = 1.023\times10^5$m/s, $E_1 = 1.173\times10^5$V/m and $E_0 = 3.792\times10^5$V/m. Also shown

is the experimental data used by Chang and Day [145] and attributed to Ruch and Kino [146], and Houston and Evans [147]. The match is excellent.

C. Solution for the Potential Distribution

The general solution of Poisson's equation (1) can be expressed as a linear superposition of two components [142–144]

$$\psi = \psi_0 + \psi_1. \tag{12}$$

ψ_0 is the Laplacian potential due to the impressed voltages on the electrodes and satisfies the equation

$$\nabla^2\psi_0 = 0 \tag{13}$$

with the boundary conditions (see Fig. 1)

$$\psi_0(0, a) = 0 \tag{14a}$$

$$\psi_0(L, a) = v_0 \tag{14b}$$

$$\frac{\partial\psi_0(x, a)}{\partial y} = 0 \tag{14c}$$

$$\psi_0(x, 0) = 0. \tag{14d}$$

ψ_1 is due to the space charge in the channel and satisfies the equation

$$\nabla^2\psi_1 = -\frac{q}{\varepsilon}(N - n) \tag{15}$$

with the boundary conditions

$$\psi_1(0, a) = 0 \tag{16a}$$

$$\psi_1(L, a) = v_1 \tag{16b}$$

$$\frac{\partial\psi_1(x, a)}{\partial y} = 0 \tag{16c}$$

$$\psi_1(x, 0) = v_{gs} - V_{bi} \tag{16d}$$

where L and a are the gate length and channel thickness, respectively, V_{bi} is the built-in voltage of the gate Schottky contact, and v_{gs} is the applied intrinsic gate–source voltage. v_0 and v_1 are unknown fractions of v_{ds}, the applied intrinsic drain–source voltage, resulting from the boundary conditions (14b) and (16b) and must be solved for in order to determine the performance of the devices. Since $v_{ds} = v_1 + v_0$, it is sufficient to solve for v_1 only.

Khatibzadeh and Trew [144] showed that a simplified solution to (13) with the boundary conditions (14a)–(14d) is given by

$$\psi_0(x, y) = \frac{v_0}{\sinh\left(\frac{\pi L}{2a}\right)} \sinh\left(\frac{\pi x}{2a}\right) \sin\left(\frac{\pi y}{2a}\right) \tag{17}$$

and the solution to (15) with the boundary conditions (16a)–(16c) can be expressed as

$$\psi_1(x, y) = \begin{cases} -\frac{q}{\varepsilon} F_1(d(x), y) + \frac{v_1}{L} x & 0 \le x \le L_1 \\ -\frac{q}{\varepsilon} F_1(d_1, y) + \frac{v_1}{L} x + \frac{q}{\varepsilon} \gamma(x - L_1) F_2(d_1, y) & L_1 < x \le L \end{cases} \tag{18}$$

where

$$F_1(d(x), y) = \int_y^a \int_z^a [1 - T(d(x), \tau)] N(\tau) d\tau dz \tag{19}$$

$$F_2(d_1, y) = \int_y^a \int_z^a T(d_1, \tau) N(\tau) d\tau dz. \tag{20}$$

T is the transition function defined by (8) and d_1 is the effective depletion-layer width in the saturation region. The piecewise transition function of (9) could be used here as well. The boundary condition (16d) was applied to (18) to solve for $d(x)$ and γ [144].

Solving for the potential ψ_1 in (18) involves two double integrations F_1 and F_2 which require significant computational effort. These numerical integrations are necessary if the doping profile is arbitrary. However, for uniform doping, i.e., if $N(y) = N_d$ in (7), the efficiency of the model can be greatly improved if (9) is used instead of (8) in (19) and (20) since (9) can be analytically integrated. This has been implemented in both OSA90/hope and HarPE [127,128] and our experiments show that the simulation time can be reduced by more than two thirds as compared with using (8).

D. Intrinsic Currents

The gate, drain and source currents can be expressed by the equations

$$i_g = i_{gc}(\phi,\ v_1(\phi,t),\ v_{gs}(\phi,t),\ v_{ds}(\phi,t),\ t) + \frac{\partial q_g(\phi,\ v_1(\phi,t),\ v_{gs}(\phi,t),\ v_{ds}(\phi,t),\ t)}{\partial t} \tag{21}$$

$$i_d = i_{dc}(\phi,\ v_1(\phi,t),\ v_{gs}(\phi,t),\ v_{ds}(\phi,t),\ t) + \frac{\partial q_d(\phi,\ v_1(\phi,t),\ v_{gs}(\phi,t),\ v_{ds}(\phi,t),\ t)}{\partial t} \tag{22}$$

$$i_s = i_{sc}(\phi,\ v_1(\phi,t),\ v_{gs}(\phi,t),\ v_{ds}(\phi,t),\ t) + \frac{\partial q_s(\phi,\ v_1(\phi,t),\ v_{gs}(\phi,t),\ v_{ds}(\phi,t),\ t)}{\partial t} \tag{23}$$

where i_{gc}, i_{dc} and i_{sc} are the gate, drain and source conduction currents, respectively, q_g, q_d and q_s stand for the total charges, respectively on the gate, drain and source electrodes, and ϕ is the parameter vector including gate length, gate width, channel thickness, doping density, etc. Equations (21)–(23) can be represented by the equivalent circuit shown in Fig. 4.

i_{gc}, i_{dc} and i_{sc} of (21)–(23) are calculated by integrating the current density J in (2) over the corresponding areas in the planes $y = 0$, $x = L$ and $x = 0$, respectively, (see Fig. 1). For example, the drain conduction current i_{dc} can be written in integral form as [148]

$$i_{dc} = \int J \cdot ds = -qW \int_0^a \left(\mu(E(L,\ y))n(L,\ y)E_x(L,\ y) + D\nabla_x n(L,\ y) \right) dy \tag{24}$$

where E_x and $\nabla_x n$ are the x components of E and ∇n, respectively, and W is the gate width.

The partial derivatives of the total charges q_g, q_d and q_s w.r.t. time t represent the displacement currents through the corresponding electrodes. Again, q_g, q_d and q_s can be written in integral form [148], for instance,

$$q_g = \varepsilon W \int_0^L E_y(x,\ 0)dx \tag{25}$$

where E_y is the y component of E.

Since $E(x,\ y)$ and $n(x,\ y)$ depend on the voltages v_1, v_{gs} and v_{ds}, the conduction currents and the total charges are nonlinear functions of v_1, v_{gs} and v_{ds}. Under normal working conditions, the gate

is reverse biased and the gate conduction current i_{gc} can be neglected. (The gate forward biasing and drain breakdown conditions may be included by introducing diodes into the model [148].) Under this assumption, the drain and source conduction currents are equal at DC. In [142–144], the solution of v_1 is obtained iteratively by forcing the difference between the drain and source conduction currents to be sufficiently small. In Section III, we discuss HB simulation where the nonlinear HB equations need to be solved iteratively. In order to avoid a double iteration loop and make the PBM computationally more efficient, we combine solving for v_1 with the HB iterations while satisfying the boundary conditions.

Using the MESFET physical parameters given in [148] we compare DC simulation results of the PBM described in this section to those of Khatibzadeh, as shown in Fig. 5. Slight discrepancies can be attributed to our modifications w.r.t. the original model of [144].

E. Performance Prediction and Parameter Extraction

A significant advantage of the PBMs over the ECMs is that directly from the physical parameter values PBM simulation can predict device performance, or even the performance of the overall circuit embedding the device. This could be done before the device is manufactured and for any range of working conditions. Obviously, validity of this approach strongly depends on model accuracy. We believe that the predictive potential of PBMs should and will provide device and circuit engineers with the opportunity to extend and improve their design capabilities.

Parameter extraction, indispensable for ECMs [5–7,149,150], may also prove useful for PBMs. Firstly, as was already mentioned in Section II.A, we use parameter extraction to determine the extrinsic device parameters. Secondly, the intrinsic physical parameters, even if they are known or measured, can be fine tuned, for example, to account for measurement errors. It should be noted that, unlike ECMs, it is relatively easy to estimate a good starting point for parameter extraction of PBMs, since the model parameters are physically meaningful and tangible. Another significant application of PBM parameter extraction is for statistical modeling at the device physical and geometrical level, in which a number of devices must be characterized from measurements. This is

further discussed in Section IV.

To illustrate PBM parameter extraction of a FET we consider the extrinsic and intrinsic model shown in Fig. 6. The intrinsic parameters are defined in Table I. S-parameter measurements [151] in the frequency range 1GHz to 21GHz at 3 bias points (gate bias 0V, -0.84V, -1.54V and drain bias 5V) are processed simultaneously. The v-E curve obtained by fitting (11) to the experimental data [146,147] is used here since no v-E measurements for this particular device are available.

Parameter extraction was carried out using the ℓ_2 optimizer [152] of HarPE [128]. Measured values of gate length L, gate width W and doping density N_d were assigned as the starting values. The optimization was performed in two stages. First, the extrinsic parasitic parameters were optimized while the intrinsic physical parameters were kept fixed. In the second stage both the intrinsic and extrinsic parameters were optimized starting from the result of the first stage. The entire parameter extraction process took approximately 5 CPU minutes and 30 iterations on a Sun SPARCstation 1. Optimizable extrinsic and intrinsic parameters before and after optimization are listed in Table II. The measured [151] and simulated S parameters at the three bias points are shown in Fig. 7.

Finally, it should be pointed out that extracting parameter values by simultaneously optimizing a large number of parameters may lead to non-unique results. Some parameter values may become non-physical due to factors such as model simplifications, insufficient measurements or measurement errors. Therefore, model tuning, keeping the parameters within their physical limits, or parameter control, may be necessary. Based on practical knowledge of the device, these concepts can be accommodated in parameter extraction by applying constraints to the parameters being optimized.

III. HARMONIC BALANCE NONLINEAR CIRCUIT ANALYSIS

The responses of a nonlinear circuit can be determined by solving a set of nonlinear state equations

$$f(\dot{\boldsymbol{x}},\ \boldsymbol{x},\ \boldsymbol{u},\ t) = \mathbf{0} \tag{26}$$

where $\boldsymbol{x} = [x_1\ x_2\ \ldots\ x_n]^T$ is the vector of state variables, typically certain voltages and/or currents, and $\boldsymbol{u} = [u_1\ u_2\ \ldots\ u_m]^T$ is the excitation vector. (26) can be solved in the time domain, the frequency domain, or a mixed frequency/time domain using respective methods.

In this section, we discuss nonlinear steady-state circuit analysis with PBMs of FETs using the mixed frequency/time-domain HB method.

A. Formulation of the Harmonic Balance Equations

The circuit nodal equations in the time domain can be written as [50]

$$f(v(t),\ t) = i(v(t)) + \frac{d}{dt}q(v(t)) + \int_{-\infty}^{t} y(t-\tau)v(\tau)d\tau + i_{ss}(t) = 0 \tag{27}$$

where t is time, $\boldsymbol{v}$ is the vector of node voltage waveforms, $\boldsymbol{i}$ is the vector of the currents entering the nodes from nonlinear resistors or nonlinear voltage controlled current sources, $\boldsymbol{q}$ is the vector of the charges entering the nodes from nonlinear capacitors, $\boldsymbol{y}$ is the matrix-valued impulse response of linear components, and $\boldsymbol{i}_{ss}$ is the vector of independent current source waveforms.

To use the HB technique, (27) is Fourier transformed into the frequency domain [50] as

$$\boldsymbol{F}(\boldsymbol{V}) = \boldsymbol{I}(\boldsymbol{V}) + j\boldsymbol{\Omega}\boldsymbol{Q}(\boldsymbol{V}) + \boldsymbol{Y}\boldsymbol{V} + \boldsymbol{I}_{ss} = \boldsymbol{0} \tag{28}$$

where $\boldsymbol{V}$, $\boldsymbol{I}_{ss}$, $\boldsymbol{I}$ and $\boldsymbol{Q}$ are the vectors that contain the Fourier coefficients of the respective time-domain waveforms at each node and all harmonics, and $\boldsymbol{Y}$ is the nodal admittance matrix for the linear elements. $\boldsymbol{\Omega}$ is the angular frequency matrix, as defined in [50].

In order to reduce the number of equations the circuit can be divided into a linear subcircuit, a nonlinear subcircuit and an excitation subcircuit, as shown in Fig. 8. Then, the quantities in (28) can be limited to the connection nodes with $\boldsymbol{Y}$ being the equivalent admittance matrix for the linear subcircuit. Further reduction can be achieved by replacing the linear and the excitation subcircuits by their Norton equivalent at the nonlinear ports. The state variables are then limited to the nonlinear port voltages, and $\boldsymbol{I}_{ss}$ and $\boldsymbol{Y}$ represent the Norton equivalent.

To use the Newton method to solve the complex HB equations, (28) is reorganized into the following real equation form by splitting the real and imaginary parts of the complex quantities

$$\overline{F}(\overline{V}) = \overline{I}(\overline{V}) + \overline{\Omega}\,\overline{Q}(\overline{V}) + \overline{Y}\,\overline{V} + \overline{I}_{ss} = 0 \tag{29}$$

where a bar stands for real quantities resulting from their complex counterparts. For example,

$$\overline{V} = \begin{bmatrix} Real(V) \\ Imag(V) \end{bmatrix}, \quad \overline{F} = \begin{bmatrix} Real(F) \\ Imag(F) \end{bmatrix}.$$

$\overline{\Omega}$ is a frequency matrix which can be written as

$$\overline{\Omega} = \begin{bmatrix} & & & & -\Omega(0) & & & \\ & & & & & -\Omega(\omega_1) & & \\ & & & & & & \cdots & \\ & & & & & & & -\Omega(\omega_H) \\ \Omega(0) & & & & & & & \\ & \Omega(\omega_1) & & & & & & \\ & & \cdots & & & & & \\ & & & \Omega(\omega_H) & & & & \end{bmatrix} \tag{30}$$

where $\Omega(\omega_i)$is a diagonal matrix whose diagonal elements are ω_i's. H is the number of harmonics used in the simulation.

It should be noted that the size of the system of equations (28) is directly proportional to the number of harmonics H. It is known that the trigonometric Fourier series exhibits slow convergence. Therefore, truncating the number of harmonic components, needed for efficiency or even feasibility, may strongly affect accuracy and convergence of the HB method, especially for high nonlinearities or excitations with many spectral components.

B. Integration of Physics-based Model with HB Equations

We now turn to the problem of efficient integration of the MESFET PBM described in Section II into the HB equations (29). The model is solved in the time domain for the gate, drain and source currents at given intrinsic voltages. In order to do that, however, one must first determine the value of the intermediate parameter v_1 in (16). In the original approach [142–144], the "pseudo-static" DC condition $i_{dc} = -i_{sc}$ was used to solve for v_1. This condition is valid at DC only when the displacement currents of (21)–(23) assume zero values. For instantaneous currents under AC excitations both terms

in (21)–(23) must be considered. Solving first for v_1 would require an additional iteration loop within the HB Newton iteration.

To avoid such a double iteration loop, our implementation treats v_1 of (16b) as an additional state variable, although it has no circuit interpretation. v_1 is directly integrated into the HB equations and allowed to vary w.r.t. time, RF input levels, and operating frequencies [8], while satisfying the boundary conditions (16). Including v_1 in the state variable vector requires augmenting (28) by the KCL equation for the pseudo-node "Z", as indicated in Fig. 4. This procedure is applied to all FETs in the circuit. For example, for a single FET circuit the state vector can be defined as

$$\boldsymbol{v}(\phi,\ t) = [v_1(\phi,\ t)\ v_{gs}(\phi,\ t)\ v_{ds}(\phi,\ t)]^T. \tag{31}$$

The nonlinear current and charge vectors of (27) can be expressed as

$$\boldsymbol{i}(\phi,\ \boldsymbol{v}(\phi,\ t),\ t) = \boldsymbol{A} \begin{bmatrix} i_{gc}(\phi,\ \boldsymbol{v}(\phi,\ t),\ t) \\ i_{dc}(\phi,\ \boldsymbol{v}(\phi,\ t),\ t) \\ i_{sc}(\phi,\ \boldsymbol{v}(\phi,\ t),\ t) \end{bmatrix} \tag{32}$$

and

$$\boldsymbol{q}(\phi,\ \boldsymbol{v}(\phi,\ t),\ t) = \boldsymbol{B} \begin{bmatrix} q_g(\phi,\ \boldsymbol{v}(\phi,\ t),\ t) \\ q_d(\phi,\ \boldsymbol{v}(\phi,\ t),\ t) \\ q_s(\phi,\ \boldsymbol{v}(\phi,\ t),\ t) \end{bmatrix} \tag{33}$$

where $\boldsymbol{A}$ and $\boldsymbol{B}$ are simple incidence matrices containing 0's, 1's and/or −1's needed to express the terminal currents and charges in terms of quantities used in (21)–(23). For an arbitrary value of v_1 (21)–(23) may not satisfy the current continuity condition

$$i_g(t) + i_d(t) + i_s(t) = 0. \tag{34}$$

However, if we augment the HB equations

$$\overline{\boldsymbol{F}}(\phi,\ \overline{\boldsymbol{V}}(\phi)) = \overline{\boldsymbol{I}}(\phi,\ \overline{\boldsymbol{V}}(\phi)) + \overline{\Omega}\,\overline{\boldsymbol{Q}}(\phi,\ \overline{\boldsymbol{V}}(\phi)) + \overline{\boldsymbol{Y}}\,\overline{\boldsymbol{V}}(\phi) + \overline{\boldsymbol{I}}_{ss} = \boldsymbol{0} \tag{35}$$

with the admittance matrix $\overline{\boldsymbol{Y}}$ modified to include the pseudo-node "Z", which is isolated from the linear part of the circuit, the solution of (35) ensures current continuity for all harmonics, i.e.,

$$\overline{I}_g + \overline{I}_d + \overline{I}_s = \mathbf{0}. \tag{36}$$

This ensures the current continuity condition (34) in the time domain. Therefore, our formulation is valid not only for DC but also for small- and large-signal RF operations, and it does not require a double iteration loop.

C. Notes on Solving the HB Equations

The Newton update for solving the HB equations can be written as

$$\overline{V}_{new}(\phi) = \overline{V}_{old}(\phi) - \left[\overline{J}(\phi, \overline{V}_{old}(\phi))\right]^{-1}\overline{F}(\phi, \overline{V}_{old}(\phi)) \tag{37}$$

where $\overline{J}(\phi, \overline{V}(\phi))$ is the Jacobian matrix used in the algorithm. From (35) (or (29)), we see that the Jacobian has the form

$$\overline{J}(\phi, \overline{V}(\phi)) = \left[\frac{\partial \overline{I}^T(\phi, \overline{V}(\phi))}{\partial \overline{V}(\phi)}\right]^T + \overline{\Omega}\left[\frac{\partial \overline{Q}^T(\phi, \overline{V}(\phi))}{\partial \overline{V}(\phi)}\right]^T + \overline{Y}. \tag{38}$$

Note that in solving the HB equations, ϕ is constant and $\overline{V}(\phi)$ is variable. Following [50], in order to calculate the entries of $\overline{J}(\phi, \overline{V}(\phi))$, we must first obtain the time-domain derivatives of i and q w.r.t. v. The time-domain derivatives of i and q w.r.t. v are evaluated by differentiating the corresponding terms of (21)-(23) w.r.t. v. After the derivatives of i and q w.r.t. v are obtained, the entries of the Jacobian matrix $\overline{J}$ can be evaluated by the Fourier transform.

Since v_1 is considered as a state variable, the entries of $\overline{J}(\phi, \overline{V}(\phi))$ include the derivatives of $\overline{I}$ and $\overline{Q}$ w.r.t. $\overline{V}_1$. For instance, if $\overline{I}_{dc}(\phi, \overline{V}(\phi), \omega_k)$ denotes the split real and imaginary parts of the kth harmonic component of the drain conduction current and $\overline{V}_1(\phi, \omega_l)$ represents the split real and imaginary parts of the lth harmonic component of variable v_1, then

$$\frac{\partial \overline{I}_{dc}^T(\phi, \overline{V}(\phi), \omega_k)}{\partial \overline{V}_1(\phi, \omega_l)} = \begin{bmatrix} G_{v_1}^R(\omega_{k-l}) + G_{v_1}^R(\omega_{k+l}) & G_{v_1}^I(\omega_{k+l}) - G_{v_1}^I(\omega_{k-l}) \\ G_{v_1}^I(\omega_{k-l}) + G_{v_1}^I(\omega_{k+l}) & G_{v_1}^R(\omega_{k-l}) - G_{v_1}^R(\omega_{k+l}) \end{bmatrix}^T \tag{39}$$

where

$$G^R_{v_1}(\omega_i) \triangleq \frac{1}{T_0}\int_0^{T_0} \frac{\partial i_{dc}(\phi,\ v(\phi),\ t)}{\partial v_1(\phi,\ t)} \cos(\omega_i t)dt \tag{40a}$$

and

$$G^I_{v_1}(\omega_i) \triangleq -\frac{1}{T_0}\int_0^{T_0} \frac{\partial i_{dc}(\phi,\ v(\phi),\ t)}{\partial v_1(\phi,\ t)} \sin(\omega_i t)dt \tag{40b}$$

and ω_i is the ith harmonic frequency. T_0 is the fundamental period. The time-domain derivative in (40) is evaluated by differentiating (24) w.r.t. v_1

$$\frac{\partial i_{dc}}{\partial v_1} = -qW\int_0^a \left(\frac{\partial \mu}{\partial E}\frac{\partial E}{\partial v_1}nE_x + \mu\frac{\partial n}{\partial v_1}E_x + \mu n\frac{\partial E_x}{\partial v_1} + D\frac{\partial(\nabla_x n)}{\partial v_1}\right)_{x=L} dy. \tag{41}$$

(41) involves additional integrations, so in our actual implementation the perturbation technique is used instead.

In Section IV we discuss further utilization of the Jacobian matrix $\overline{J}$ at the solution of the HB equations: it can be reused in adjoint analysis for optimization.

IV. GRADIENT-BASED OPTIMIZATION

Circuit design optimization with ECMs has been extensively studied and is available in some commercial software packages. Such optimization adjusts passive components to achieve desired circuit performance or yield with fixed active devices. Little work has been devoted so far to design optimization with PBMs. This section addresses several aspects of physics-based circuit design using gradient optimization and HB simulation.

A. Sensitivity Analysis

To facilitate efficient gradient-based optimization for circuit design we need to provide the optimizer with the gradient, i.e., the partial derivatives of circuit responses w.r.t. design variables. This is commonly referred to as sensitivity analysis. The most popular method of sensitivity analysis is the conventional *P*erturbation *A*pproximation *S*ensitivity *T*echnique (PAST). In this method, the

first-order derivative of $f(\boldsymbol{\phi})$ w.r.t. ϕ_i is estimated by

$$\frac{\partial f(\boldsymbol{\phi})}{\partial \phi_i} = \frac{f(\boldsymbol{\phi} + \Delta\phi_i \boldsymbol{u}_i) - f(\boldsymbol{\phi})}{\Delta\phi_i} \tag{42}$$

where $\Delta\phi_i \boldsymbol{u}_i$ denotes the perturbation of the ith variable, $\Delta\phi_i$ is the perturbation size and $\boldsymbol{u}_i$ is a unit vector which has 1 in the ith position and zeros elsewhere. This method is straightforward and easy to implement. However, it may not be accurate enough and the computational effort involved, especially for large-scale problems, may be prohibitive.

Bandler, Chen, Daijavad and Madsen [153] proposed an *I*ntegrated *G*radient *A*pproximation *T*echnique (IGAT) which utilizes the Broyden update [154]

$$\nabla f(\boldsymbol{\phi}_{new}) = \nabla f(\boldsymbol{\phi}_{old}) + \frac{f(\boldsymbol{\phi}_{new}) - f(\boldsymbol{\phi}_{old}) - (\nabla f(\boldsymbol{\phi}_{old}))^T \Delta\boldsymbol{\phi}}{\Delta\boldsymbol{\phi}^T \Delta\boldsymbol{\phi}} \Delta\boldsymbol{\phi} \ . \tag{43}$$

and the special iteration of Powell [155]. Perturbations with (42) are used to obtain an initial approximation as well as regular corrections. $\boldsymbol{\phi}_{old}$ and $\boldsymbol{\phi}_{new}$ are two different points and $\Delta\boldsymbol{\phi} = \boldsymbol{\phi}_{new} - \boldsymbol{\phi}_{old}$. IGAT is robust and has been applied to both microwave performance-driven design [153] and yield optimization [63].

Efficient and accurate sensitivity analysis for HB can be achieved by the *E*xact *A*djoint *S*ensitivity *T*echnique (EAST) developed by Bandler, Zhang and Biernacki [156], which is a generalization of the linear adjoint sensitivity analysis technique. For example, the sensitivity of an output voltage V_{out} w.r.t. a parameter ϕ_i of a nonlinear element at branch b can be expressed by

$$\frac{\partial \overline{V}_{out}}{\partial \phi_i} = \begin{cases} -\sum_k Real\left[\hat{V}_b(k) G_b^*(k)\right] & \text{if } \phi_i \in \text{nonlinear current sources} \\ -\sum_k Imag\left[\hat{V}_b(k) G_b^*(k)\right] & \text{if } \phi_i \in \text{nonlinear capacitors} \end{cases} \tag{44}$$

where the complex quantity $\hat{V}_b(k)$ is the voltage of branch b at harmonic k and is obtained from the

adjoint network. $G_b(k)$ denotes the sensitivity expression of the element containing variable ϕ_i [156]. * stands for the conjugate of a complex number. This technique exhibits high accuracy and computational efficiency but suffers from implementation complexity.

To combine the efficiency of EAST and simplicity of PAST, Bandler *et al.* proposed the *F*easible *A*djoint *S*ensitivity *T*echnique (FAST) [157]. It features high speed gradient computation as well as ease in implementation. It is particularly suitable for general purpose CAD programs. We choose FAST here for incorporating PBMs into efficient gradient-based optimization.

B. Integration of FAST with Physics-Based Models

Consider a vector of circuit responses

$$\boldsymbol{R}(\boldsymbol{\phi}) = \mathfrak{R}(\boldsymbol{\phi}, \overline{\boldsymbol{V}}(\boldsymbol{\phi})) \tag{45}$$

which may include output voltages, currents, powers, power gains, etc. Let $\boldsymbol{S}$ be a set of design specifications. Then the objective function for a design problem can be expressed as

$$U(\boldsymbol{\phi}) = U(\boldsymbol{R}(\boldsymbol{\phi}), \boldsymbol{S}). \tag{46}$$

The corresponding design optimization problem is to

$$\underset{\boldsymbol{\phi}}{\textit{minimize}} \quad U(\boldsymbol{\phi}). \tag{47}$$

In order use a gradient-based optimizer to solve (47), the derivatives of U w.r.t. each variable ϕ_i in $\boldsymbol{\phi}$ need to be calculated. Let ϕ_i be a generic design variable such as a device dimension or doping density. The sensitivity of U w.r.t. ϕ_i can be obtained by differentiating (46) w.r.t. ϕ_i

$$\frac{\partial U}{\partial \phi_i} = \left[\frac{\partial U}{\partial \boldsymbol{R}}\right]^T \frac{\partial \boldsymbol{R}}{\partial \phi_i}. \tag{48}$$

$\frac{\partial U}{\partial \boldsymbol{R}}$ depends on the form of the objective function. $\frac{\partial \boldsymbol{R}}{\partial \phi_i}$ can be derived from (45) as

$$\frac{\partial \boldsymbol{R}(\boldsymbol{\phi})}{\partial \phi_i} = \frac{\partial \mathfrak{R}(\boldsymbol{\phi}, \overline{\boldsymbol{V}}(\boldsymbol{\phi}))}{\partial \phi_i} + \left[\frac{\partial \mathfrak{R}^T(\boldsymbol{\phi}, \overline{\boldsymbol{V}}(\boldsymbol{\phi}))}{\partial \overline{\boldsymbol{V}}(\boldsymbol{\phi})}\right]^T \frac{\partial \overline{\boldsymbol{V}}(\boldsymbol{\phi})}{\partial \phi_i} \tag{49}$$

where $\frac{\partial \mathfrak{R}}{\partial \phi_i}$ and $\frac{\partial \mathfrak{R}^T}{\partial \overline{\boldsymbol{V}}}$ may be calculated analytically or by perturbation. The FAST technique is

applied to calculate $\frac{\partial \overline{V}}{\partial \phi_i}$.

Assume that the solution of the HB equation is $\overline{V} = \overline{V}_{sol}$, i.e.,

$$\overline{F}(\boldsymbol{\phi}, \overline{V}_{sol}) = \mathbf{0}. \tag{50}$$

The FAST technique approximates the gradient by

$$\overline{e}^T \frac{\partial \overline{V}(\boldsymbol{\phi})}{\partial \phi_i} \approx - \hat{\overline{V}}^T \frac{\overline{F}(\boldsymbol{\phi} + \Delta\phi_i u_i, \overline{V}_{sol})}{\Delta \phi_i} \tag{51}$$

where $\overline{e}$ is a vector containing 1's and 0's used to select the real or imaginary part of an output voltage of interest. $\hat{\overline{V}}$ is obtained by solving the adjoint system

$$[\overline{J}(\boldsymbol{\phi}, \overline{V}(\boldsymbol{\phi}))]^T \hat{\overline{V}} = \overline{e} \tag{52}$$

where $\overline{J}(\boldsymbol{\phi}, \overline{V}(\boldsymbol{\phi}))$ is the Jacobian matrix, as defined by (38), at the solution of the HB equations. In an efficient implementation, it can be available in the form of LU factors.

As an example, consider the sensitivity of an output voltage w.r.t. the gate width W of a FET, i.e., $\overline{e}^T \frac{\partial \overline{V}(\boldsymbol{\phi})}{\partial W}$. We need to obtain the adjoint solution $\hat{\overline{V}}$ and evaluate the HB residual function $\overline{F}(W + \Delta W, \overline{V}_{sol})$. By reusing the Jacobian matrix available at the HB solution, the adjoint system can be solved with relatively little additional effort. The HB residual function is evaluated from (34) as

$$\overline{F}(W + \Delta W, \overline{V}_{sol}) = \overline{I}(W + \Delta W, \overline{V}_{sol}) + \overline{\Omega}\overline{Q}(W + \Delta W, \overline{V}_{sol}) + \overline{Y}\,\overline{V}_{sol} + \overline{I}_{ss}. \tag{53}$$

Note that $\overline{V}_{sol}$ is constant at this stage, so no iterations are necessary. For instance, i_{dc}, needed to evaluate the first term in the r.h.s. of (53), can be calculated by replacing W by $W + \Delta W$ in (24), where E and n are determined from v_{sol}, the inverse Fourier transform of $\overline{V}_{sol}$. The resulting i_{dc} is then transformed to the frequency domain and used in (53). This provides a high speed yet simple gradient evaluation procedure for gradient optimizers.

C. Algorithm for Optimization

Step 1 Initialization for Optimization.

Step 1.1 Input the circuit topology, design specifications, matching circuit elements and device physical parameters.

Step 1.2 Initialize the design variable vector ϕ. Assign values to all parameters in the circuit including the physical parameters and parasitic parameters of the FETs.

Step 2 Time Domain Simulation.

Step 2.1 Initialize $\overline{V}(\phi)$.

Step 2.2 Convert $\overline{V}(\phi)$ to $v(\phi, t)$, i.e., v_1, v_{gs} and v_{ds}, using the inverse Fourier transform. Calculate the gate, drain and source conduction currents $i(\phi, v(\phi, t), t)$ and gate, drain and source total charges $q(\phi, v(\phi, t), t)$.

Step 3 Frequency Domain Simulation.

Step 3.1 Use the forward Fourier transform to obtain $\overline{I}(\phi, \overline{V}(\phi))$ and $\overline{Q}(\phi, \overline{V}(\phi))$ from $i(\phi, v(\phi, t), t)$ and $q(\phi, v(\phi, t), t)$.

Step 3.2 Solve the HB equation using the Newton update (37). Note that at this stage ϕ is constant and $\overline{V}(\phi)$ is variable. If $\overline{V}(\phi)$ is the solution of the HB equation $\overline{F}(\phi, \overline{V}(\phi)) = 0$, then go to *Step 4*. Otherwise, update $\overline{V}(\phi)$ and go to *Step 2.2*.

Step 4 Optimization of Parameter ϕ.

Step 4.1 If ϕ is optimal, stop.

Step 4.2 Solve the adjoint system (52) using the Jacobian matrix at the solution of the HB equation. Calculate $\frac{\partial \overline{V}(\phi)}{\partial \phi_i}$ using (51). Evaluate $\frac{\partial R(\phi)}{\partial \phi_i}$ using (49) and then $\frac{\partial U(\phi)}{\partial \phi_i}$ using (48), for $i = 1, 2, ..., n$, where n is the number of optimizable parameters.

Step 4.3 Update ϕ according to the optimization algorithm. Go to *Step 2*.

This algorithm is illustrated by the flowchart in Fig. 9.

V. STATISTICAL MODELING

Statistical variations of device parameters in the manufacturing process cause performance deviations. The ultimate purpose of statistical modeling is to characterize devices for accurate yield analysis and optimization. In this section we address statistical modeling of FETs with PBMs.

A. Parameter Extraction and Statistical Estimation

Our approach to statistical modeling is based on parameter extraction and statistical estimation through postprocessing. It requires measurements taken on a large sample of devices, which may include DC, small-signal and large-signal data. For each device, the model parameters are extracted from the corresponding measurements, resulting in a sample of models. This sample of models is postprocessed to estimate the statistics of the model parameters, including the mean values, standard deviations, correlation matrix, etc. Efficient, consistent and reliable parameter extraction is essential for this approach.

Suppose we have K sets of measurement data, each containing m measured responses

$$\boldsymbol{S}^i = [S_1^i \; S_2^i \; \ldots \; S_m^i]^T \tag{54}$$

corresponding to the ith device, $i = 1, 2, \ldots, K$, where K is the total number of devices measured. Let

$$\boldsymbol{\phi}^i = [\phi_1^i \; \phi_2^i \; \ldots \; \phi_n^i]^T \tag{55}$$

denote the model parameters of the ith device and

$$\boldsymbol{R}(\boldsymbol{\phi}^i) = [R_1(\boldsymbol{\phi}^i) \; R_2(\boldsymbol{\phi}^i) \; \ldots \; R_m(\boldsymbol{\phi}^i)]^T \tag{56}$$

be the model responses corresponding to the measurements $\boldsymbol{S}^i$. The parameter extraction problem can be formulated as

$$\min_{\boldsymbol{\phi}^i} \sum_{j=1}^{m} w_j^i \, | R_j(\boldsymbol{\phi}^i) - S_j^i |^p \qquad 1 \le p \tag{57}$$

where w_j^i is a weighting factor and $p = 1$ or $p = 2$ leads to ℓ_1 or ℓ_2 (least squares) optimization, respectively. Optimization is performed for each device measured, i.e., for $i = 1, 2, \ldots, K$.

Often, a multidimensional normal distribution is assumed for the model parameters. It is fully described by the mean values, standard deviations and pair-wise correlation coefficients estimated from the sample of models. In cases where the sample distribution appears substantially different from normal, we utilize the marginal discrete density function (DDF) approach [84]. A discretized joint probability density function has also been proposed [74,158].

B. Statistical ECMs

Statistical models can be considered at the device response level, the equivalent circuit model level (statistical ECMs) and the physical parameter level (statistical PBMs), as shown in Fig. 10.

ECM statistical modeling attempts to characterize the distribution of the equivalent circuit parameters such as inductors and capacitors [73,84]. The main advantage of this approach is that many ECMs are available in microwave CAD software and ECM simulation is usually efficient. However, it is difficult or even impossible to relate the statistical distributions of ECM parameters to those of the device physical parameters. Statistical variations in a single physical parameter may affect many ECM parameters, and at the same time each ECM parameter may be affected by many physical parameters. Consequently, the equivalent circuit model parameters are correlated and such correlations are difficult to estimate. Furthermore, this nonlinear mapping may result in complicated and non-Gaussian distributions.

In a recent paper by Bandler *et al.* [86], statistical modeling of GaAs MESFETs using the Materka ECM [3] was investigated. Even though for individual device models the fit of the ECM responses to the measurements is excellent, the statistical model based on the extracted ECM sample failed to satisfactorily reproduce the original measurement statistics.

C. Statistical PBMs

Statistical PBMs characterize the distributions of device physical parameters [86]. With PBMs it is easier to identify the parameters that are subject to significant statistical variations and the parameters which are correlated (e.g., geometrical dimensions). The statistics of some physical parameters may even be directly available from measurements. At this level, the typical assumption of normal distribution is often justified. Unlike ECMs, by attempting to characterize statistical behaviour of the parameters that are actually subject to random variations in the real world, PBM statistical modeling is closer to reality and we believe it is more accurate and reliable. An obvious disadvantage of PBMs is that simulation may be more time consuming.

As an example, we use the Ladbrooke model [159] and the Khatibzadeh and Trew model [144]

to illustrate PBM statistical modeling.

The Ladbrooke model uses a small-signal equivalent circuit whose component values are derived from the physical parameters and the bias conditions. The equivalent circuit of the Ladbrooke model is shown in Fig. 11. g_m, τ, r_0, C_{gs}, C_{gd}, R_i, R_d, R_s, and L_g are functions of the physical parameters and bias conditions, for example [159],

$$g_m = \frac{\varepsilon v_s W}{d} \tag{58}$$

$$C_{gd} = \frac{2\varepsilon W}{1 + \frac{2X}{L}} \tag{59}$$

$$L_g = \frac{\mu_0 d W}{m^2 L} + L_{g0} \tag{60}$$

where ε is the permittivity of GaAs, v_s the saturation electron drift velocity, W the gate width, L the gate length, μ_0 the permeability of free space, m the number of gate fingers, and L_{g0} is introduced to include the inductances from gate bond wires and pads. d is the equivalent depletion depth which is determined as

$$d = \sqrt{2\varepsilon \frac{V_{B0} - V_{G'S'}}{qN_d}} \tag{61}$$

and X is the voltage dependent space-charge layer extension calculated as

$$X = a_0(V_{D'G'} + V_{B0}) \sqrt{\frac{2\varepsilon}{qN_d(V_{B0} - V_{G'S'})}} \tag{62}$$

where V_{B0} is the zero-bias barrier potential, N_d the doping density, and a_0 is a proportionality coefficient. In our implementation the drain output resistor r_0 is approximated by [86]

$$r_0 = r_{01} V_{D'S'}(r_{03} - V_{G'S'}) + r_{02} \tag{63}$$

where r_{01}, r_{02} and r_{03} are fitting parameters, $V_{G'S'}$, $V_{D'G'}$ and $V_{D'S'}$ are the intrinsic gate-to-source, drain-to-gate and drain-to-source DC operating voltages, respectively (see Fig. 11). R_g, L_d, L_s, G_{ds} and C_{ds} are assumed to be linear elements. The value of the gate width W is known and we keep it

as a constant. The model parameters to be extracted are

$$\{L, a, N_d, v_s, V_{B0}, a_0, r_{01}, r_{02}, r_{03}, L_{g0}, R_g, L_d, L_s, G_{ds}, C_{ds}\}$$

where a is the channel thickness.

The parameters of the Khatibzadeh and Trew model are listed in Table I.

Statistical modeling was performed on a sample of GaAs MESFET measurements provided by Plessey Research Caswell [151]. 69 individual devices (data sets) from two wafers were used. Each device represents a four finger 0.5μm gate length GaAs MESFET with equal finger width of 75μm. Each data set contains small-signal S parameters measured under three different bias conditions and at frequencies from 1GHz to 21GHz with a 0.4GHz step. DC drain bias current is also included in the measurements.

HarPE [128] was used to carry out statistical modeling. Parameter extraction was performed first for each individual device by matching simultaneously the DC and small-signal S-parameter responses to the corresponding measurements [6]. Then, the resulting sample of 69 models was postprocessed to obtain the mean values of the parameters. In order to improve consistency of the parameter extraction process, individual device models were extracted again using those mean values as the initial starting point. The new resulting sample of models was then postprocessed to obtain the parameter statistics, including the mean values, standard deviations, discrete distribution functions (DDF) [84], as well as the correlation matrix.

The parameter mean values and standard deviations for the Ladbrooke model and for the Khatibzadeh and Trew model are listed in Table III. The histograms of the FET gate length L and doping density N_d for both models are shown in Figs. 12 and 13. Table III indicates that there exist significant discrepancies in some common parameters in the two models. For example, the standard deviations of the parameters of the Khatibzadeh and Trew model are noticeably smaller than those of the Ladbrooke model. Although slight differences may exist because of different approximations and structures adopted by the two models these results are not satisfactory and further investigation is under way [160].

The two statistical models were examined using Monte Carlo simulations. The statistical S-parameter responses generated by the models were compared with the measurements. The comparison was made at the bias point V_{GS} = 0V and V_{DS} = 5V and at frequency 11GHz. Monte Carlo simulation was performed with 400 outcomes from the mean values, standard deviations, correlations and DDFs of the model parameters. The mean values and standard deviations of the measured and the simulated S parameters from the Ladbrooke model and from the Khatibzadeh and Trew model are listed in Table IV. The histograms of one S parameter are plotted in Fig. 14.

The match of the standard deviations of the measured S parameters and of those simulated by the Ladbrooke model is quite good, as shown in Table IV. The mean values from the Ladbrooke model do not fit the measurements well, which may indicate that the model is not flexible enough. The mean value match by the Khatibzadeh and Trew model is better than that by the Ladbrooke model. However, the standard deviations of the S parameters from the Khatibzadeh and Trew model are smaller than those from the measurement except for $|S_{21}|$. This is consistent with the observation that the standard deviations in the Khatibzadeh and Trew model are very small (see Table III).

VI. YIELD OPTIMIZATION OF MMICs

Random variations in the manufacturing process may lead to some circuits failing to meet design specifications. Yield optimization, which takes into account the manufacturing tolerances, model uncertainties, variations of process parameters and environmental uncertainties, etc., has become an important design tool to reduce the cost of manufacturing.

In this section, we present yield optimization of MMICs with PBMs. As design variables we directly consider physical parameters for both active devices and passive components. The parameters may include, for example, FET gate length, gate width, doping density, the number of turns of spiral inductors, geometrical dimensions of metal-insulator-metal (MIM) capacitors, etc. Statistical PBMs are employed to generate random circuit outcomes for simulation. The efficient FAST sensitivity technique is utilized to permit high speed gradient-based yield optimization.

A. Formulation of Yield Optimization Problem

Assume that there are N_{fail} failed circuits out of a total of N outcomes. The production yield is simply defined as

$$Y = 1 - \frac{N_{fail}}{N}. \tag{64}$$

Let the parameters of a nominal circuit be $\boldsymbol{\phi}^0$. The manufactured outcomes $\boldsymbol{\phi}^i$, $i = 1, 2, ..., N$, are spread around $\boldsymbol{\phi}^0$ according to the statistical distributions of the parameters and can be represented by

$$\boldsymbol{\phi}^i = \boldsymbol{\phi}^0 + \Delta\boldsymbol{\phi}^i. \tag{65}$$

For the ith outcome and the jth design specification S_j, $j = 1, 2, ..., m$, the error is defined as

$$e_j(\boldsymbol{\phi}^i) = R_j(\boldsymbol{\phi}^i) - S_j \tag{66a}$$

if S_j is an upper specification, or as

$$e_j(\boldsymbol{\phi}^i) = S_j - R_j(\boldsymbol{\phi}^i) \tag{66b}$$

if S_j is a lower specification.

During yield optimization, which takes place at the design stage, the outcomes $\boldsymbol{\phi}^i$ cannot be the manufactured ones. Instead, they are generated from the statistical models, and the yield optimization problem is defined for those simulated random outcomes. Let all the errors for the ith outcome be assembled into the vector

$$\boldsymbol{e}(\boldsymbol{\phi}^i) = [e_1(\boldsymbol{\phi}^i)\ e_2(\boldsymbol{\phi}^i)\ ...\ e_m(\boldsymbol{\phi})]^T. \tag{67}$$

If all the entries of $\boldsymbol{e}(\boldsymbol{\phi}^i)$ are nonpositive, the outcome $\boldsymbol{\phi}^i$ is acceptable, i.e., it meets all the specifications. From (67) we create the generalized ℓ_p function $v(\boldsymbol{\phi}^i)$ as

$$v(\boldsymbol{\phi}^i) = \begin{cases} \left[\sum_{j \in J(\boldsymbol{\phi}^i)} [e_j(\boldsymbol{\phi}^i)]^p\right]^{1/p} & \text{if } J(\boldsymbol{\phi}^i) \neq \varnothing \\ -\left[\sum_{j=1}^{m} [-e_j(\boldsymbol{\phi}^i)]^{-p}\right]^{-1/p} & \text{if } J(\boldsymbol{\phi}^i) = \varnothing \end{cases} \tag{68}$$

where

$$J(\phi^i) = \{ j \mid e_j(\phi^i) \geq 0 \}. \tag{69}$$

The one-sided ℓ_1 objective function for yield optimization [72] can be formulated as

$$U(\phi^0) = \sum_{i \in I} \alpha_i \, v(\phi^i) \tag{70}$$

where

$$I = \{ i \mid v(\phi^i) > 0 \} \tag{71}$$

and α_i are positive multipliers. If we chose α_i as [72]

$$\alpha_i = \frac{1}{| v(\phi^i) |} \tag{72}$$

the value of function $U(\phi^0)$ would be equal to N_{fail} and the yield would be

$$Y(\phi^0) = 1 - \frac{U(\phi^0)}{N} . \tag{73}$$

Hence, the relation between yield and the error functions is established, so maximization of yield can be converted to minimization of $U(\phi^0)$, i.e.,

$$\underset{\phi^0}{\text{minimize}} \; U(\phi^0). \tag{74}$$

In our implementation α_i are assigned according to (72) only at the starting point and then it is kept fixed during optimization. As a consequence, $U(\phi^0)$ is no longer equal to N_{fail} when optimization proceeds, but it provides a continuous approximation to N_{fail} [72]. A continuous "yield probability function" has been recently proposed in [161] to be used in place of (70).

B. Physics-Based Models for MMIC Passive Components

We use the PBM described in Section II to model GaAs MESFETs. Passive components are modeled through their equivalent circuits and the corresponding n-port $\boldsymbol{Y}$ matrices. The element values of the equivalent circuit elements are derived from material and geometrical parameters. Since the MMICs are manufactured on a common semi-insulating substrate these equivalent models are

grounded, e.g., a "two terminal component" is represented by a two-port. From these equivalent circuits we calculate the corresponding Y matrices. In general,

$$I = Y(\phi)V \tag{75}$$

where ϕ stands for physical parameters, and I and V are port current and voltage vectors.

For MIM capacitors ϕ includes the geometrical dimensions of the metal plate, the permittivity and the thickness of the dielectric film. For spiral inductors, ϕ includes the substrate height, the conductor width and spacing, and the number of turns. The configurations and schematics of spiral inductors, MIM capacitors and planar resistors are shown in Fig. 15. For instance, the value of capacitance C in the equivalent circuit for an MIM capacitor can be evaluated by [162]

$$C = \frac{10^{-3}\varepsilon_{rd} w l}{36\pi d} \tag{76}$$

where C is in pF, ε_{rd} is the relative permittivity of the dielectric film, w and l are the width and length of the metal plate in μm, respectively, and d is the thickness of the dielectric film in μm.

In this way all the passive components, as well as active devices (with the exception of the extrinsic parasitics), can be simulated and optimized in terms of physical parameters.

C. Quadratic Approximation of Responses and Gradients

Yield optimization requires substantial computational effort for circuit simulations and, if gradient optimization is used, for gradient evaluations. Quadratic approximation is an efficient approach to speed up the optimization process [163,118,164].

In quadratic approximation the circuit response $R(\phi)$ is approximated by a multidimensional quadratic polynomial of the form

$$R(\phi) \approx a_0 + \sum_{i=1}^{n} a_i(\phi_i - r_i) + \sum_{\substack{j,i=1 \\ j \geq i}}^{n} b_{ij}(\phi_i - r_i)(\phi_j - r_j) \tag{77}$$

where

$$r = [r_1\ r_2\ \ldots\ r_n]^T \tag{78}$$

is a known reference point and

$$\boldsymbol{a} = [a_0 \; a_1 \; \ldots \; a_n]^T \tag{79a}$$

$$\boldsymbol{b} = [b_{11} \; b_{22} \; \ldots \; b_{nn} \; b_{12} \; b_{13} \; \ldots \; b_{n-1,n}]^T \tag{79b}$$

are the quadratic model parameters to be determined. According to [118,164], $\boldsymbol{a}$ and $\boldsymbol{b}$ can be extremely efficiently determined using k, $n+1 \le k \le 2n+1$, function values calculated at k predetermined base points.

The gradient of $R(\boldsymbol{\phi})$ is a vector of functions, each function being the partial derivative of $R(\boldsymbol{\phi})$ w.r.t. one designable variable. In yield optimization we typically deal with four types of parameters, namely, n_{DS} designable variables $\boldsymbol{\phi}_{DS}$ with statistics, n_D designable variables $\boldsymbol{\phi}_D$ without statistics, n_{FS} non-designable variables $\boldsymbol{\phi}_{FS}$ with statistical variations, and n_F fixed parameters $\boldsymbol{\phi}_F$. The gradients of $R(\boldsymbol{\phi})$ with respect to the designable variables can be written as

$$\nabla R = \left[\left(\frac{\partial R}{\partial \boldsymbol{\phi}_{DS}^0} \right)^T \quad \left(\frac{\partial R}{\partial \boldsymbol{\phi}_D^0} \right)^T \right]^T. \tag{80}$$

The dimension of ∇R is $(n_{DS}+n_D)$. Each element in ∇R can also be approximated by its quadratic model of the form of (77).

For yield optimization we need to calculate all the responses of interest and their gradients at a number of statistical outcomes. Each statistical outcome is generated in a $(n_{DS}+n_{FS})$-dimensional space from the corresponding distributions of the statistical variables $\boldsymbol{\phi}_{DS}$ and $\boldsymbol{\phi}_{FS}$. Following (65), the statistical variables can be expressed as

$$\boldsymbol{\phi}_S = [\boldsymbol{\phi}_{DS}^T \; \boldsymbol{\phi}_{FS}^T]^T = [(\boldsymbol{\phi}_{DS}^0)^T \; (\boldsymbol{\phi}_{FS}^0)^T]^T + [(\Delta\boldsymbol{\phi}_{DS})^T \; (\Delta\boldsymbol{\phi}_{FS})^T]^T. \tag{81}$$

For efficiency, we build the models of the circuit responses and their gradients in the $(n_{DS}+n_{FS})$-dimensional space using $\boldsymbol{\phi}_{DS}$ and $\boldsymbol{\phi}_{FS}$ as the variables in the quadratic models (77). The models are built at each optimization iteration for the updated nominal point and utilized for as many statistical

outcomes as desired.

D. FAST Gradient-Based Yield Optimization

Gradient-based yield optimization involves repeated simulation of a large number of statistical outcomes and requires sensitivity analysis to estimate the gradients of the error functions. Therefore, an effective and efficient approach to gradient calculation is very important. Two gradient estimation techniques IGAT and FAST, as discussed in Section IV, have been used in yield optimization of nonlinear circuits [63]. Here, we use FAST for physics-based yield optimization.

In order to solve the yield optimization problem (74), we need to calculate the gradients of the objective function U w.r.t. the designable variables. Let ϕ_k^0 be a generic designable variable out of $\boldsymbol{\phi}^0$. Differentiating (68) w.r.t. ϕ_k^0 we obtain, if $J(\boldsymbol{\phi}^i) \neq \varnothing$,

$$\frac{\partial v(\boldsymbol{\phi}^i)}{\partial \phi_k^0} = \left[\sum_{j \in J(\boldsymbol{\phi}^i)} [e_j(\boldsymbol{\phi}^i)]^p\right]^{\frac{1}{p}-1} \sum_{j \in J(\boldsymbol{\phi}^i)} [e_j(\boldsymbol{\phi}^i)]^{p-1} \left[\frac{\partial e_j(\boldsymbol{\phi}^i)}{\partial \boldsymbol{\phi}^i}\right]^T \frac{\partial \boldsymbol{\phi}^i}{\partial \phi_k^0}. \tag{82}$$

From (65) we have $\frac{\partial \boldsymbol{\phi}^i}{\partial \phi_k^0} = \boldsymbol{u}_k$, unless a different than (65) relationship exists between $\boldsymbol{\phi}^i$ and $\boldsymbol{\phi}^0$ (e.g., a relative perturbation). Following (66a) and (66b) the computation of $\frac{\partial e_j(\boldsymbol{\phi}^i)}{\partial \boldsymbol{\phi}^i}$ can be converted to the calculation of the gradients of circuit responses by expressing the gradient of $e_j(\boldsymbol{\phi}^i)$ w.r.t. the lth element ϕ_l^i in $\boldsymbol{\phi}^i$ as

$$\frac{\partial e_j(\boldsymbol{\phi}^i)}{\partial \phi_l^i} = \pm \frac{\partial R_j(\boldsymbol{\phi}^i)}{\partial \phi_l^i} \tag{83}$$

where the sign depends on the type of the specification S_j. If S_j is an upper (lower) specification, the positive (negative) sign is used. Finally, the FAST technique is used to evaluate $\frac{\partial R_j(\boldsymbol{\phi}^i)}{\partial \phi_k^i}$.

E. Yield Optimization of A Three Stage X-band MMIC Amplifier

We consider a three stage small-signal X-band cascadable MMIC amplifier shown in Fig. 16. The design is based on the circuit topology and the fabrication layout described in [165], but with different parameter values. The amplifier contains three MESFETs using an interdigitated structure

with two gate fingers of dimensions 150μm×1.0μm. The matching circuits are composed of inductors and capacitors arranged in bandpass topology. All passive components are realized using lumped MMIC elements: spiral inductors, MIM capacitors and bulk resistors. The second and third MESFETs are biased through 1500Ω GaAs bulk resistors. The drains and the first gate bias are bypassed by high value MIM capacitors. The input-output matching circuit includes a series capacitor to make the amplifier cascadable without additional components.

The amplifier is to meet the following specifications: in the passband (8GHz - 12GHz) gain = 14±1.5dB, input and output VSWR < 2.5; in the stopband (below 6GHz or above 15GHz) gain < 2dB.

We use the PBMs for both the MESFETs and the passive elements. Since all devices are made from the same material and on the same wafer, they share common parameters. All three MESFETs have the same values for the critical electric field, saturation velocity, relative permittivity, built-in potential, low-field mobility and high-field diffusion coefficient. All the MIM capacitors have the same dielectric film, and all bulk resistors have the same sheet resistance. The geometrical parameters can have different values for different devices, including the gate length, gate width, and channel thickness of the MESFETs, the metal plate area of the MIM capacitors, and the number of turns of the spiral inductors. The doping densities of the MESFETs are also considered as independent parameters.

First, a nominal design is performed using minimax optimization [166]. As in a traditional design, only the matching circuits are optimized. The parameters of the active devices (MESFETs) have fixed values. There are 14 design variables, namely, S_{C1}, S_{C2}, S_{C3}, S_{C4} (the area of the metal plate of MIM capacitors C_1, C_2, C_3 and C_4), n_{L1}, n_{L2}, ..., n_{L10} (the number of turns of the spiral inductors L_1, L_2, ..., L_{10}). The values of the capacitors and inductors given in [165] were used to select the initial values for these variables. The nominal solution was achieved by minimax optimization after 15 iterations (about 5 minutes on a Sun SPARCstation 1). The gain and input VSWR before and after optimization are shown in Fig. 17. The values of the design variables before and after optimization are listed in Table V.

The minimax nominal design is then used as the starting point for yield optimization. A total of 37 parameters are considered as statistical variables. They include the gate length, gate width, channel thickness and doping density of the MESFETs, as well as the geometrical parameters of the passive elements. The extrinsic parasitic parameters of MESFETs are assumed independent, non-designable and without statistical variations. The mean values and standard deviations of the statistical variables are listed in Table VI. The correlation matrix used is given in Table VII. The most significant correlations are between the corresponding parameters for different devices. For instance, the gate lengths of the three MESFETs are strongly correlated. In addition to the number of turns of the 10 spiral inductors, the metal plate area of the 4 MIM capacitors, the gate length, gate width, channel thickness and doping density of the MESFETs are chosen as the variables for yield optimization.

At the starting point (i.e., the minimax nominal design), the yield was 26% as estimated by Monte Carlo analysis with 200 statistical outcomes. The yield was improved to 69% at the solution of yield optimization (about 4 and a half hours CPU time on a Sun SPARCstation 1). The solution is given in Table VIII. The Monte Carlo sweeps of gain and input VSWR before and after yield optimization are shown in Figs. 18 and 19.

VII. TWO-DIMENSIONAL (2D) FIELD-BASED MESFET SIMULATION AND MODELING

Among PBMs, field-based numerical models are considered to be the most accurate in terms of the simulation results they provide. For MESFETs, a number of numerical models such as the 2D drift-diffusion model [130, 133] have been proposed. Although conventional microwave CAD programs may have difficulties accommodating field-based models, the new generation of CAD systems should be able to do so with an open architecture. The Datapipe feature of OSA90/hope [127] is designed to functionally integrate external simulators. In this section we demonstrate 2D field-based MESFET simulation and modeling utilizing the Datapipe feature.

A. 2D Drift-Diffusion MESFET Model

We use a 2D drift-diffusion MESFET model based on numerical techniques presented by Reiser [130] and Snowden *et al.* [133].

The model makes the following assumptions: (1) neglecting minority carriers, (2) neglecting thermal generation and recombination effects, and (3) describing the carrier flow by the diffusion equations. The basic model equations are described by equations (1)-(5) in Section II. The diffusion coefficient D is determined from the Einstein relation

$$D = \frac{kT}{q}\mu \tag{84}$$

with Boltzmann's constant k and the absolute temperature T. The electron mobility μ is calculated by (10).

Two-dimensional Poisson's equations and current continuity equations with the boundary conditions approximated according to the physical nature of the device are solved using the finite difference method to simulate the internal device physics.

B. Simulation Using Datapipe of OSA90/hope

The Datapipe feature of OSA90/hope [127] is designed to utilize UNIX interprocess pipes for high-speed data communication between OSA90/hope and external programs. Using Datapipe, external models and simulators can be functionally integrated into the overall simulation, optimization and statistical environment. The basic Datapipe architecture is illustrated in Fig. 20.

We apply this concept to 2D field-based MESFET simulation. The 2D field simulator runs as an external program, concentrating on intensive number crunching operations such as solving the Poisson's equations and current continuity equations. OSA90/hope interacts with the user, accepts and parses parameter values through an input file, organizes simulation (sweep) ranges, passes the necessary data to the external simulator, postprocesses the results returned from the external simulator, and provides graphics display capabilities.

We consider a 0.5×300μm GaAs MESFET with the physical parameters listed in Table IX. The source and drain lengths are equivalent ohmic contact length. Since the substrate has a very high

resistivity and its effect on the results can almost be neglected in the finite difference simulation, a small value rather than the actual value of substrate thickness is considered in order to reduce computation time. The approximated doping profile is listed in Table X. We used the 2D model in DC simulation at 56 bias points, which took about 14 hours of CPU time on a Sun SPARCstation 1. The simulated DC results are indicated in Fig. 21 by circles.

C. The Plessey Model [167]

Field-based simulation provides accurate results but is very time-consuming. Often, field-based simulation is used to generate data for ECM modeling. We utilize a modified Statz model from Plessey [167] to match the results from our 2D field simulation. The Plessey model equation for the FET drain current is as follows

$$I_{ds} = \frac{I_{dss}(V_{gs} - V_t)^2}{1 + b(V_{gs} - V_t)}(1 + \lambda V_{ds})\tanh(\alpha V_{ds}) + \left[1 + \frac{V_{ds}}{V_{t1}}\right] G_{dst} V_{ds} \tanh(\alpha V_{ds}) \tag{85}$$

where

$$V_{t1} = V_t(1 - \beta V_{ds}). \tag{86}$$

I_{dss}, V_t, G_{dst}, b, α, β and λ are the parameters to be determined. The model equation is implemented in the OSA90/hope input file using expressions.

The Plessey model parameters are extracted by ℓ_1 optimization of OSA90/hope, matching the DC data at 56 bias points. The extraction took about 3 minutes of CPU time on a Sun SPARCstation 1. The model parameter values before and after optimization are listed in Table XI. The DC drain currents calculated by the 2D field simulator and by the Plessey model are compared in Fig. 21.

VIII. CONCLUSIONS

We have presented our approach towards physics-oriented microwave circuit optimization. We have addressed device modeling, parameter extraction, nonlinear simulation, nominal design, statistical modeling and yield optimization.

Analytical large-signal physical models of MESFETs have been discussed and new developments presented. Nonlinear circuit analysis with PBMs integrated into the HB equations have been described.

PBMs provide flexibility for engineers to perform designs based on physical parameters and to foresee the characteristics of the circuits before fabrication. Although some phenomena of the FETs are not fully accommodated at present we believe that continuing research on and improvements of PBMs will address the unsolved problems in the near future.

FAST has been shown to be suitable for high speed gradient calculations for circuit optimization employing physical, geometrical and process-related parameters of devices as design variables. Hierarchical, nonlinear, yield-driven optimization has been demonstrated.

Statistical modeling of active devices with physics-based models has been explored. Our procedure has been illustrated through new implementations of the Ladbrooke model and the Khatibzadeh and Trew model. The results from the Ladbrooke model have demonstrated the feasibility of using PBMs for statistical modeling, though further investigation of the Khatibzadeh and Trew model for statistical purposes is needed.

Physics-based statistical models have been applied in physics-based yield-driven optimization suitable for MMICs. Both passive and active elements have been related through material and geometrical statistical parameters.

Effective multidimensional quadratic functions have been employed to simultaneously approximate responses and gradients. Our novel theoretical developments have been incorporated into OSA90/hope and HarPE. They are thereby available to the microwave community. OSA90/hope's novel Datapipe structure constitutes the first microwave CAD product of its kind. The open architecture feature enables device and circuit designers to solve a variety of relevant linear/nonlinear/statistical modeling, simulation and optimization problems with both circuit and physical parameters.

ACKNOWLEDGEMENTS

The authors would like to express their appreciation to Dr. Rolf H. Jansen of Jansen Microwave, Ratingen, Germany, Guest Co-Editor of this Special Issue, for several significantly inspiring discussions. The authors thank Dr. Robert J. Trew of North Carolina State University, Raleigh, NC, for useful discussions and providing essential data. The authors acknowledge some original work done by Dr. Jian Song which has been integrated into our presentation. Thanks are also due to Dr. D. Mike Brookbanks of GEC-Marconi Materials Research, Caswell, Northamptonshire, England, for technical discussions and generously providing measurement data. Thanks are also extended to his colleague Dr. Ron G. Arnold. Thanks are due to Dr. Peter H. Ladbrooke of GaAs Code Ltd., Cambridge, England, for helpful discussions and comments [168]. Thanks are given to Dr. Walter R. Curtice of W.R. Curtice Consulting, Princeton Junction, NJ, for helpful criticisms and discussions. Finally, thanks are extended to the reviewers for helpful comments, constructive criticisms and suggestions to improve this manuscript.

REFERENCES

[1] W.R. Curtice, "A MESFET model for use in the design of GaAs integrated circuits," *IEEE Trans. Microwave Theory Tech.*, vol. MTT-28, 1980, pp. 448-456.

[2] W.R. Curtice and M. Ettenberg, "A nonlinear GaAs FET model for use in the design of output circuits for power amplifiers," *IEEE Trans. Microwave Theory Tech.*, vol. MTT-33, 1985, pp. 1383-1394.

[3] A. Materka and T. Kacprzak, "Computer calculation of large-signal GaAs FET amplifier characteristics," *IEEE Trans. Microwave Theory Tech.*, vol. MTT-33, 1985, pp. 129-135.

[4] H. Statz, P. Newman, I.W. Smith, R.A. Pucel and H.A. Haus, "GaAs FET device and circuit simulation in SPICE," *IEEE Trans. Electron Devices*, vol. ED-34, 1987, pp. 160-169.

[5] V.D. Hwang and T. Itoh, "An efficient approach for large-signal modeling and analysis of GaAs MESFET," *IEEE Trans. Microwave Theory Tech.*, vol. MTT-35, 1987, pp. 396-402.

[6] J.W. Bandler, S.H. Chen, S. Ye and Q.J. Zhang, "Integrated model parameter extraction using large-scale optimization concepts," *IEEE Trans. Microwave Theory Tech.*, vol. 36, 1988, pp. 1629-1638.

[7] J.W. Bandler, Q.J. Zhang, S. Ye and S.H. Chen, "Efficient large-signal FET parameter extraction using harmonics," *IEEE Trans. Microwave Theory Tech.*, vol. 37, 1989, pp. 2099-2108.

[8] J.W. Bandler, Q.J. Zhang and Q. Cai, "Nonlinear circuit optimization with dynamically integrated physical device models," *IEEE Int. Microwave Symp. Dig.* (Dallas, TX), 1990, pp. 303-306.

[9] R.J. Gilmore and M.B. Steer, "Nonlinear circuit analysis using the method of harmonic balance-a review of the art. Part I. introductory concepts," *Int. J. Microwave and Millimetre-Wave Computer-Aided Engineering*, vol. 1, 1991, pp. 22-37.

[10] L.O. Chua and P. Lin, *Computer-Aided Analysis of Electronic Circuits: Algorithms and Computational Techniques*. Engelwood Cliffs, NJ: Prentice-Hall, 1975.

[11] S. Skelboe, "Computation of the periodic steady-state response of nonlinear networks by extrapolation methods," *IEEE Trans. Circuits Syst.*, vol. CAS-27, 1980, pp. 161-175.

[12] S. Skelboe, "Time-domain steady-state analysis of nonlinear electrical systems," *Proc. IEEE*, vol. 70, 1982, pp. 1210-1228.

[13] J. Vlach and K. Singhal, *Computer Methods for Circuit Analysis and Design*. New York: Van Nostrand Reinhold, 1983.

[14] A.K. Jastrzebski and M.I. Sobhy, "Analysis of microwave circuits using state-space approach," *Proc. IEEE Int. Symp. Circuits Syst.* (Montreal, Canada), 1984, pp. 1119-1122.

[15] M.I. Sobhy and A.K. Jastrzebski, "Direct integration methods of nonlinear microwave circuits," *Proc. 15th European Microwave Conf.* (Paris, France), 1985, pp. 1110-1118.

[16] L.W. Nagel and D.O. Pederson, *SPICE (Simulation Program with Integrated Circuit Emphasis)*, Electronics Research Laboratory, University of California, Memo ERL-M382, April, 1973.

[17] S.W. Director, "A method for quick determination of the periodic steady-state in nonlinear networks," *Proc. 9th Allerton Conf. Circuits Syst. Theory*, (Urbana, IL), 1971, pp. 131-139.

[18] T.J. Aprille, Jr. and T.N. Trick, "Steady-state analysis of nonlinear circuits with periodic inputs," *Proc. IEEE*, vol. 60, 1972, pp. 108-114.

[19] T.J. Aprille, Jr. and T.N. Trick, "A computer algorithm to determine the steady-state response of nonlinear oscillators," *IEEE Trans. Circuit Theory*, vol. CT-19, 1972, pp. 354-360.

[20] F.R. Colon and T.N. Trick, "Fast periodic steady-state analysis for large-signal electronic circuits," *IEEE J. Solid-State Circuits*, vol. SC-8, 1973, pp. 260-269.

[21] S.W. Director and K.W. Current, "Optimization of forced nonlinear periodic circuits," *IEEE Trans. Circuits Syst.*, vol. CAS-23, 1976, pp. 329-335.

[22] M.S. Nakhla and F.H. Branin, Jr., "Determining the periodic response of nonlinear systems by a gradient method," *Int. J. Circuit Theory Appl.*, vol. 5, 1977, pp. 255-273.

[23] M.B. Steer, C.R. Chang and G.W. Rhyne, "Computer-aided analysis of nonlinear microwave circuits using frequency-domain nonlinear analysis techniques: the state of the art," *Int. J. Microwave and Millimetre-Wave Computer-Aided Engineering*, vol. 1, 1991, pp. 181-200.

[24] R.G. Sea, "An algebraic formula for amplitudes of intermodulation products involving an arbitrary number of frequencies," *Proc. IEEE*, vol. 56, 1968, pp. 1388-1389.

[25] R.G. Sea and A.G. Vacroux, "On the computation of intermodulation products for a power series nonlinearity," *Proc. IEEE*, 1969, pp. 337-338.

[26] M.B. Steer and P.J. Khan, "An algebraic formula for the output of a system with large-signal multifrequency excitation," *Proc. IEEE*, 1983, pp. 177-179.

[27] G.W. Rhyne, M.B. Steer and B.D. Bates, "Frequency-domain nonlinear circuit analysis using generalized power series," *IEEE Trans. Microwave Theory Tech.*, vol. MTT-36, 1988, pp. 379-387.

[28] V. Volterra, *Theory of Functionals and of Integral and Integro-Differential Equations.* London: Blackie & Son, 1930.

[29] E. Bedrosian and S.O. Rice, "The output properties of Volterra systems (nonlinear systems with memory) driven by harmonic and Gaussian inputs," *Proc. IEEE*, vol. 59, 1971, pp. 1688-1707.

[30] J.J. Bussgang, L. Ehrman and J.W. Graham, "Analysis of nonlinear systems with multiple inputs," *Proc. IEEE*, vol. 62, 1974, pp. 1088-1119.

[31] D.D. Weiner and J.F. Spina, *Sinusoidal Analysis and Modeling of Weakly Nonlinear Circuits.* New YorK: Van Nostrand Reinhold, 1980.

[32] I.W. Sandberg, "Expansions for nonlinear systems," *Bell Syst. Tech. J.*, vol. 61, 1982, pp. 159-199.

[33] S.A. Maas, "A general-purpose computer program for the Volterra-series analysis of nonlinear microwave circuits," *IEEE Int. Microwave Symp. Dig.* (New York, NY), 1988, pp. 311-314.

[34] A. Ushida and L.O. Chua, "Frequency-domain analysis of nonlinear circuits driven by multi-tone signals," *IEEE Trans. Circuits Syst.*, vol. CAS-31, 1984, pp. 766-779.

[35] J.H. Haywood and Y.L. Chow, "Intermodulation distortion analysis using a frequency-domain harmonic balance technique," *IEEE Trans. Microwave Theory Tech.*, vol. MTT-36, 1988, pp. 1251-1257.

[36] C.R. Chang, M.B. Steer and G.W. Rhyne, "Frequency-domain spectral balance using the arithmetic operator method," *IEEE Trans. Microwave Theory Tech.*, vol. MTT-37, 1989, pp. 1681-1688.

[37] G.L. Heiter, "Characterization of nonlinearities in microwave devices and systems," *IEEE Trans. Microwave Theory Tech.*, vol. MTT-21, 1973, pp. 797-805.

[38] R.B. Swerdlow, "Analysis of intermodulation noise in frequency converters by Volterra series," *IEEE Trans. Microwave Theory Tech.*, vol. MTT-26, 1978, pp. 305-313.

[39] R.S. Tucker, "Third-order intermodulation distortion and gain compression in GaAs FET's," *IEEE Trans. Microwave Theory Tech.*, vol. MTT-27, 1979, pp. 400-408.

[40] R.A. Minasian, "Intermodulation distortion analysis of MESFET amplifiers using Volterra series representation," *IEEE Trans. Microwave Theory Tech.*, vol. MTT-28, 1980, pp. 1-8.

[41] C.L. Law and C.S. Aitchison, "Prediction of wide-band power performance of MESFET distributed amplifiers using the Volterra series representation," *IEEE Trans. Microwave Theory Tech.*, vol. MTT-34, 1986, pp. 1308-1317.

[42] G.W. Rhyne and M.B. Steer, "Generalized power series analysis of intermodulation distortion in a MESFET amplifier: simulation and experiment," *IEEE Trans. Microwave Theory Tech.*, vol. MTT-35, 1987, pp. 1248-1255.

[43] Y. Hu, J. Obregon and J.C. Mollier, "Nonlinear analysis of microwave FET oscillators using Volterra series," *IEEE Trans. Microwave Theory Tech.*, vol. 37, 1989, pp. 1689-1693.

[44] C.R. Chang and M.B. Steer, "Frequency-domain nonlinear microwave circuit simulation using the arithmetic operator method," *IEEE Trans. Microwave Theory Tech.*, vol. 38, 1990, pp. 1139-1143.

[45] W.J. Cunningham, *Introduction to Nonlinear Analysis*. New York: McGraw-Hill, 1958.

[46] J.C. Lindenlaub, "An approach for finding the sinusoidal steady-state response of nonlinear systems," *Proc. 7th Allerton Conf. Circuit Syst. Theory* (Chicago, IL), 1969, pp. 323-327.

[47] M.S. Nakhla and J. Vlach, "A piecewise harmonic-balance technique for determination of periodic response of nonlinear systems," *IEEE Trans. Circuits Syst.*, vol. CAS-23, 1976, pp. 85-91.

[48] A.I. Mees, *Dynamics of Feedback Systems*. New York: Wiley, 1981.

[49] V. Rizzoli, A. Lipparini, and E. Marazzi, "A general-purpose program for nonlinear microwave circuit design," *IEEE Trans. Microwave Theory Tech.*, vol. 31, 1983, pp. 762-770.

[50] K. S. Kundert and A. Sangiovanni-Vincentelli, "Simulation of nonlinear circuits in the frequency domain," *IEEE Trans. Computer-Aided Design*, vol. CAD-5, 1986, pp. 521-535.

[51] V. Rizzoli, C. Cecchetti, A. Lipparini, and F. Mastri, "General-purpose harmonic balance analysis of nonlinear microwave circuits under multitone excitation," *IEEE Trans. Microwave Theory Tech.*, vol. 36, 1988, pp. 1650-1660.

[52] R.J. Gilmore and M.B. Steer, "Nonlinear circuit analysis using the method of harmonic balance-a review of the art. Part II. advanced concepts," *Int. J. Microwave and Millimetre-Wave Computer-Aided Engineering*, vol. 1, 1991, pp. 159-180.

[53] F. Filicori, V.A. Monaco and C. Naldi, "Simulation and design of microwave class-C amplifiers through harmonic analysis," *IEEE Trans. Microwave Theory Tech.*, vol. MTT-27, 1979, pp. 1043-1051.

[54] R.G. Hicks and P.J. Khan, "Numerical analysis of subharmonic mixers using accurate and approximate models," *IEEE Trans. Microwave Theory Tech.*, vol. MTT-30, 1982, pp. 2113-2120.

[55] W.R. Curtice, "Nonlinear analysis of GaAs MESFET amplifiers, mixers, and distributed amplifiers using harmonic balance technique," *IEEE Trans. Microwave Theory Tech.*, vol. 35, 1987, pp. 441-447.

[56] P.W. Van Der Walt, "Efficient technique for solving nonlinear mixer pumping problem," *Electronics Lett.*, vol 21, 1985, pp. 899-900.

[57] S. El-Rabaie, J.A.C. Stewart, V.F. Fusco and J.J. McKeown, "A novel approach for the large signal analysis and optimisation of microwave frequency doublers", *IEEE Int. Microwave Symp. Dig.* (New York, NY), 1988, pp. 1119-1122.

[58] J.W. Bandler, R.M. Biernacki, S.H. Chen, J. Song, S. Ye and Q.J. Zhang, "Analytically unified DC/small-signal/large-signal circuit design," *IEEE Trans. Microwave Theory Tech.*, vol. 39, 1991, pp. 1076-1082.

[59] V.D. Hwang, Y-C. Shih, H.M. Le and T. Itoh, "Nonlinear modeling and verification of MMIC amplifiers using the waveform-balance method", *IEEE Trans. Microwave Theory Tech.*, vol. 37, 1989, pp. 2125-2133.

[60] R. Gilmore, "Nonlinear circuit design using the modified harmonic balance algorithm", *IEEE Trans. Microwave Theory Tech.*, vol. MTT-34, 1986, pp. 1294-1307.

[61] A. Lipparini, E. Marazzi and V. Rizzoli, "A new approach to the computer-aided design of nonlinear networks and its application to microwave parametric frequency dividers," *IEEE Trans. Microwave Theory Tech.*, vol. MTT-30, 1982, pp. 1050-1058.

[62] V. Rizzoli and A. Neri, "State of the art and present trends in nonlinear microwave CAD techniques", *IEEE Trans. Microwave Theory Tech.*, vol. 36, 1988, pp. 343-365.

[63] J.W. Bandler, Q.J. Zhang, J. Song and R.M. Biernacki, "FAST gradient based yield optimization of nonlinear circuits", *IEEE Trans. Microwave Theory Tech.*, vol. 38, 1990, pp. 1701-1710.

[64] R.H. Jansen, R.G. Arnold and I.G. Eddison, "A comprehensive CAD approach to the design of MMICs up to mm-wave frequencies", *IEEE Trans. Microwave Theory Tech.*, vol. 36, 1988, pp. 208-219.

[65] R.H. Jansen, I.G. Eddison and R.G. Arnold, "Recent developments in CAD of high packing density MMICs", *MIOP 1989* (Sindelfingen, West Germany), 1989, Paper 1.3.

[66] R.H. Jansen, "Progress in passive and active MMIC device modeling", *Workshop on Progress in Microwave CAD and in CAD Applications Dig.* (Ratingen, West Germany), 1989, pp. 173-196.

[67] F.A. Myers, "Advanced GaAs MMIC elements and circuits", *Workshop on Progress in Microwave CAD and in CAD Applications Dig.* (Ratingen, West Germany), 1989, pp. 197-203.

[68] R. Goyal, M. Golio and W. Thomann, "Device Modeling", in *Monolithic Microwave Integrated Circuits: Technology & Design*, R. Goyal Ed. Boston: Artech House, 1989, Chapter 4.

[69] E.D. Cohen, "MIMIC from the Department of Defense perspective", *IEEE Trans. Microwave Theory Tech.*, vol. 38, 1990, pp. 1171-1174.

[70] C.M. Snowden, "Microwave and millimeter-wave device and circuit design based on physical modeling," *Int. J. on Microwave and Millimetre-Wave Computer-Aided Engineering*, vol. 1, 1991, pp. 4-21.

[71] R.J. Trew, "MESFET models for microwave CAD applications," *Int. J. on Microwave and Millimetre-Wave Computer-Aided Engineering*, vol. 1, 1991, pp. 143-158.

[72] J.W. Bandler and S.H. Chen, "Circuit optimization: the state of the art", *IEEE Trans. Microwave Theory Tech.*, vol. 36, 1988, pp. 424-443.

[73] J. Purviance, D. Criss and D. Monteith, "FET model statistics and their effects on design centering and yield prediction for microwave amplifiers," *IEEE Int. Microwave Symp. Dig.* (New York, NY), 1988, pp. 315-318.

[74] R.W. Dutton, D.A. Divekar, A.G. Gonzalez, S.E. Hansen and D.A. Antoniadis, "Correlation of fabrication process and electrical device parameter variations," *IEEE J. Solid-State Circuits*, vol. SC-12, 1977, pp. 349-355.

[75] D.A. Divekar, R.W. Dutton and W.J. McCalla, "Experimental study of Gummel-Poon model parameter correlations for bipolar junction transistors," *IEEE J. Solid-State Circuits*, vol. SC-12, 1977, pp. 552-559.

[76] M.A. Styblinski, "Factor analysis model of resistor correlations for monolithic integrated circuits," *Proc. IEEE Int. Symp. Circuits Syst.* (Tokyo, Japan), 1977, pp. 776-777.

[77] P.J. Rankin, "Statistical modeling for integrated circuits," *IEE Proc.*, vol. 129, Pt. G, No. 4, 1982, pp. 186-191.

[78] S. Freeman, "Statistical techniques for calibrating simulation models of analog circuits and devices," *Proc. IEEE Int. Symp. Circuits Syst.* (Montreal, Canada), 1984, pp. 684-688.

[79] S. Liu and K. Singhal, "A statistical model for MOSFETs," *Proc. IEEE Int. Conf. Computer-Aided Design* (Santa Clara, CA), 1985, pp. 78-80.

[80] P. Cox, P. Yang, S.S. Mahant-Shetti and P. Chatterjee, "Statistical modeling for efficient parametric yield estimation of MOS VLSI circuits," *IEEE Trans. Electron Devices*, vol. ED-32, 1985, pp. 471-478.

[81] N. Herr and J.J. Barnes, "Statistical circuit simulation modeling of CMOS VLSI," *IEEE Trans. Computer-Aided Design*, vol. CAD-5, 1986, pp. 15-22.

[82] C.J.B. Spanos and S.W. Director, "Parameter extraction for statistical IC process characterization," *IEEE Trans. Computer-Aided Design*, vol. CAD-5, 1986, pp. 66-78.

[83] J.E. Purviance, M.C. Petzold and C. Potratz, "A linear statistical FET model using principal component analysis," *IEEE Trans. Microwave Theory Tech.*, vol. 37, 1989, pp. 1389-1394.

[84] J.W. Bandler, R.M. Biernacki, S.H. Chen, J. Loman, M. Renault and Q.J. Zhang, "Combined discrete/normal statistical modeling of microwave devices," *Proc. European Microwave Conf.* (Wembley, England), 1989, pp. 205-210.

[85] J. Purviance, M. Meehan and D. Collins, "Properties of FET parameter statistical data bases," *IEEE Int. Microwave Symp. Dig.* (Dallas, TX), 1990, pp. 567-570.

[86] J.W. Bandler, R.M. Biernacki, S.H. Chen, J. Song, S. Ye and Q.J. Zhang, "Statistical modeling of GaAs MESFETs," *IEEE Int. Microwave Symp. Dig.* (Boston, MA), 1991, pp. 87-90.

[87] A.R. Jha, R. Goyal and B. Manz, "Introduction," in *Monolithic Microwave Integrated Circuits: Technology & Design*, R. Goyal Ed. Boston: Artech House, 1989, Chapter 1.

[88] B.J. Karafin, "The optimum assignment of component tolerances for electrical networks," *Bell Syst. Tech. J.*, vol. 50, 1971, pp. 1225-1242.

[89] J.F. Pinel and K.A. Roberts, "Tolerance assignment in linear networks using nonlinear programming," *IEEE Trans. Circuit Theory*, vol. CT-19, 1972, pp. 475-479.

[90] J.W. Bandler, "Optimization of design tolerances using nonlinear programming," *Proc. 6th Princeton Conf. on Information Science and Systems* (Princeton, NJ), 1972, pp. 655-659. Also in *Computer-Aided Filter Design*, G. Szentirmai, Ed. New York: IEEE Press, 1973.

[91] J.W. Bandler, "The tolerance problem in optimal design," *Proc. European Microwave Conf.* (Brussels, Belgium), 1973, Paper A.13.1.(I).

[92] J.W. Bandler, "Optimization of design tolerances using nonlinear programming," *J. Optimization Theory and Applications*, vol. 14, 1974, pp. 99-114.

[93] J.W. Bandler, P.C. Liu and H. Tromp, "A nonlinear programming approach to optimal design centering, tolerancing and tuning," *IEEE Trans. Circuits Syst.*, vol. CAS-23, 1976, pp. 155-165.

[94] J.W. Bandler, P.C. Liu and H. Tromp, "Integrated approach to microwave design," *IEEE Trans. Microwave Theory Tech.*, vol. MTT-24, 1976, pp. 584-591.

[95] S.W. Director and G.D. Hachtel, "The simplicial approximation approach to design centering," *IEEE Trans. Circuits Syst.*, vol. CAS-24, 1977, pp. 363-372.

[96] J.W. Bandler and H.L. Abdel-Malek, "Optimal centering, tolerancing, and yield determination via updated approximations and cuts," *IEEE Trans. Circuits Syst.*, vol. CAS-25, 1978, pp. 853-871.

[97] E. Polak and A. Sangiovanni-Vincentelli, "Theoretical and computational aspects of the optimal design centering, tolerancing, and tuning problem," *IEEE Trans. Circuits Syst.*, vol. CAS-26, 1979, pp. 795-813.

[98] H.L. Abdel-Malek and J.W. Bandler, "Yield optimization for arbitrary statistical distributions: Part I-theory," *IEEE Trans. Circuits Syst.*, vol. CAS-27, 1980, pp. 245-253.

[99] R.S. Soin and R. Spence, "Statistical exploration approach to design centering," *Proc. IEE*, vol. 127, pt. G., 1980, pp. 260-269.

[100] M.A. Styblinski and A. Ruszczynski, "Stochastic approximation approach to statistical circuit design," *Electronics Lett.*, vol. 19, 1980, pp. 300-302.

[101] K. Singhal and J.F. Pinel, "Statistical design centering and tolerancing using parametric sampling," *IEEE Trans. Circuits Syst.*, vol. CAS-28, 1981, pp. 692-702.

[102] T. Downs, A.S. Cook and G. Rogers, "A partitioning approach to yield estimation for large circuit and systems," *IEEE Trans. Circuits Syst.*, vol. CAS-31, 1984, pp. 472-485.

[103] J.W. Bandler and A.E. Salama, "Functional approach to microwave postproduction tuning," *IEEE Trans. Microwave Theory Tech.*, vol. MTT-33, 1985, pp. 302-310.

[104] A.J. Strojwas and A. Sangiovanni-Vincentelli, Eds., *IEEE Trans. Computer-Aided Design*, Special Issue on Statistical Design of VLSI Circuits, vol. CAD-5, 1986, pp. 5-169.

[105] P. Yang, D.E. Hocevar, P.F. Cox, C. Machala and P.K. Chatterjee, "An integrated and efficient approach for MOS VLSI statistical circuit design," *IEEE Trans. Computer-Aided Design*, vol. CAD-5, 1986, pp. 5-14.

[106] M.L. Stein, "An efficient method of sampling for statistical circuit design," *IEEE Trans. Computer-Aided Design*, vol. CAD-5, 1986, pp. 23-29.

[107] M.A. Styblinski, "Problems of yield gradient estimation for truncated probability density functions," *IEEE Trans. Computer-Aided Design*, vol. CAD-5, 1986, pp. 30-38.

[108] M.A. Styblinski and L.J. Opalski, "Algorithms and software tools for IC yield optimization based on fundamental fabrication parameters," *IEEE Trans. Computer-Aided Design*, vol. CAD-5, 1986, pp. 79-89.

[109] J.P. Spoto, W.T. Coston and C.P. Hernandez, "Statistical integrated circuit design and characterization," *IEEE Trans. Computer-Aided Design*, vol. CAD-5, 1986, pp. 90-103.

[110] S.R. Nassif, A.J. Strojwas and S.W. Director, "A methodology for worst-case analysis of integrated circuits," *IEEE Trans. Computer-Aided Design*, vol. CAD-5, 1986, pp. 104-113.

[111] W. Maly, A.J. Strojwas and S.W. Director, "VLSI yield prediction and estimation: a unified framework," *IEEE Trans. Computer-Aided Design*, vol. CAD-5, 1986, pp. 114-130.

[112] D. Riley and A. Sangiovanni-Vincentelli, "Models for a new profit-based methodology for statistical design of integrated circuits," *IEEE Trans. Computer-Aided Design*, vol. CAD-5, 1986, pp. 131-169.

[113] L.J. Opalski and M.A. Styblinski, "Generalization of yield optimization problem: maximum income approach," *IEEE Trans. Computer-Aided Design*, vol. CAD-5, 1986, pp. 346-360.

[114] Y. Aoki, H. Masuda, S. Shimada and S. Sato, "A new design-centering methodology for VLSI device development," *IEEE Trans. Computer-Aided Design*, vol. CAD-6, 1987, pp. 452-461.

[115] T.K. Yu, S.M. Kang, I.N. Hajj and T.N. Trick, "Statistical performance modeling and parametric yield estimation of MOS VLSI," *IEEE Trans. Computer-Aided Design*, vol. CAD-6, 1987, pp. 1013-1022.

[116] D.E. Hocevar, P.F. Cox and P. Yang, "Parametric yield optimization for MOS circuit blocks," *IEEE Trans. Computer-Aided Design*, vol. CAD-7, 1988, pp. 645-658.

[117] J.W. Bandler, R.M. Biernacki, S.H. Chen, M. Renault, J. Song and Q.J. Zhang, "Yield optimization of large scale microwave circuits," *Proc. European Microwave Conf.* (Stockholm, Sweden), 1988, pp. 255-260.

[118] R.M. Biernacki, J.W. Bandler, J. Song and Q.J. Zhang, "Efficient quadratic approximation for statistical design," *IEEE Trans. Circuits Syst.*, vol. 36, 1989, pp. 1449-1454.

[119] J.W. Bandler, Q.J. Zhang, J. Song and R.M. Biernacki, "Yield optimization of nonlinear circuits with statistically characterized devices," *IEEE Int. Microwave Symp. Dig.* (Long Beach, CA), 1989, pp. 649-652.

[120] M.D. Meehan, T. Wandinger and D.A. Fisher, "Accurate design centering and yield prediction using the 'truth model'," *IEEE Int. Microwave Symp. Dig.* (Boston, MA), 1991, pp. 1201-1204.

[121] J. Purviance and M. Meehan, "CAD for statistical analysis and design of microwave circuits", *Int. J. Microwave and Millimeter-Wave Computer-Aided Engineering*, vol. 1, 1991, pp. 59-76.

[122] R.J. Gilmore, M. Eron and T. Zhang, "Yield optimization of a MMIC distributed amplifier using physically-based device models," *IEEE Int. Microwave Symp. Dig.* (Boston, MA), 1991, pp. 1205-1208.

[123] J.W. Bandler, Q. Cai, R.M. Biernacki, S.H. Chen and Q.J. Zhang, "Physics-based design and yield optimization of MMICs," *Proc. European Microwave Conf.* (Stuttgart, Germany), 1991, pp. 1515-1520.

[124] C.H. Corbex, A.F. Gerodolle, S.P. Martin and A.R. Poncet, "Data structuring for process and device simulations," *IEEE Trans. Computer-Aided Design*, vol. 7, 1988, pp. 489-500.

[125] J.R.F. McMacken and S.G. Chamberlain, "CHORD: a modular semiconductor device simulation development tool incorporating external network models," *IEEE Trans. Computer-Aided Design*, vol. 8, 1989, pp. 826-836.

[126] P. Lloyd, H.K. Dirks, E.J. Prendergast and K. Singhal, "Technology CAD for competitive products," *IEEE Trans. Computer-Aided Design*, vol. 9, 1990, pp. 1209-1216.

[127] *OSA90/hope*™, Optimization Systems Associates Inc., P.O. Box 8083, Dundas, Ontario, Canada L9H 5E7, 1991.

[128] *HarPE™*, Optimization Systems Associates Inc., P.O. Box 8083, Dundas, Ontario, Canada L9H 5E7, 1991.

[129] D.P. Kennedy and R.R. O'Brien, "Computer aided two dimensional analysis of the junction field-effect transistor," *IBM J. Res. Devel.*, vol. 14, 1970, pp. 95-116.

[130] M. Reiser, "A two-dimensional numerical FET model for DC, AC and large-signal analysis," *IEEE Trans. Electron Devices*, vol. ED-20, 1973, pp. 35-45.

[131] T. Wada and J. Frey, "Physical basis of short-channel MESFET operation," *IEEE Trans. Electron Devices*, vol. ED-26, 1979, pp. 476-490.

[132] W.R. Curtice and Y.H. Yun, "A temperature model for the GaAs MESFET," *IEEE Trans. Electron Devices*, vol. ED-28, 1981, pp. 954-962.

[133] C.M. Snowden, M.J. Hawes and D.V. Morgan, "Large-signal modeling of GaAs MESFET operation," *IEEE Trans. Electron Devices*, vol. ED-30, 1983, pp. 1817-1824.

[134] C.M. Snowden and D. Loret, "Two-dimensional hot-electron models for shot-gate-length GaAs MESFETs," *IEEE Trans. Electron Devices*, vol. ED-34, 1987, pp. 212-223.

[135] W. Shockley, "A unipolar 'field-effect' transistor", *Proc. IRE*, vol. 40, 1952, pp. 1365-1376.

[136] J.A. Turner and B.L.H. Wilson, "Implications of carrier velocity saturation in a gallium arsenide field-effect transistor," *Proc. Symp. Gallium Arsenide*, 1968, pp. 195-204.

[137] A.B. Grebene and S.K. Ghandhi, "General theory for pinched operation of the junction-gate FET," *Solid-State Electronics*, vol. 12, 1969, pp. 573-589.

[138] K. Lehovec and R. Zuleeg, "Voltage-current characteristics of GaAs J-FETs in the hot electron range", *Solid-State Electronics*, vol. 13, 1970, pp. 1415-1426.

[139] A. Pucel, A. Haus and H. Statz, "Signal and noise properties of gallium arsenide microwave field-effect transistors", in *Advances in Electronics and Electron Physics*, vol. 38. New York: Academic Press, 1975, pp. 195-265.

[140] T.H. Chen and M.S. Shur, "Analytic models for ion-implanted GaAs FET's," *IEEE Trans. Electron Devices*, vol. ED-32, 1985, pp. 18-28.

[141] T.H. Chen and M.S. Shur, "A capacitance model for GaAs MESFETs," *IEEE Trans. Electron Devices*, vol. ED-32, 1985, pp. 883-891.

[142] K. Yamaguchi and H. Kodera, "Drain conductance of junction gate FET's in the hot electron range", *IEEE Trans. Electron Devices*, vol. ED-23, 1976, pp. 545-553.

[143] A. Madjar and F.J. Rosenbaum, "A large-signal model for the GaAs MESFET", *IEEE Trans. Microwave Theory Tech.*, vol. MTT-29, 1981, pp. 781-788.

[144] M.A. Khatibzadeh and R.J. Trew, "A large-signal, analytic model for the GaAs MESFET", *IEEE Trans. Microwave Theory Tech.*, vol. 36, 1988, pp. 231-238.

[145] C.S. Chang and D.Y.S. Day, "Analytic theory for current-voltage characteristics and field distribution of GaAs MESFET's", *IEEE Trans. Electron Devices*, vol. 36, 1989, pp. 269-280.

[146] J.G. Ruch and G.S. Kino, "Measurement of the velocity-field characteristic of gallium arsenide", *Appl. Phys. Lett.*, vol. 10, 1967, pp. 40-42.

[147] P.A. Houston and A.G.R. Evans, "Electron drift velocity in n-GaAs at high electric fields", *Solid-State Electronics*, vol. 20, 1977, pp. 197-204.

[148] M.A. Khatibzadeh, "Large-signal modeling of gallium-arsenide field-effect transistors", Ph.D. dissertation, North Carolina State University, Raleigh, NC, 1987.

[149] H. Fukui, "Determination of the basic device parameters of a GaAs MESFET," *Bell Syst. Tech. J.*, vol. 58, 1979, pp. 771-797.

[150] W.R. Curtice, "GaAs MESFET modeling and nonlinear CAD," *IEEE Trans. Microwave Theory Tech.*, vol. 36, 1988, pp. 220-230.

[151] Measurement data provided by Plessey Research Caswell Ltd., Caswell, Towcester, Northamptonshire, England NN12 8EQ, 1990.

[152] J.W. Bandler, S.H. Chen and M.L. Renault, "KMOS-a fortran library for nonlinear optimization," Department of Electrical and Computer Engineering, McMaster University, Hamilton, Canada, Report SOS-87-1-R, 1987.

[153] J.W. Bandler, S.H. Chen, S. Daijavad and K. Madsen, "Efficient optimization with integrated gradient approximations," *IEEE Trans. Microwave Theory Tech.*, vol. 36, 1988, pp. 444-455.

[154] C.G. Broyden, "A class of methods for solving nonlinear simultaneous equations," *Mathematics of Computation*, vol. 19, 1965, pp. 577-593.

[155] M.J.D. Powell, "A Fortran subroutine for unconstrained minimization, requiring first derivatives of the objective functions," Atomic Energy Research Establishment, Harwell, Berkshire, England, Rep. AERE-R. 6469, 1970, pp. 20-27.

[156] J.W. Bandler, Q.J. Zhang and R.M. Biernacki, "A unified theory for frequency domain simulation and sensitivity analysis of linear and nonlinear circuits," *IEEE Trans. Microwave Theory Tech.*, vol. 36, 1988, pp. 1661-1669.

[157] J.W. Bandler, Q.J. Zhang and R.M. Biernacki, "Practical, high-speed gradient computation for harmonic balance simulators," *IEEE Int. Microwave Symp. Dig.* (Long Beach, CA), 1989, pp. 363-366.

[158] H.L. Abdel-Malek and J.W. Bandler, "Yield optimization for arbitrary statistical distributions: Part II-implementation," *IEEE Trans. Circuits and Syst.*, vol. CAS-27, 1980, pp. 253-262.

[159] P.H. Ladbrooke, *MMIC Design: GaAs FETs and HEMTs*. Norwood, MA: Artech House, 1989.

[160] J.W. Bandler, S. Ye, Q. Cai, R.M. Biernacki and S.H. Chen, "Predictable yield-driven circuit optimization," *IEEE Int. Microwave Symp. Dig.* (Albuquerque, NM), 1992.

[161] J.W. Bandler, S.H. Chen and R.M. Biernacki, "A new formulation for yield optimization," *IEEE Int. Microwave Symp. Dig.* (Albuquerque, NM), 1992.

[162] I.J. Bahl, "Transmission Lines and Lumped Elements", in *Microwave Solid State Circuit Design*, I.J. Bahl and P. Bhartia, Eds. New York: Wiley, 1988, Chapter 2.

[163] R.M. Biernacki and M.A. Styblinski, "Statistical circuit design with a dynamic constraint approximation scheme," *Proc. IEEE Int. Symp. Circuits Syst.* (San Jose, CA), 1986, pp. 976-979.

[164] J.W. Bandler, R.M. Biernacki, S.H. Chen, J. Song, S. Ye and Q.J. Zhang, "Gradient quadratic approximation scheme for yield-driven design," *IEEE Int. Microwave Symp. Dig.* (Boston, MA), 1991, pp. 1197-1200.

[165] C. Kermarrec and C. Rumelhard, "Microwave monolithic integrated circuits", in *GaAs MESFET Circuit Design*, R. Soares Ed. Boston: Artech House, 1988, Chapter 9.

[166] J.W. Bandler, W. Kellermann and K. Madsen, "A superlinearly convergent minimax algorithm for microwave circuit design", *IEEE Trans. Microwave Theory Tech.*, vol. MTT-33, 1985, pp. 1519-1530.

[167] D.M. Brookbanks, Plessey Research Caswell Ltd., Caswell, Towcester, Northamptonshire, England NN12 8EQ, Private Communication, 1990.

[168] P.H. Ladbrooke, GaAs Code Ltd., St. John's Innovation Center, Cowley, Cambridge CB4 4WS, U.K., Private Communication, July 15, 1991.

FIGURE CAPTIONS

Fig. 1. Active region of a MESFET.

Fig. 2. Electron drift velocity versus electric field: (——) typical v-E curve, (---) piecewise linear approximation and (-·-) quadratic approximation.

Fig. 3. Comparison of calculated and experimental v-E data for GaAs: (——) calculated from Equation (11), (○) experimental data from Ruch and Kino [146], and (□) experimental data from Houston and Evans [147].

Fig. 4. Equivalent circuit for the intrinsic model.

Fig. 5. Comparison of our approach with that of Khatibzadeh's on DC characteristics: (——) our results and (○) Khatibzadeh's results [148].

Fig. 6. Circuit topology for parameter extraction showing the intrinsic FET and its associated extrinsic elements.

Fig. 7. Comparison of measured (○) and calculated (——) S parameters at 3 bias points for parameter extraction. (a) gate bias 0V, (b) gate bias -0.84V and (c) gate bias -1.54V. Drain bias is 5V.

Fig. 8. Partition of a circuit for harmonic balance simulation.

Fig. 9. Flowchart for design optimization of nonlinear FET circuits using HB.

Fig. 10. Different levels of statistical modeling.

Fig. 11. Topology for the Ladbrooke GaAs MESFET small-signal model where $I_d=g_m V_g \exp(-j\omega\tau)$.

Fig. 12. Histograms of gate length L. (a) the Ladbrooke model. (b) the Khatibzadeh and Trew model.

Fig. 13. Histograms of doping density N_d. (a) the Ladbrooke model. (b) the Khatibzadeh and Trew model.

Fig. 14. Histograms of $|S_{21}|$ at V_{GS}=0V and V_{DS}=5V and at 11GHz from (a) measurements, (b) the Ladbrooke model, and (c) the Khatibzadeh and Trew model.

Fig. 15. Configuration of passive devices and their corresponding two port equivalent circuits [160]: (a) spiral inductor, (b) MIM capacitor and (c) planar resistor.

Fig. 16. Circuit diagram of an X-band amplifier [163].

Fig. 17. (a) Gain and (b) input VSWR versus frequency before (---) and after (——) nominal design optimization.

Fig. 18. Monte Carlo sweep of gain versus frequency (a) before and (b) after yield optimization.

Fig. 19. Monte Carlo sweep of input VSWR versus frequency (a) before and (b) after yield optimization.

Fig. 20. Schematic diagram of Datapipe using inter-program pipe communication (IPPC), where user's programs may be user's in-house programs such as special purpose simulators, control programs, etc.

Fig. 21. Comparison of DC characteristics simulated by the 2D field-based simulator (o) and calculated by the Plessey model (——).

TABLE I

MESFET INTRINSIC PARAMETERS

Parameter	Notation	Unit
Gate Length	L	μm
Gate Width	W	μm
Channel Thickness	a	μm
Doping Density	N_d	$1/m^3$
Critical Electric Field	E_c	V/m
Saturation Velocity	v_s	m/s
Relative Permittivity	ε_r	—
Built-in Potential	V_{bi}	V
Low-Field Mobility	μ_0	m^2/Vs
High-Field Diffusion Coefficient	D_0	m^2/s

TABLE II

EXTRACTED PARAMETERS FOR
THE KHATIBZADEH AND TREW MODEL

Parameter	Before Optimization	After Optimization	Plessey Data [151]
$L(\mu m)$	0.551	0.571	0.551
$W(\mu m)$	300.0	301.6	300.0
$N_d(1/m^3)$	2.235×10^{23}	2.093×10^{23}	2.235×10^{23}
$a(\mu m)$	0.200	0.167	—
$V_{bi}(V)$	0.700	0.672	—
$R_g(\Omega)$	2.200	2.302	—
$R_d(\Omega)$	3.500	3.524	—
$R_s(\Omega)$	2.500	2.704	—
L_g(nH)	0.050	0.028	—
L_d(nH)	0.050	0.010	—
L_s(nH)	0.080	0.036	—
C_{ge}(pF)	0.100	0.123	—
C_{de}(pF)	0.050	0.055	—
$G_{ds}(1/\Omega)$	0.003	0.003	—

Other parameters are fixed as

$E_1 = 1.173\times10^5$V/m
$v_s = 1.023\times10^5$m/s
$D_0 = 0.001m^2/s$
$\varepsilon_r = 12.9$
$C_x = 10$pF

TABLE III

STATISTICAL PARAMETERS FOR THE LADBROOKE AND THE KHATIBZADEH AND TREW MODELS

Ladbrooke Model			Khatibzadeh and Trew Model		
Para.	Mean	Dev.(%)	Para.	Mean	Dev.(%)
$L(\mu m)$	0.5559	2.93	$L(\mu m)$	0.5496	1.29
$a(\mu m)$	0.1059	3.64	$a(\mu m)$	0.1310	1.38
$N_d(1/m^3)$	3.140×10^{23}	1.71	$N_d(1/m^3)$	2.219×10^{23}	0.98
$v_s(m/s)$	7.608×10^{4}	3.48	$W(\mu m)$	295.24	1.48
$V_{B0}(V)$	0.6785	4.94	$V_{bi}(V)$	0.699	1.62
a_0	1.031	7.03	$\mu_0(m^2/Vs)$	0.3932	1.16
$r_{01}(\Omega/V^2)$	1.090×10^{-2}	0.44	$E_c(V/m)$	3.255×10^{5}	1.38
$r_{02}(\Omega)$	628.2	6.86	$R_d(\Omega)$	4.001	0.06
$r_{03}(V)$	13.99	0.44	$R_s(\Omega)$	1.697	0.17
$R_g(\Omega)$	3.392	4.99	$R_g(\Omega)$	3.500	0.12
$L_{g0}(nH)$	2.414×10^{-2}	20.7	$L_g(nH)$	2.94×10^{-2}	0.13
$L_d(nH)$	6.117×10^{-2}	18.6	$L_d(nH)$	8.0×10^{-3}	0.06
$L_s(nH)$	2.209×10^{-2}	10.6	$L_s(nH)$	3.9×10^{-2}	0.85
$G_{ds}(1/\Omega)$	2.163×10^{-3}	2.72	$G_{ds}(1/\Omega)$	3.6×10^{-3}	0.61
$C_{ds}(pF)$	5.429×10^{-2}	2.71	$C_{de}(pF)$	5.27×10^{-2}	0.78
			$C_{ge}(pF)$	0.1504	1.89

TABLE IV

MEAN VALUES AND STANDARD DEVIATIONS OF MEASURED AND SIMULATED S PARAMETERS AT 11GHZ

	Measured S parameters [151]		Simulated S parameters			
			Ladbrooke Model		Khatibzadeh and Trew Model	
	Mean	Dev.(%)	Mean	Dev.(%)	Mean	Dev.(%)
$\lvert S_{11} \rvert$	0.773	.988	.7856	.764	.8085	0.32
$\angle S_{11}$	-114.3	1.36	-119.3	1.10	-116.2	0.69
$\lvert S_{21} \rvert$	1.919	.802	1.679	1.34	1.834	1.22
$\angle S_{21}$	93.35	.856	94.06	.835	91.69	0.33
$\lvert S_{12} \rvert$	.0765	3.77	.07542	3.68	.0785	2.07
$\angle S_{12}$	34.00	2.51	31.98	2.33	31.61	0.94
$\lvert S_{22} \rvert$	0.5957	1.48	.5838	1.54	.5446	1.11
$\angle S_{22}$	-38.69	2.10	-36.86	1.42	-40.64	0.98

TABLE V

VARIABLES FOR NOMINAL DESIGN

Design Variable	Before Optimization	After Optimization	Design Variable	Before Optimization	After Optimization
$S_{C1}(\mu m^2)$	353.1	326.8	n_{L4}	3.68	3.63
$S_{C2}(\mu m^2)$	2014.4	2022.4	n_{L5}	2.13	2.17
$S_{C3}(\mu m^2)$	212.3	218.2	n_{L6}	2.61	2.58
$S_{C4}(\mu m^2)$	354.2	352.2	n_{L7}	2.42	2.62
n_{L1}	3.06	2.78	n_{L8}	2.45	2.43
n_{L2}	3.56	3.66	n_{L9}	2.88	2.78
n_{L3}	2.84	2.96	n_{L10}	3.09	3.01

S_{Ci} is the area of the metal plate of MIM capacitor C_i.
n_{Li} is the number of turns of the spiral inductor L_i.

TABLE VI

ASSUMED DISTRIBUTIONS FOR STATISTICAL VARIABLES

Variable	Mean	Dev.(%)	Variable	Mean	Dev.(%)
$N_d(1/m^3)$	1.0×10^{23}	7.0	$d(\mu m)$	0.1	4.0
$L(\mu m)$	1.0	3.5	$S_{C1}(\mu m^2)$	326.8	3.5
$a(\mu m)$	0.3	3.5	$S_{C2}(\mu m^2)$	2022.4	3.5
$W(\mu m)$	300	2.0	$S_{C3}(\mu m^2)$	218.2	3.5
$W_L(\mu m)$	20	3.0	$S_{C4}(\mu m^2)$	352.2	3.5
$S_L(\mu m)$	10	3.0			

The doping density N_d, gate length L, channel thickness a and gate width W of the three MESFETs have the same distribution. The conductor width W_L and spacing S_L of the 10 spiral inductors L_1, L_2, ..., L_{10} have the same distribution. d is the thickness of the dielectric film for all MIM capacitors. S_{Ci} is the area of the metal plate of MIM capacitor C_i.

TABLE VII

ASSUMED PARAMETER CORRELATIONS FOR THE THREE MESFETS

	a_{F1}	L_{F1}	W_{F1}	N_{dF1}	a_{F2}	L_{F2}	W_{F2}	N_{dF2}	a_{F3}	L_{F3}	W_{F3}	N_{dF3}
a_{F1}	1.00	0.00	0.00	-0.25	0.80	0.00	0.00	-0.20	0.78	0.00	0.00	-0.10
L_{F1}	0.00	1.00	0.00	-0.10	0.00	0.80	0.00	-0.05	0.00	0.78	0.00	-0.05
W_{F1}	0.00	0.00	1.00	0.00	0.00	0.00	0.80	0.00	0.00	0.00	0.78	0.00
N_{dF1}	-0.25	-0.10	0.00	1.00	-0.20	-0.05	0.00	0.80	-0.15	-0.05	0.00	0.78
a_{F2}	0.80	0.00	0.00	-0.20	1.00	0.00	0.00	-0.25	0.80	0.00	0.00	-0.20
L_{F2}	0.00	0.80	0.00	-0.05	0.00	1.00	0.00	-0.10	0.00	0.80	0.00	-0.10
W_{F2}	0.00	0.00	0.80	0.00	0.00	0.00	1.00	0.00	0.00	0.00	0.80	0.00
N_{dF2}	-0.20	-0.05	0.00	0.80	-0.25	-0.10	0.00	1.00	-0.20	-0.05	0.00	0.80
a_{F3}	0.78	0.00	0.00	-0.15	0.80	0.00	0.00	-0.20	1.00	0.00	0.00	-0.25
L_{F3}	0.00	0.78	0.00	-0.05	0.00	0.80	0.00	-0.05	0.00	1.00	0.00	-0.10
W_{F3}	0.00	0.00	0.78	0.00	0.00	0.00	0.80	0.00	0.00	0.00	1.00	0.00
N_{dF3}	-0.10	-0.05	0.00	0.78	-0.20	-0.10	0.00	0.80	-0.25	-0.10	0.00	1.00

The subscripts $F1$, $F2$ and $F3$ are used to differentiate the parameters of three different FETs.

TABLE VIII

DESIGN VARIABLES FOR YIELD OPTIMIZATION

Design Variable	Before Optimization	After Optimization	Design Variable	Before Optimization	After Optimization
$a(\mu m)$	0.3	0.31	n_{L2}	3.66	3.66
$L(\mu m)$	1.0	0.99	n_{L3}	2.96	3.03
$W(\mu m)$	300	308	n_{L4}	3.63	3.65
$N_d(1/m^3)$	1.0×10^{23}	1.03×10^{23}	n_{L5}	2.17	2.23
$S_{C1}(\mu m^2)$	326.8	322.7	n_{L6}	2.58	2.51
$S_{C2}(\mu m^2)$	2022.4	2006.3	n_{L7}	2.62	2.62
$S_{C3}(\mu m^2)$	218.2	222.9	n_{L8}	2.43	2.44
$S_{C4}(\mu m^2)$	352.2	356.7	n_{L9}	2.78	2.78
n_{L1}	2.78	2.74	n_{L10}	3.01	3.09

TABLE IX

PARAMETERS FOR THE 0.5μm GaAs MESFET

Source Length	0.15μm
Source-Gate Gap	0.50μm
Gate Length	0.50μm
Drain-Gate Gap	0.60μm
Drain Length	0.15μm
Gate Width	300μm
Channel Thickness	0.15μm
Buffer Layer Thickness	0.20μm
Substrate Thickness	0.05μm
Schottky Barrier Height	0.80V
Temperature	350°K
Doping of Active Layer	$1.5\times10^{23}/m^3$
Doping at Contacts	$3.7\times10^{23}/m^3$
Substrate Impurity Level	$1.0\times10^{10}/m^3$

TABLE X

DOPING PROFILE FOR THE 0.5μm GaAs MESFET

Grid No.	Doping($1/m^3$)	Grid No.	Doping($1/m^3$)
0	1.5000×10^{23}	17	1.7705×10^{22}
1	1.5000×10^{23}	18	7.7109×10^{21}
2	1.5000×10^{23}	19	3.1290×10^{21}
3	1.5000×10^{23}	20	1.2247×10^{21}
4	1.5000×10^{23}	21	4.7939×10^{20}
5	1.5000×10^{23}	22	1.9453×10^{20}
6	1.5000×10^{23}	23	8.4721×10^{19}
7	1.5000×10^{23}	24	4.0886×10^{19}
8	1.5000×10^{23}	25	2.2485×10^{19}
9	1.5000×10^{23}	26	1.4419×10^{19}
10	1.5000×10^{23}	27	1.0967×10^{19}
11	1.5000×10^{23}	28	1.0000×10^{19}
12	1.5000×10^{23}	29	1.0000×10^{19}
13	1.3676×10^{23}	30	1.0000×10^{19}
14	1.0402×10^{23}	31	1.0000×10^{19}
15	6.6710×10^{22}	32	1.0000×10^{19}
16	3.6687×10^{22}		

TABLE XI

PARAMETERS FOR THE PLESSEY MODEL

Parameter	Before Optimization	After Optimization
I_{dss}(mA)	60	52.49
V_t(V)	-4.0	-4.10
b(V)	1.5×10^{-3}	2.23×10^{-6}
$\lambda(1/\Omega)$	0.01	0.011
$\alpha(1/V)$	14.5	3.316
$G_{dst}(1/\Omega)$	3.0×10^{-3}	2.47×10^{-3}
$\beta(1/V)$	16.5	20.0

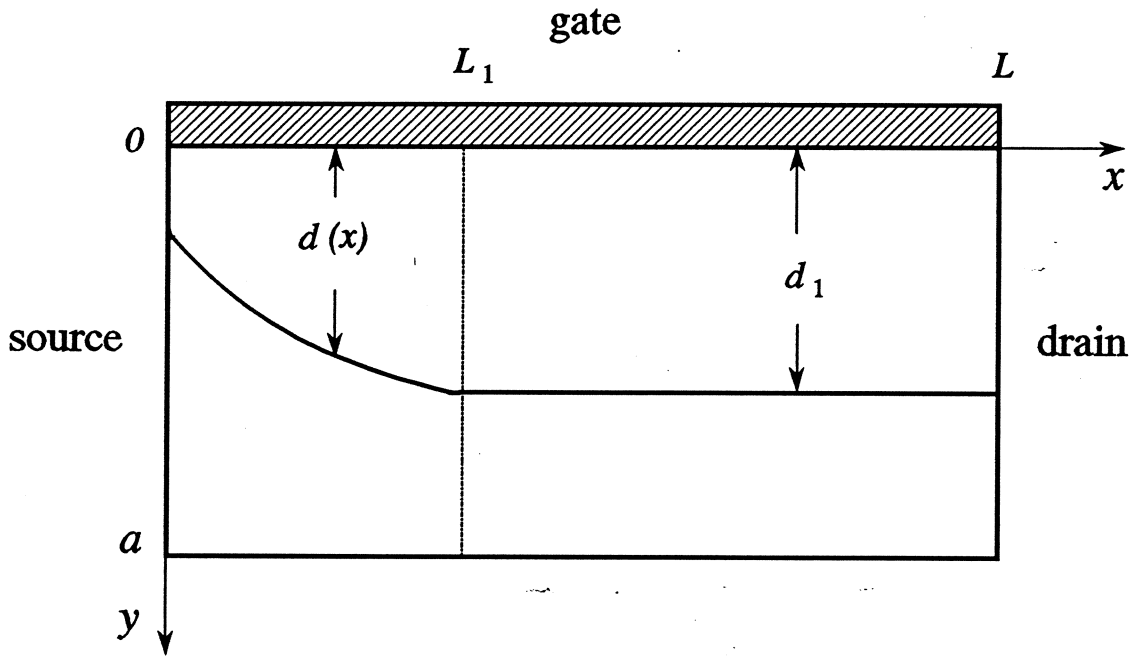

Fig. 1

Authors: John W. Bandler *et al.*

Title: Physics-Oriented Statistical Modeling, Simulation and Optimization

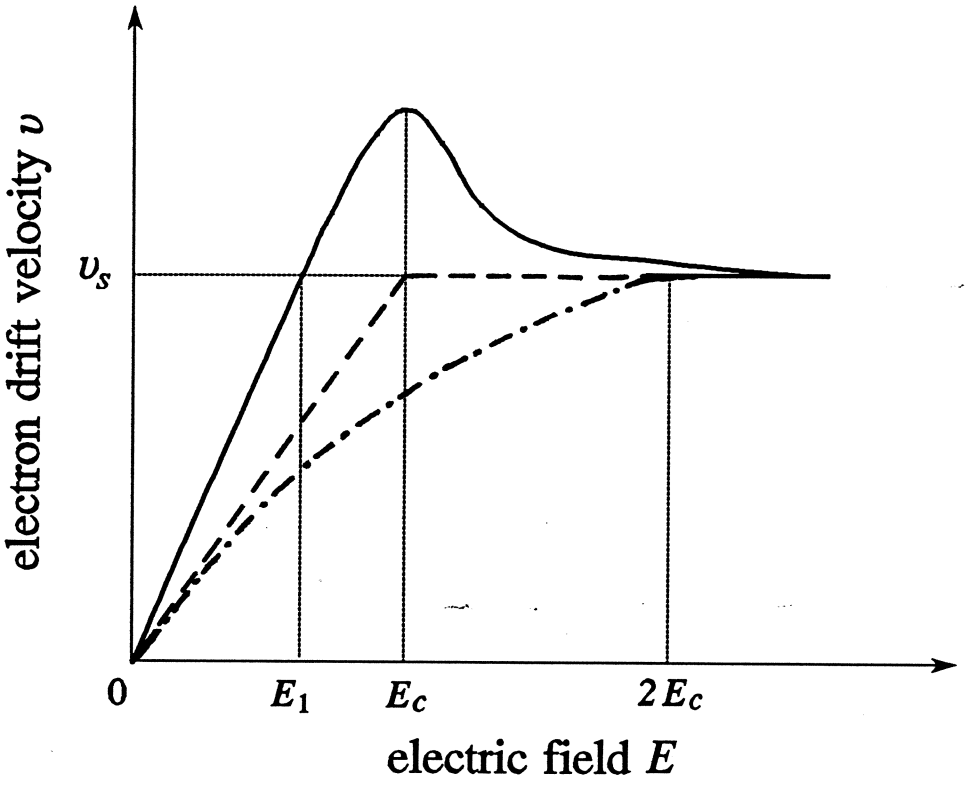

Fig. 2

Authors: John W. Bandler *et al.*

Title: Physics-Oriented Statistical Modeling, Simulation and Optimization

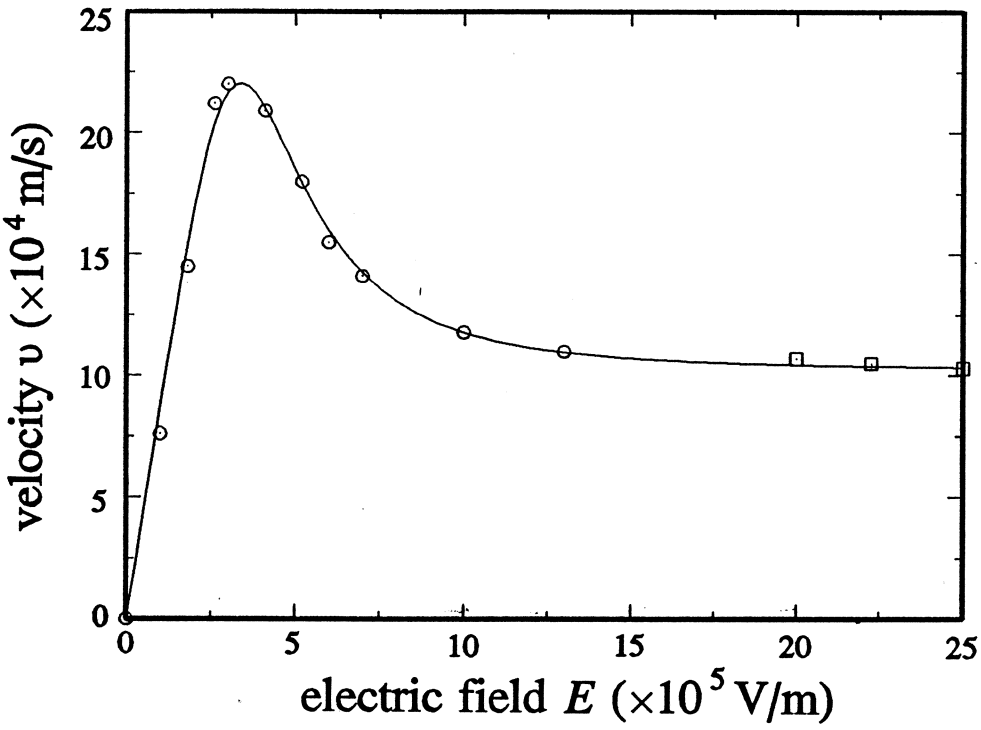

Fig. 3

Authors: John W. Bandler *et al.*

Title: Physics-Oriented Statistical Modeling, Simulation and Optimization

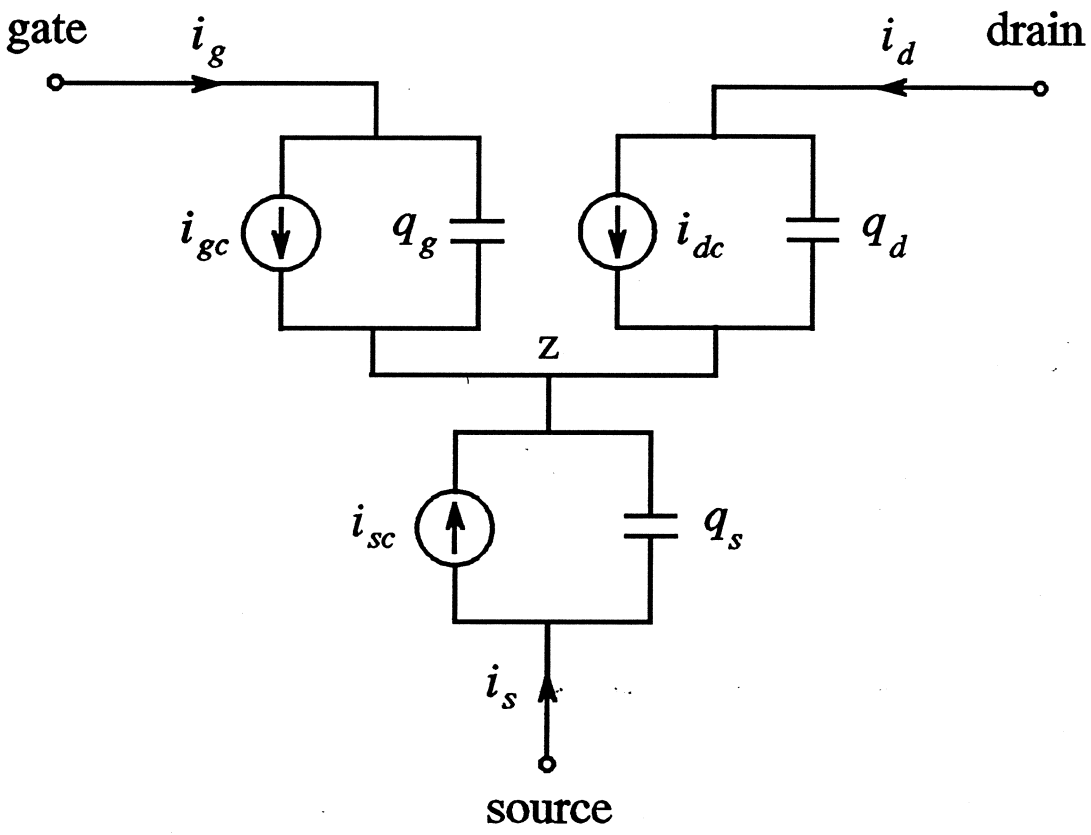

Fig. 4

Authors: John W. Bandler *et al.*

Title: Physics-Oriented Statistical Modeling, Simulation and Optimization

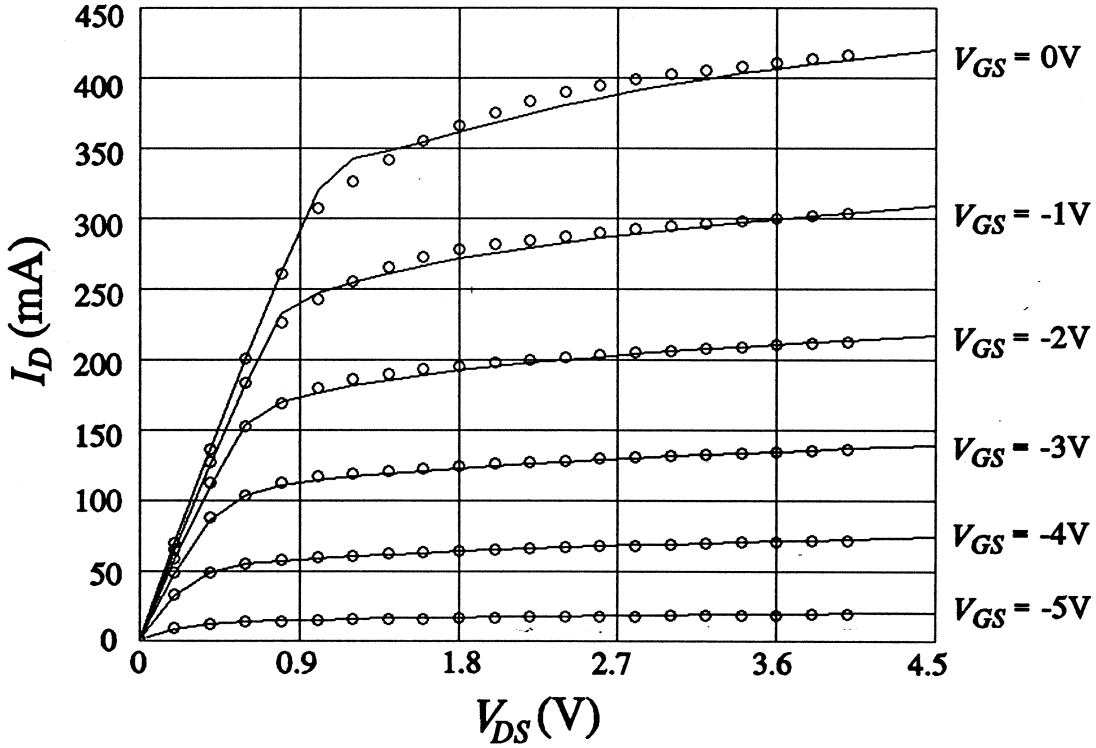

Fig. 5

Authors: John W. Bandler *et al.*

Title: Physics-Oriented Statistical Modeling, Simulation and Optimization

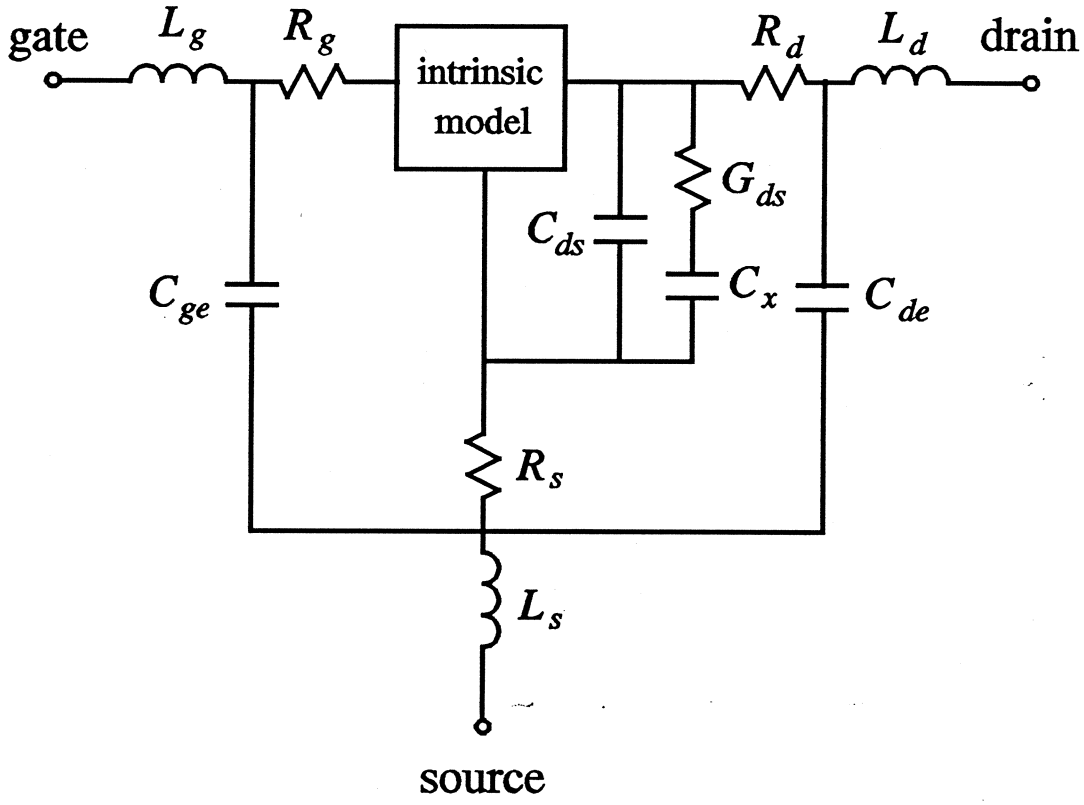

Fig. 6

Authors: John W. Bandler *et al.*

Title: Physics-Oriented Statistical Modeling, Simulation and Optimization

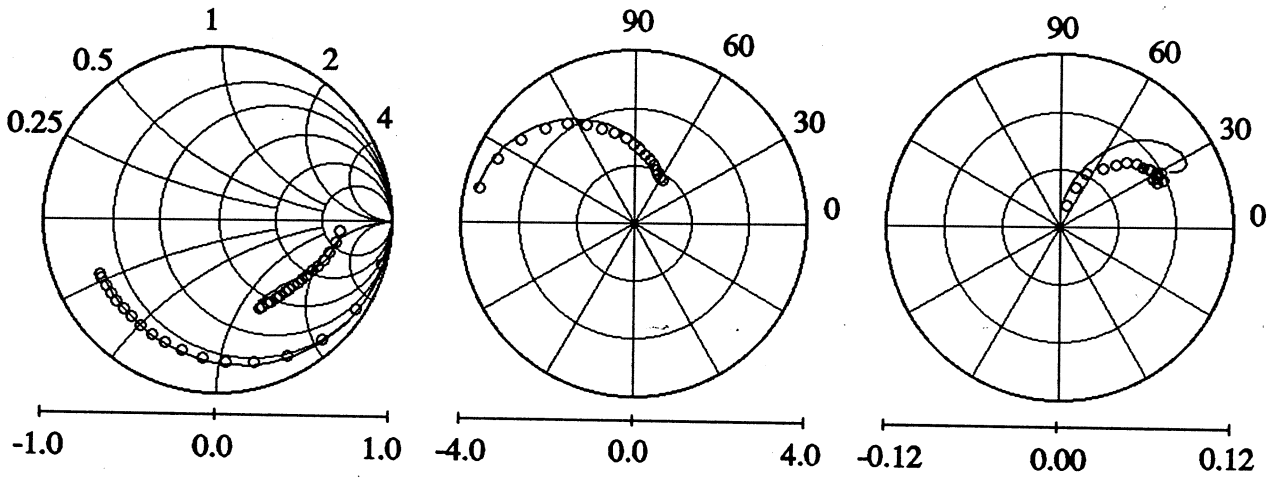

Fig. 7 (a)

Authors: John W. Bandler *et al.*

Title: Physics-Oriented Statistical Modeling, Simulation and Optimization

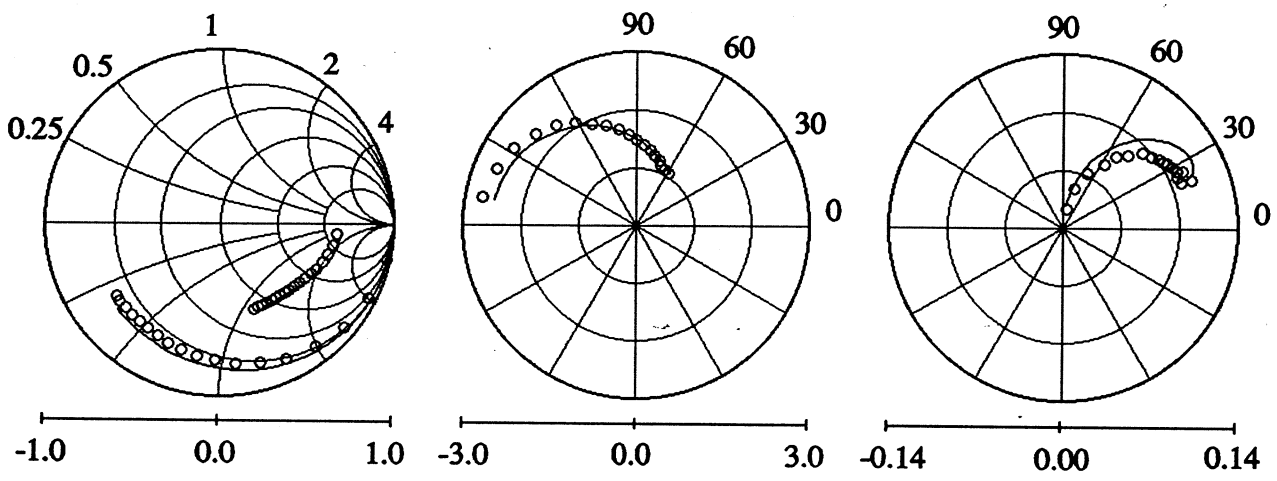

Fig. 7 (b)

Authors: John W. Bandler *et al.*

Title: Physics-Oriented Statistical Modeling, Simulation and Optimization

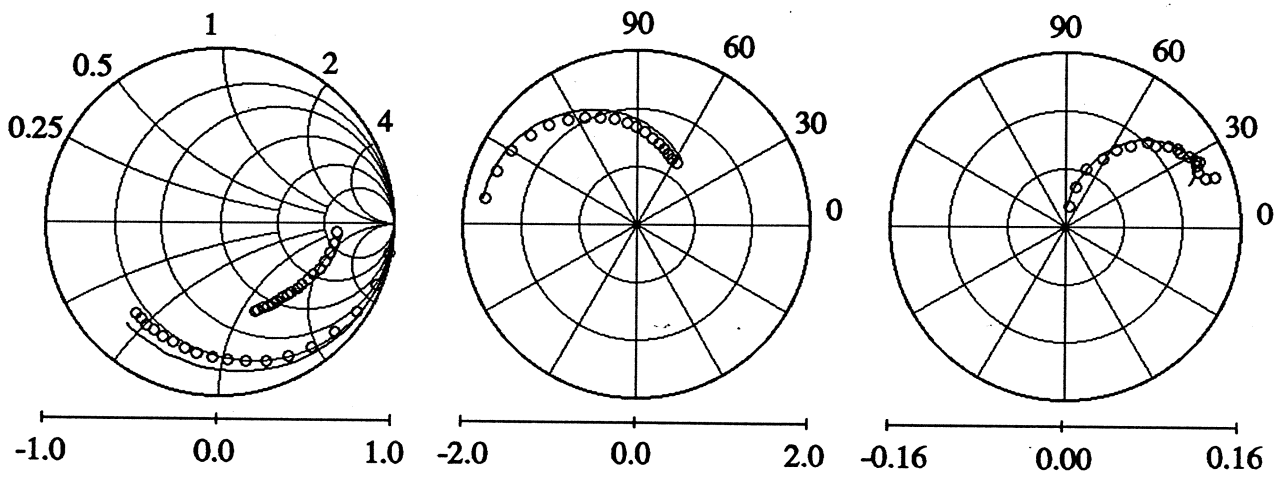

Fig. 7 (c)

Authors: John W. Bandler *et al.*

Title: Physics-Oriented Statistical Modeling, Simulation and Optimization

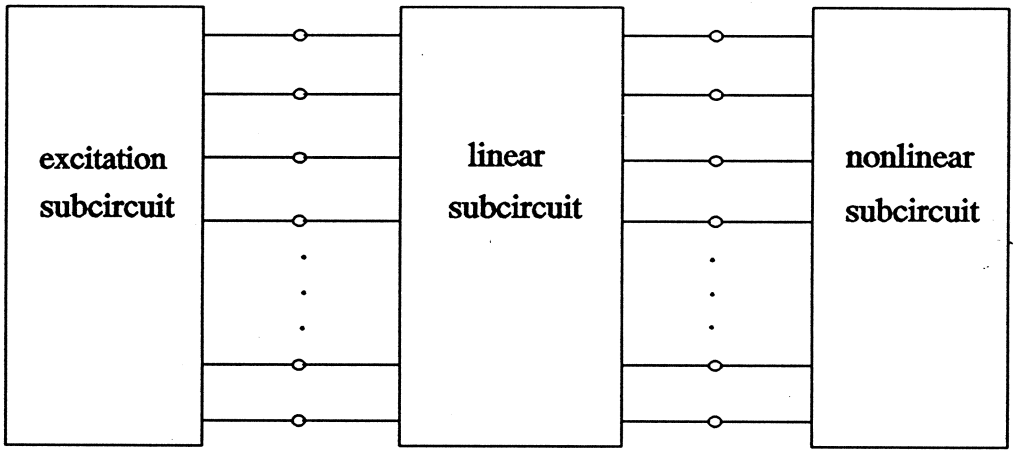

Fig. 8

Authors: John W. Bandler *et al.*

Title: Physics-Oriented Statistical Modeling, Simulation and Optimization

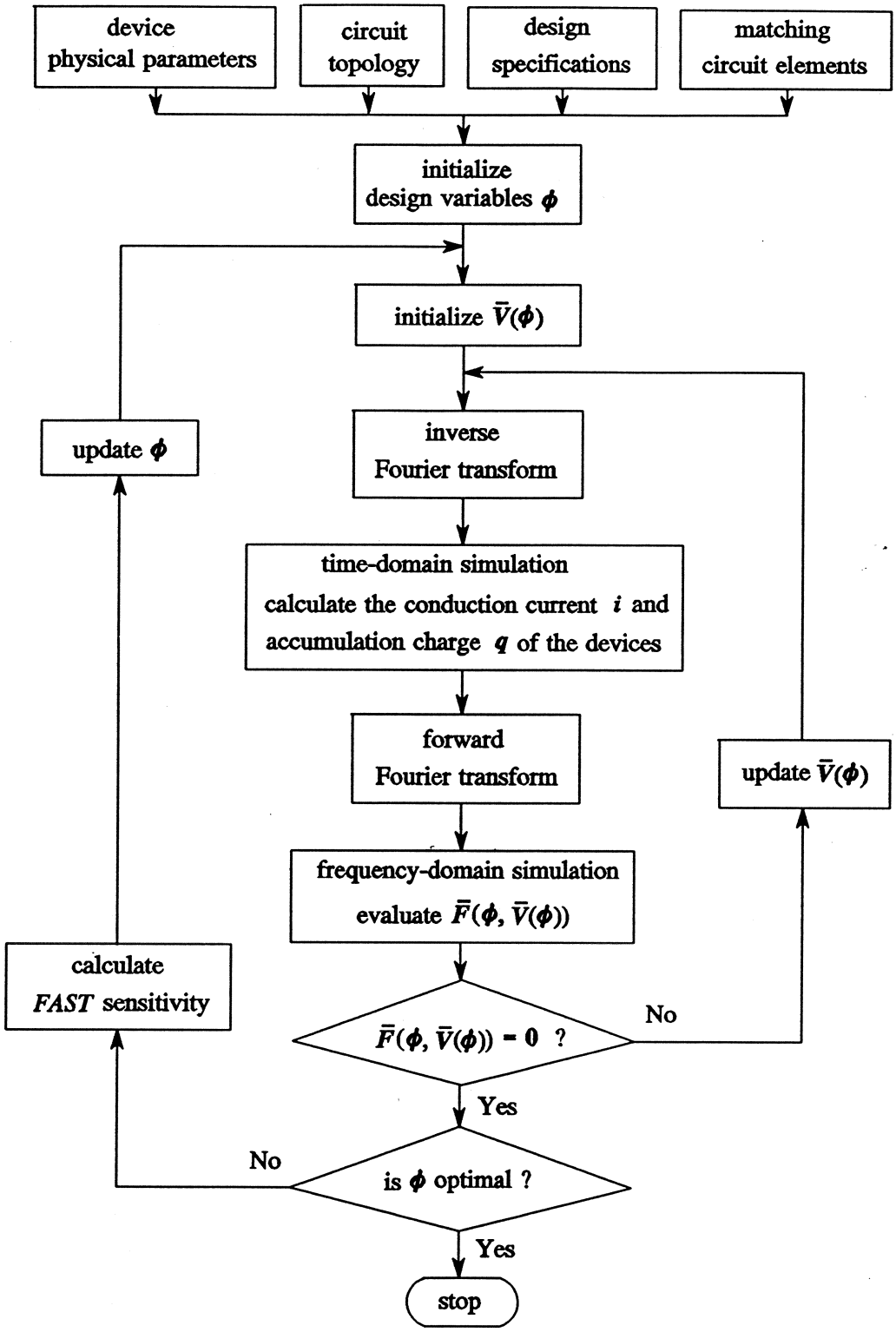

Fig. 9

Authors: John W. Bandler *et al.*

Title: Physics-Oriented Statistical Modeling, Simulation and Optimization

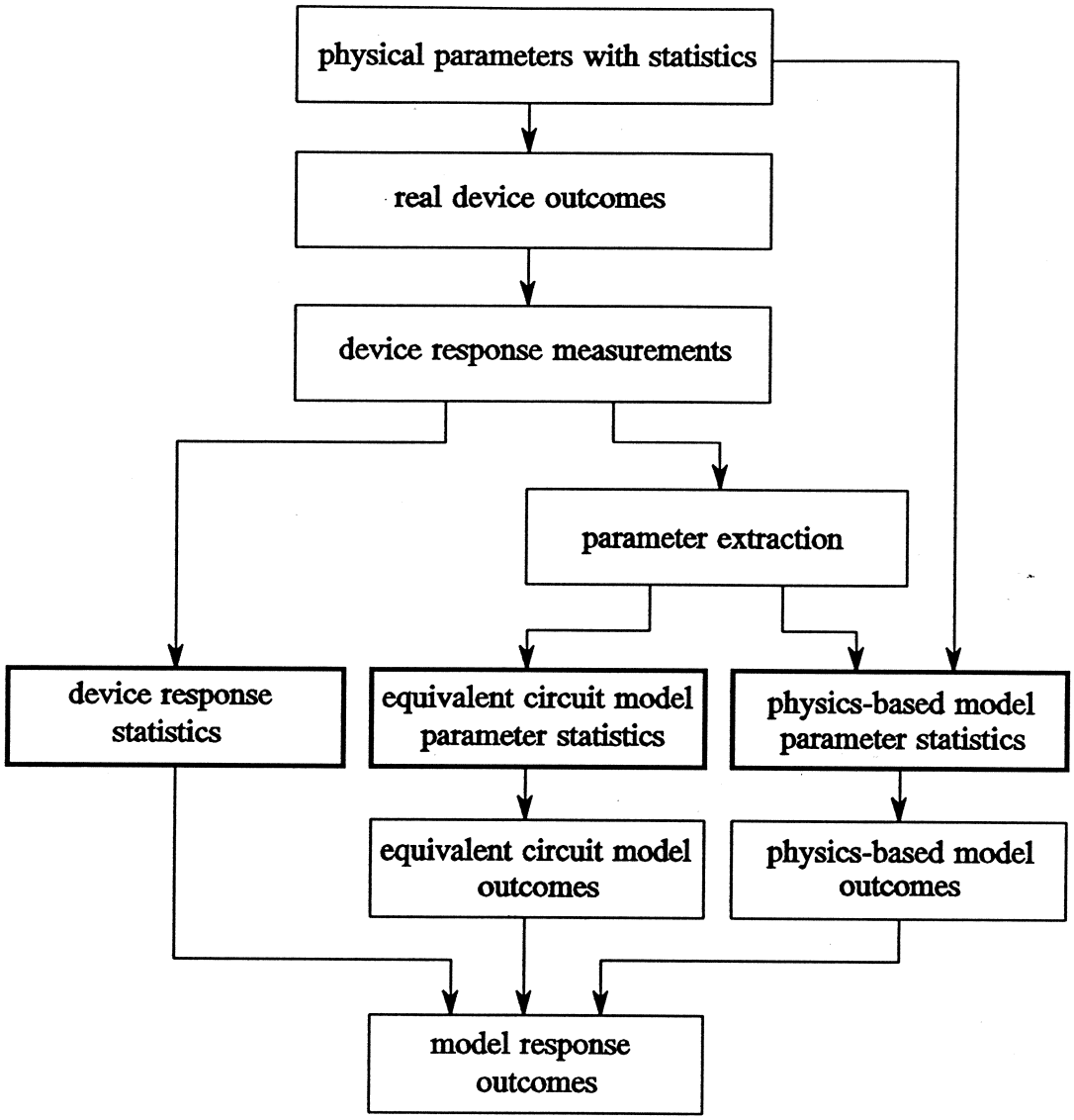

Fig. 10

Authors: John W. Bandler *et al.*

Title: Physics-Oriented Statistical Modeling, Simulation and Optimization

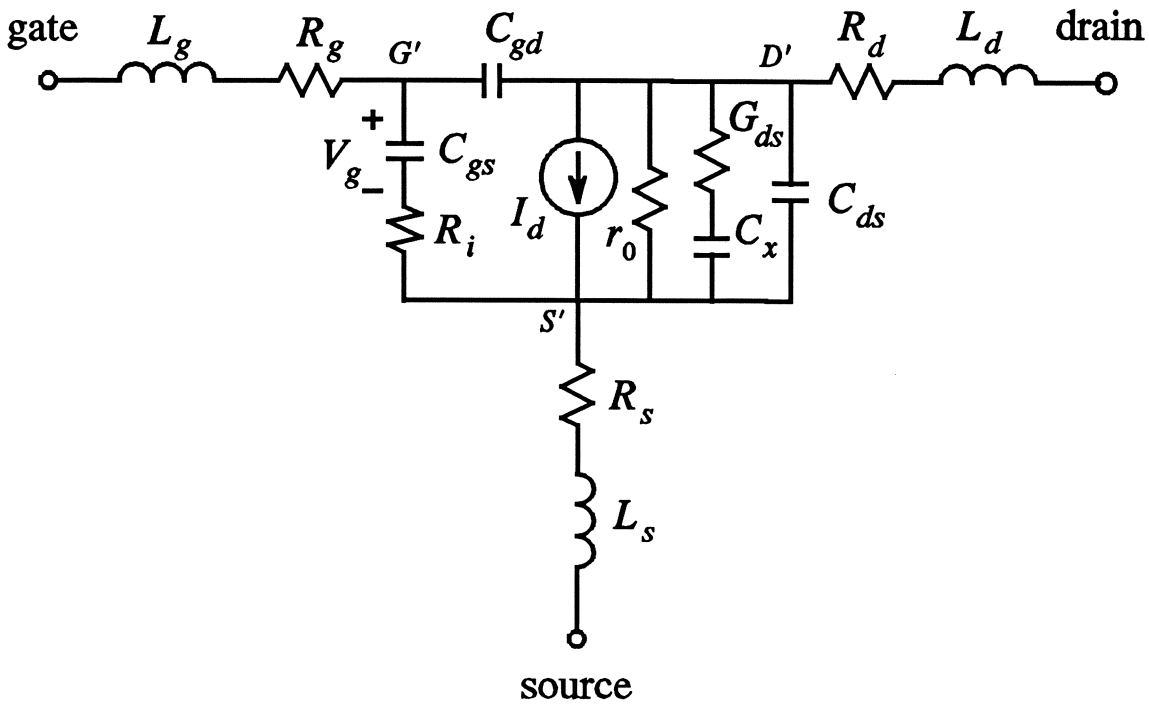

Fig. 11

Authors: John W. Bandler *et al.*

Title: Physics-Oriented Statistical Modeling, Simulation and Optimization

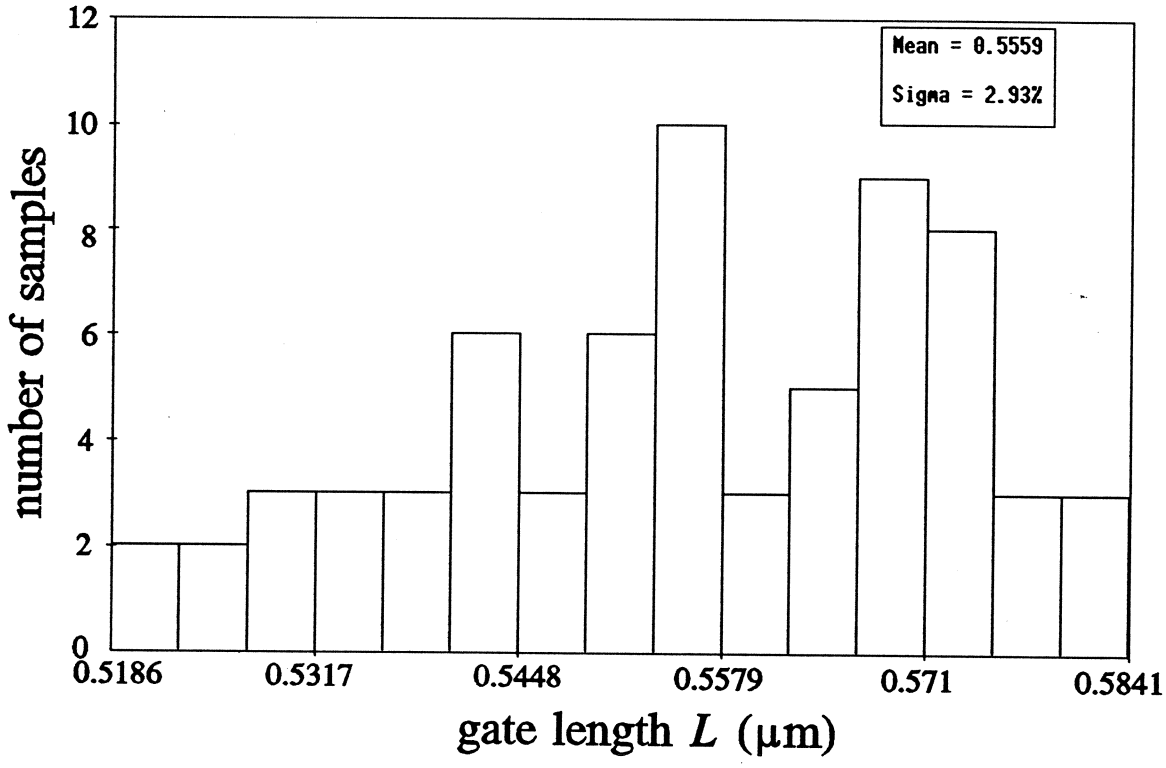

Fig. 12 (a)

Authors: John W. Bandler *et al.*

Title: Physics-Oriented Statistical Modeling, Simulation and Optimization

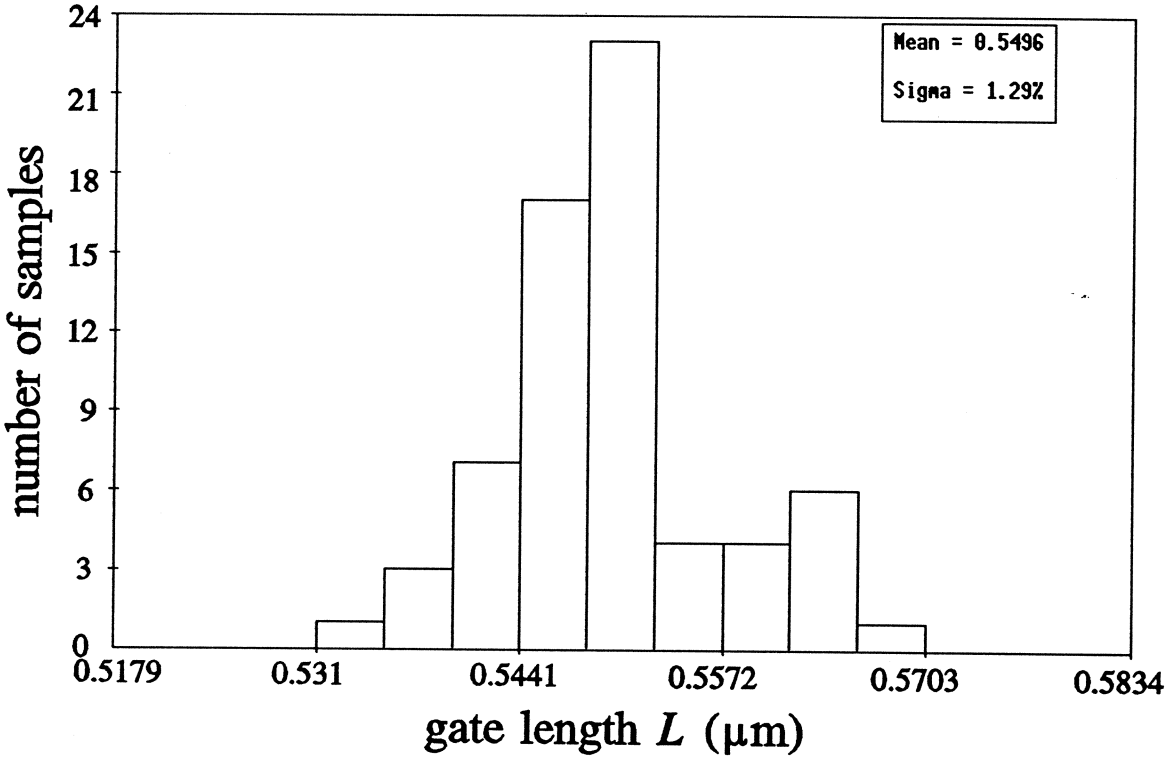

Fig. 12 (b)

Authors: John W. Bandler *et al.*

Title: Physics-Oriented Statistical Modeling, Simulation and Optimization

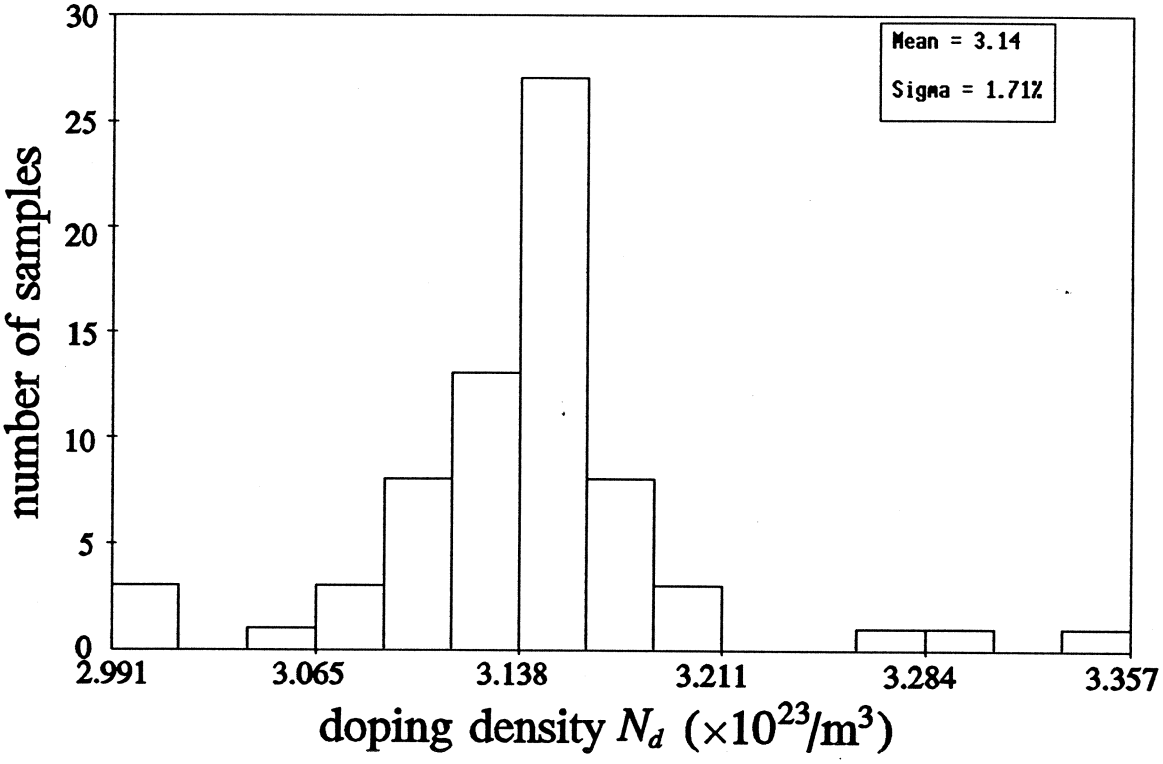

Fig. 13 (a)

Authors: John W. Bandler *et al.*

Title: Physics-Oriented Statistical Modeling, Simulation and Optimization

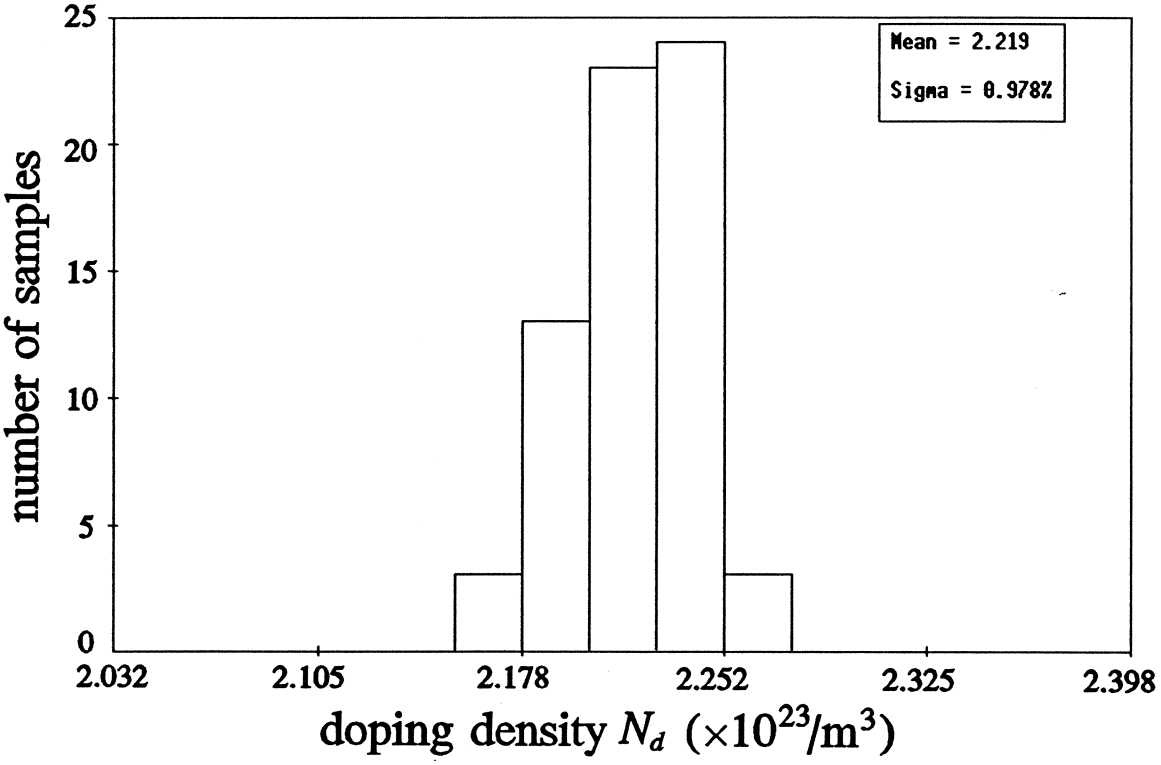

Fig. 13 (b)

Authors: John W. Bandler *et al.*

Title: Physics-Oriented Statistical Modeling, Simulation and Optimization

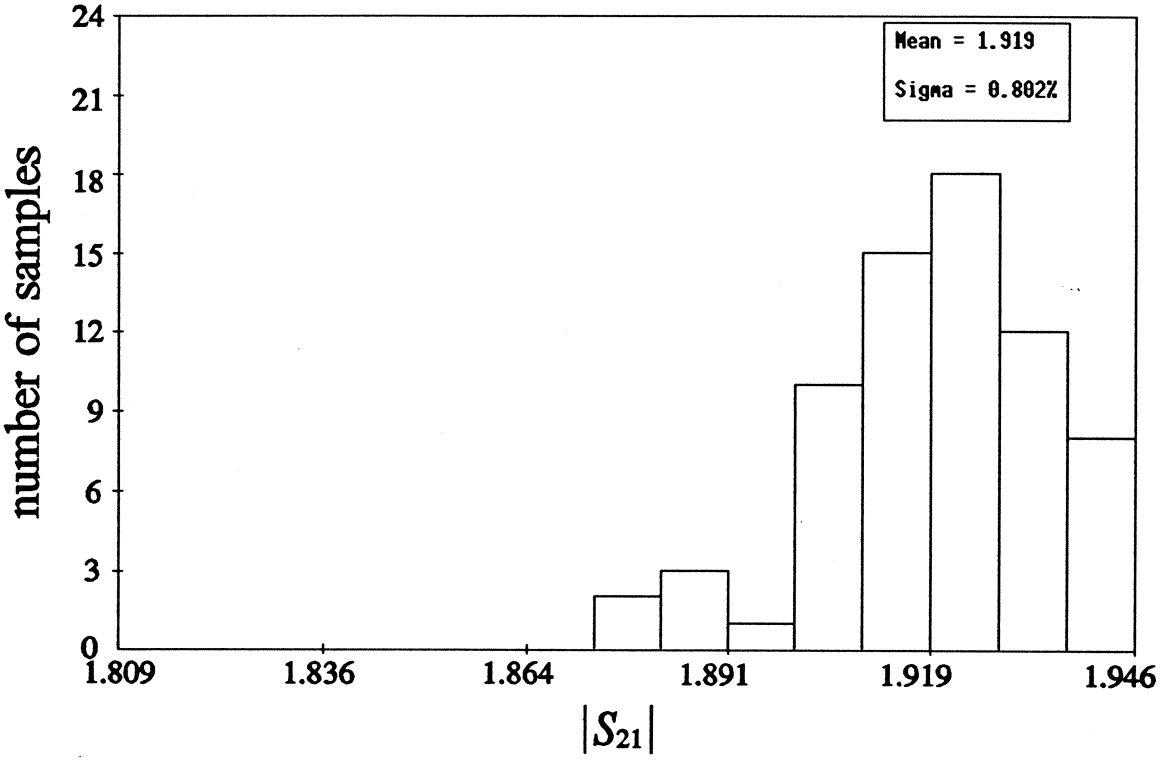

Fig. 14 (a)

Authors: John W. Bandler *et al.*

Title: Physics-Oriented Statistical Modeling, Simulation and Optimization

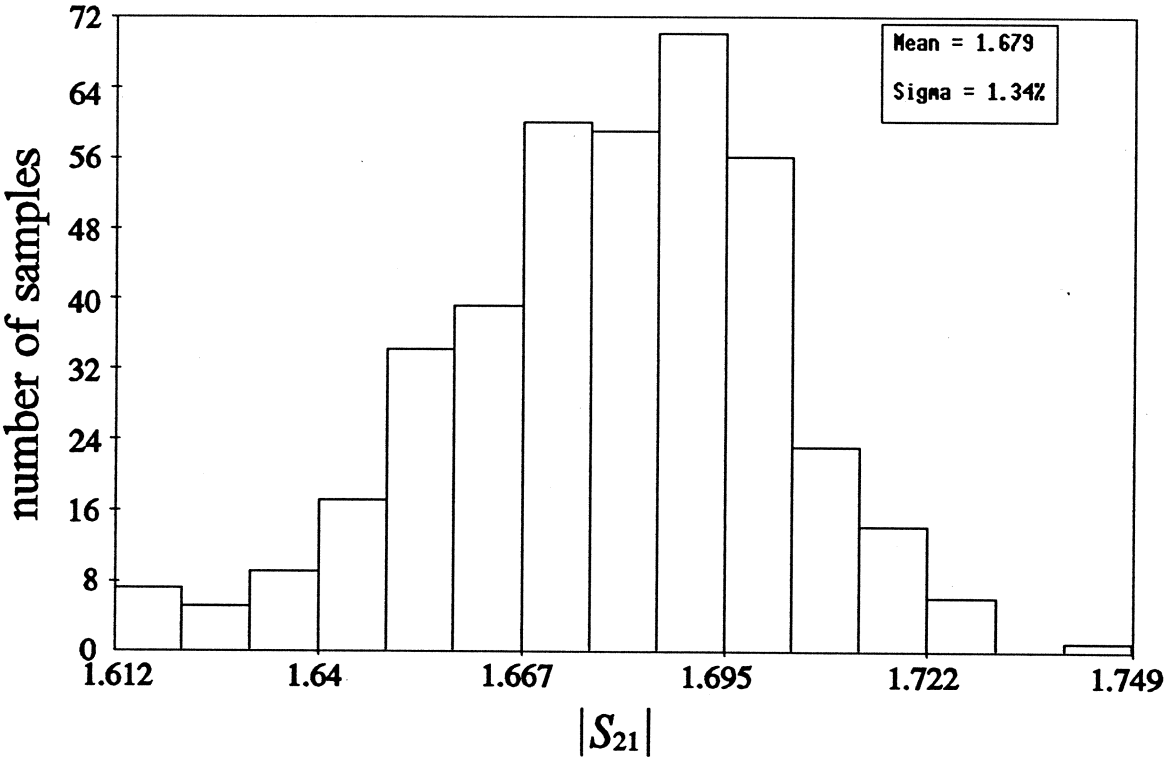

Fig. 14 (b)

Authors: John W. Bandler *et al.*

Title: Physics-Oriented Statistical Modeling, Simulation and Optimization

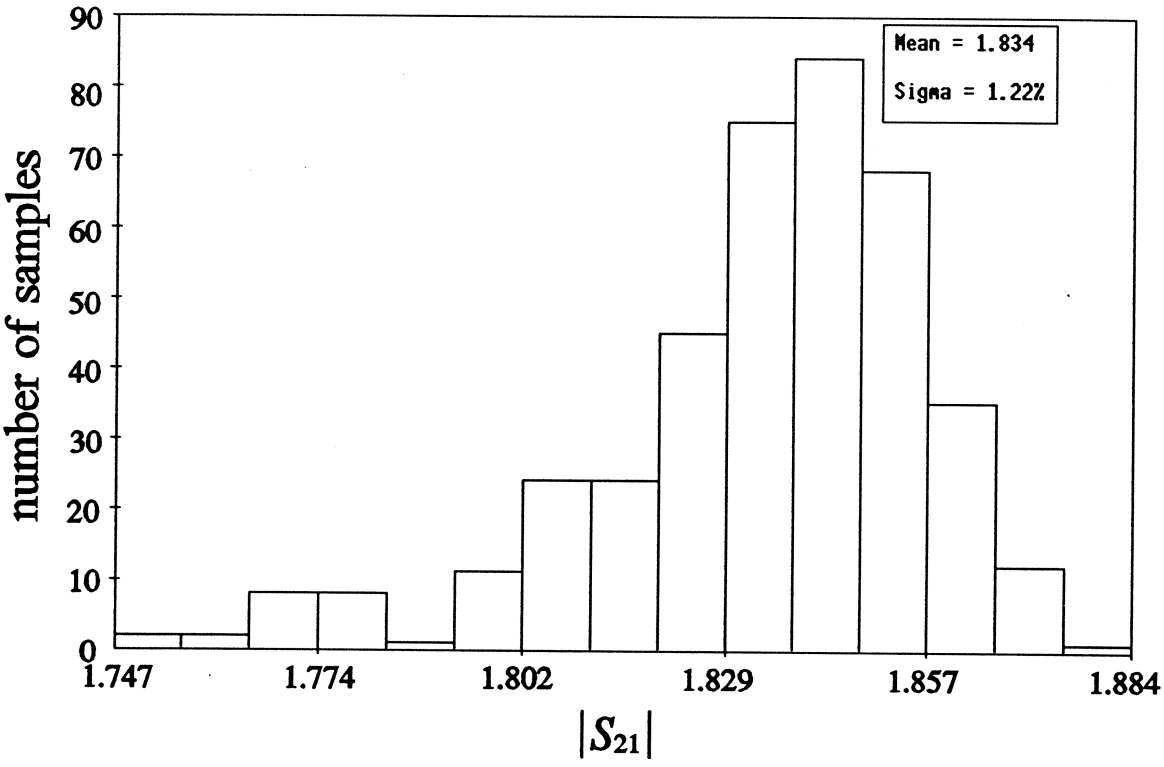

Fig. 14 (c)

Authors: John W. Bandler *et al.*

Title: Physics-Oriented Statistical Modeling, Simulation and Optimization

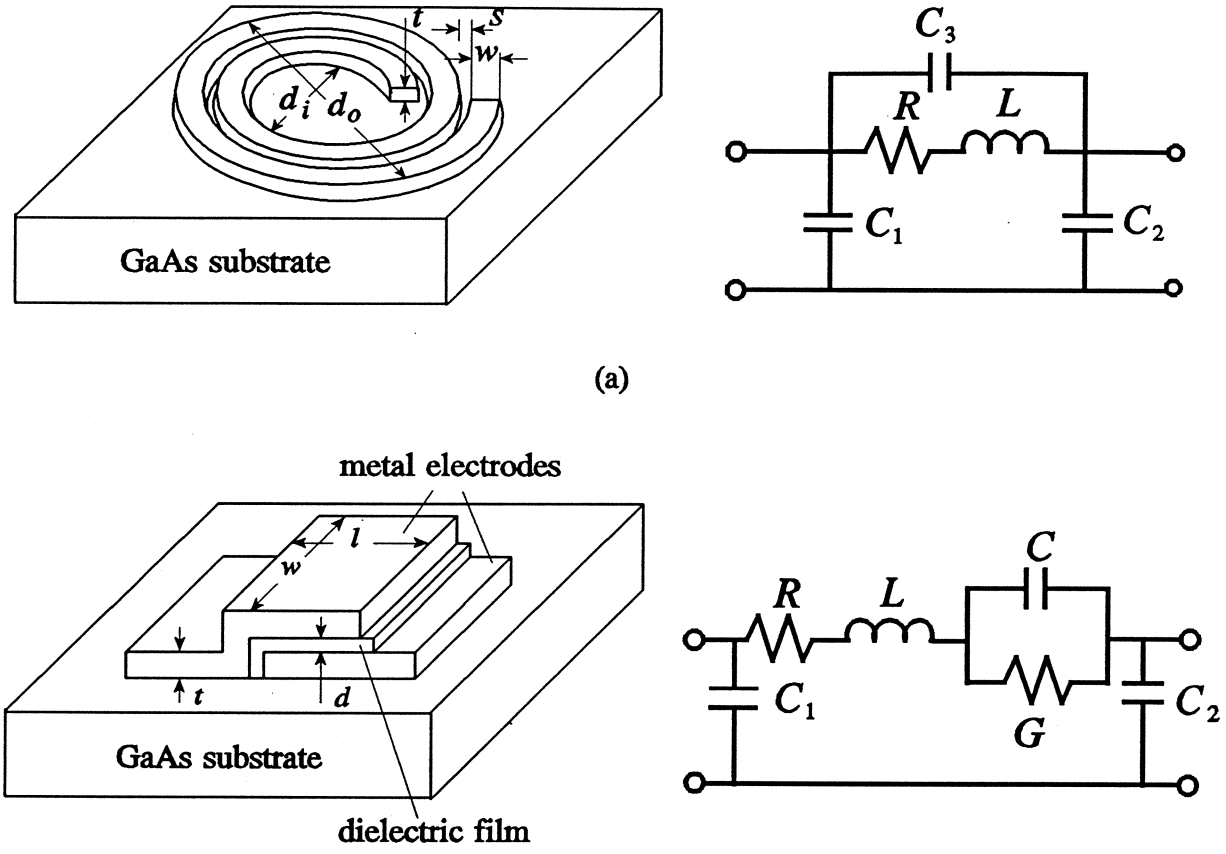

Fig. 15

Authors: John W. Bandler *et al.*

Title: Physics-Oriented Statistical Modeling, Simulation and Optimization

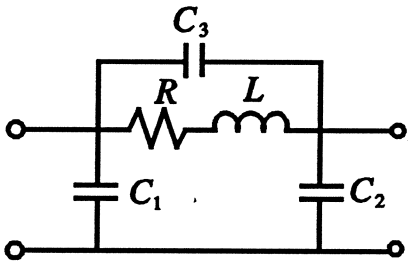

Fig. 15 (a) --- right

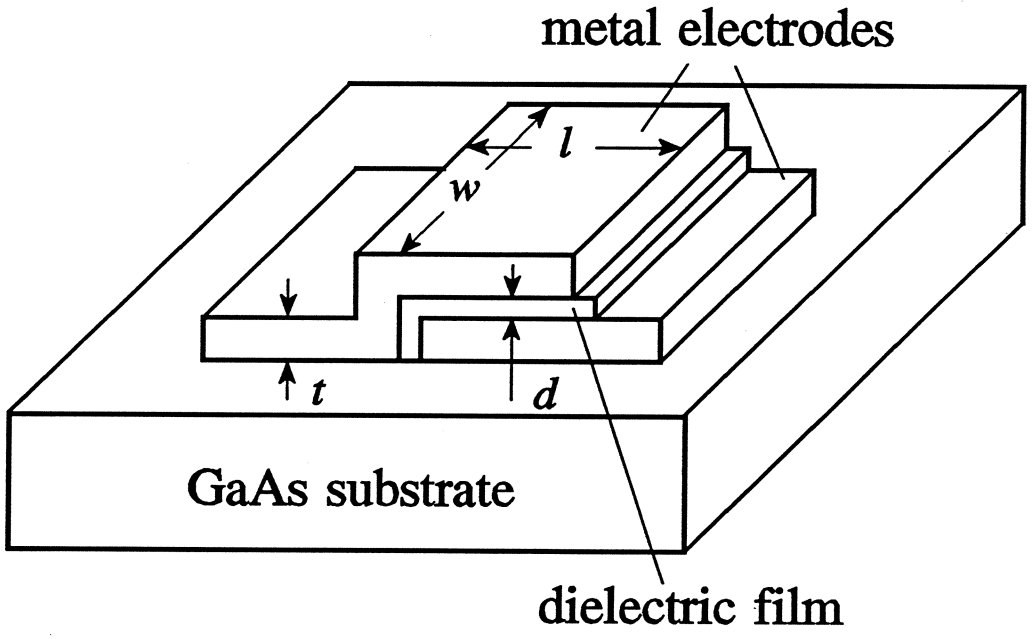

Fig. 15 (b) --- left

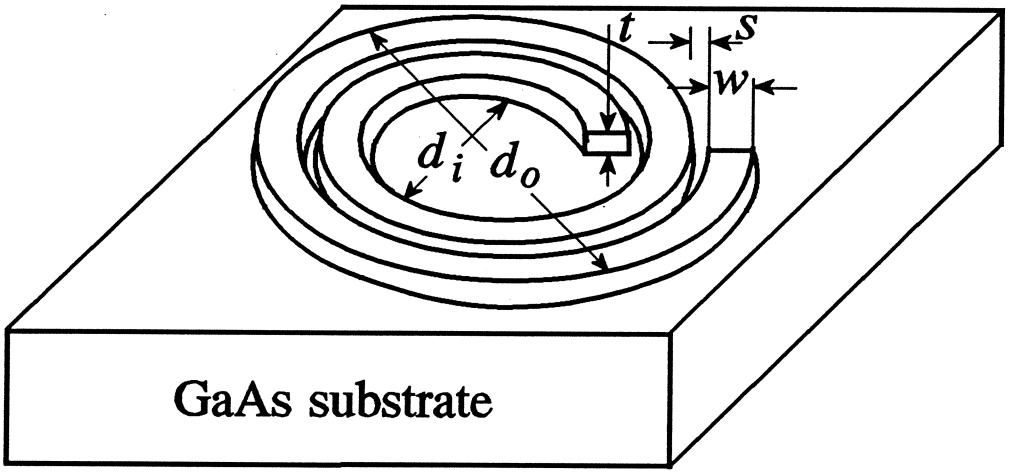

Fig. 15 (a) --- left

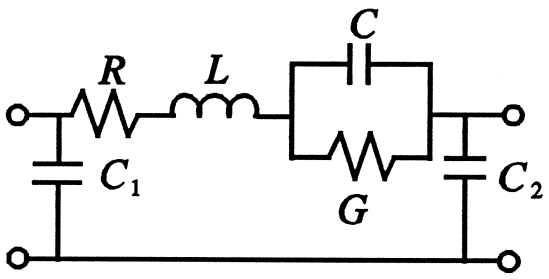

Fig. 15 (b) --- right

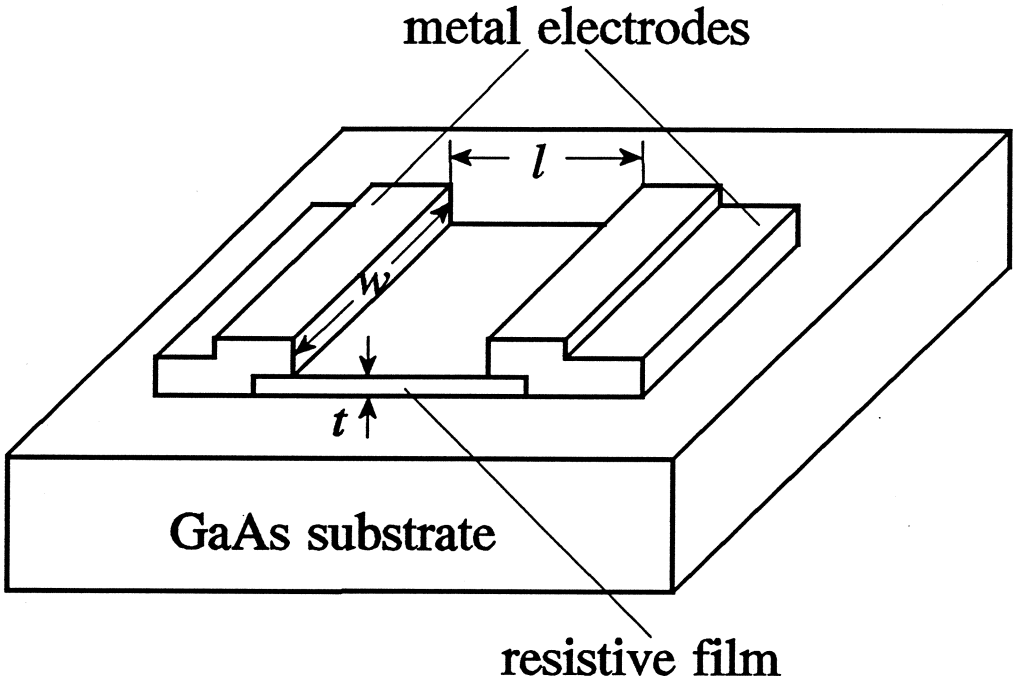

Fig. 15 (c) --- left

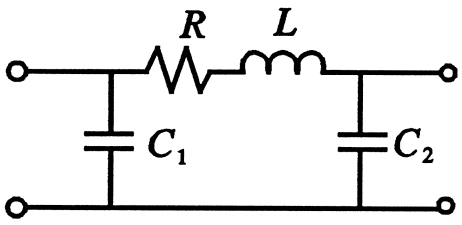

Fig. 15 (c) --- right

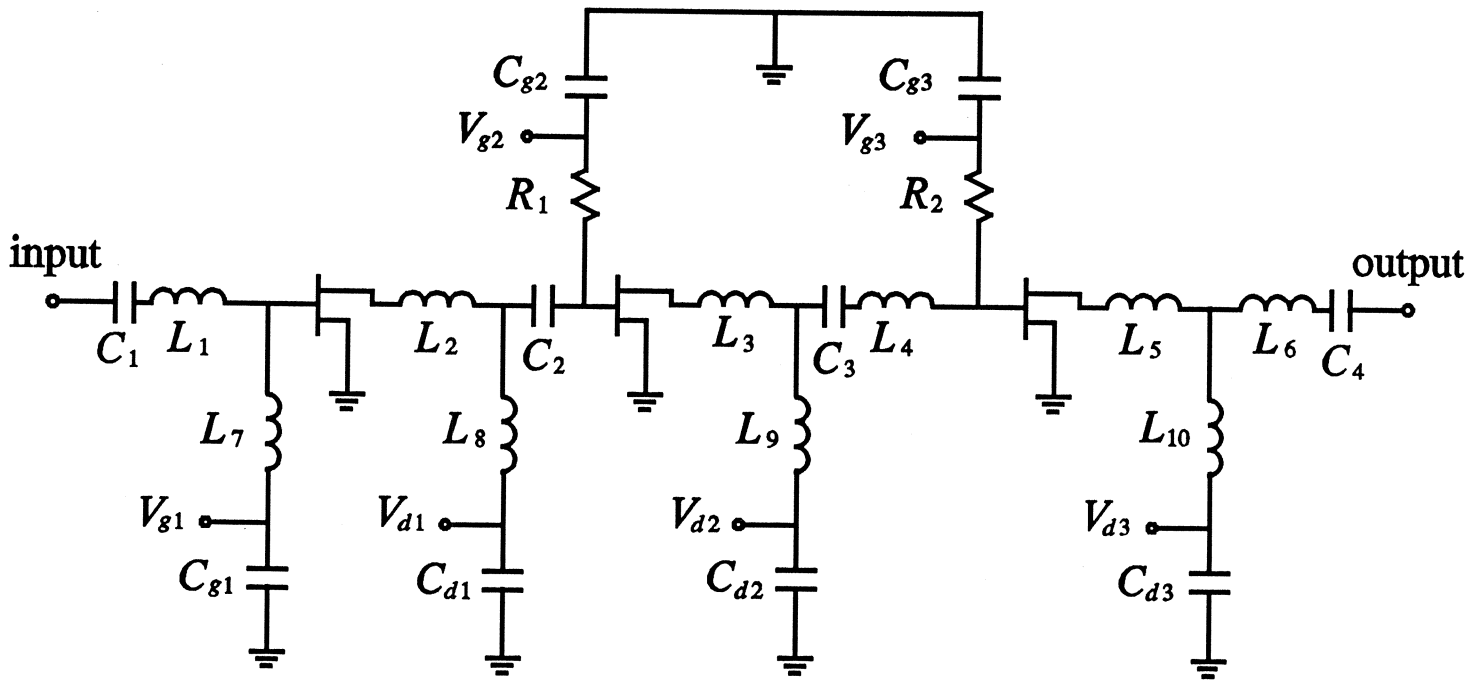

Fig. 16

Authors: John W. Bandler *et al.*

Title: Physics-Oriented Statistical Modeling, Simulation and Optimization

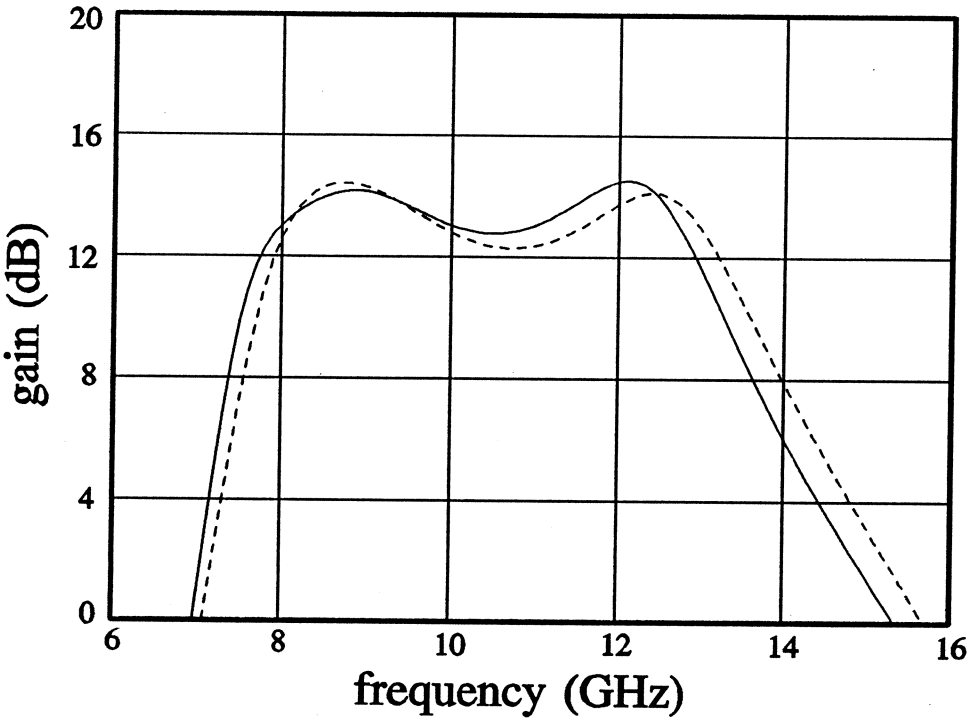

Fig. 17 (a)

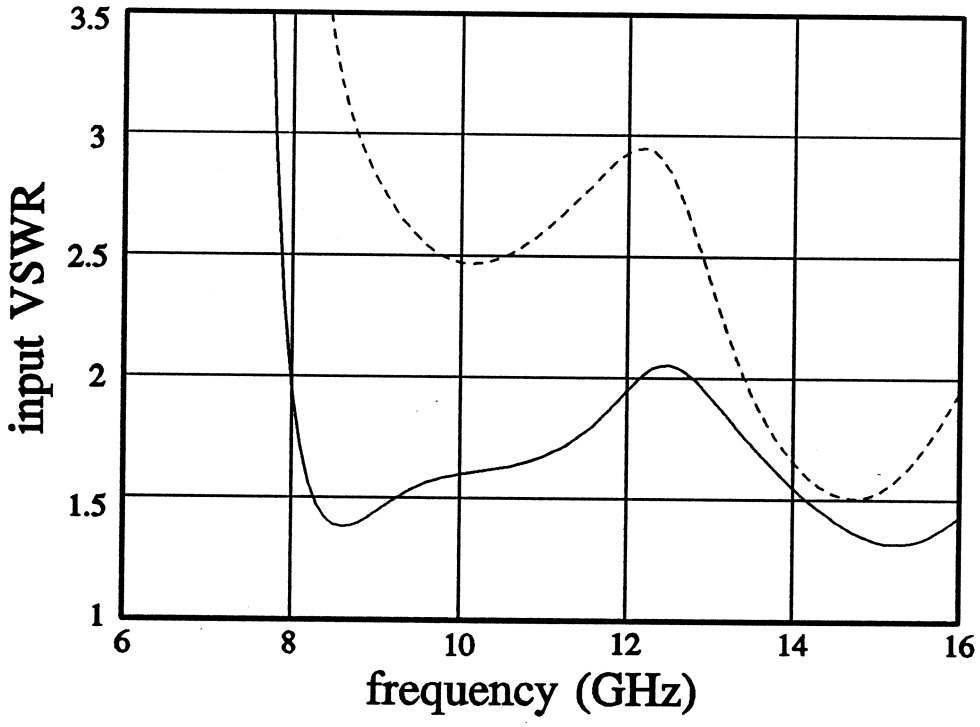

Fig. 17 (b)

Authors: John W. Bandler *et al.*

Title: Physics-Oriented Statistical Modeling, Simulation and Optimization

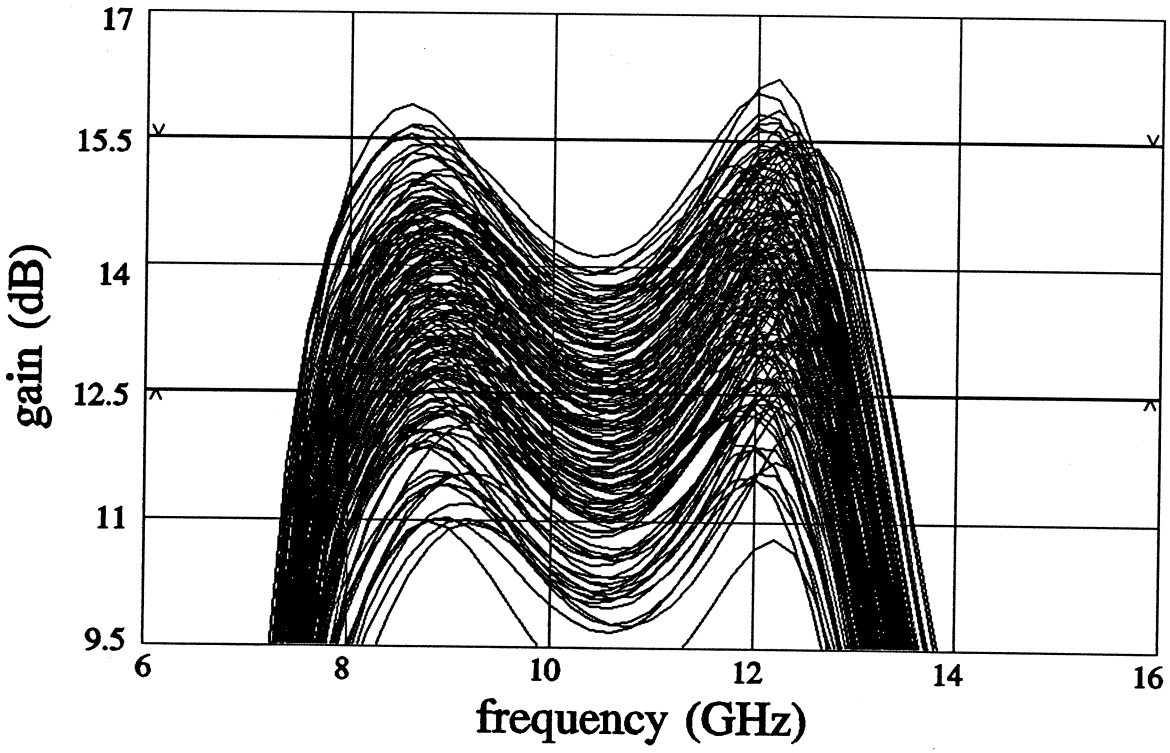

Fig. 18 (a)

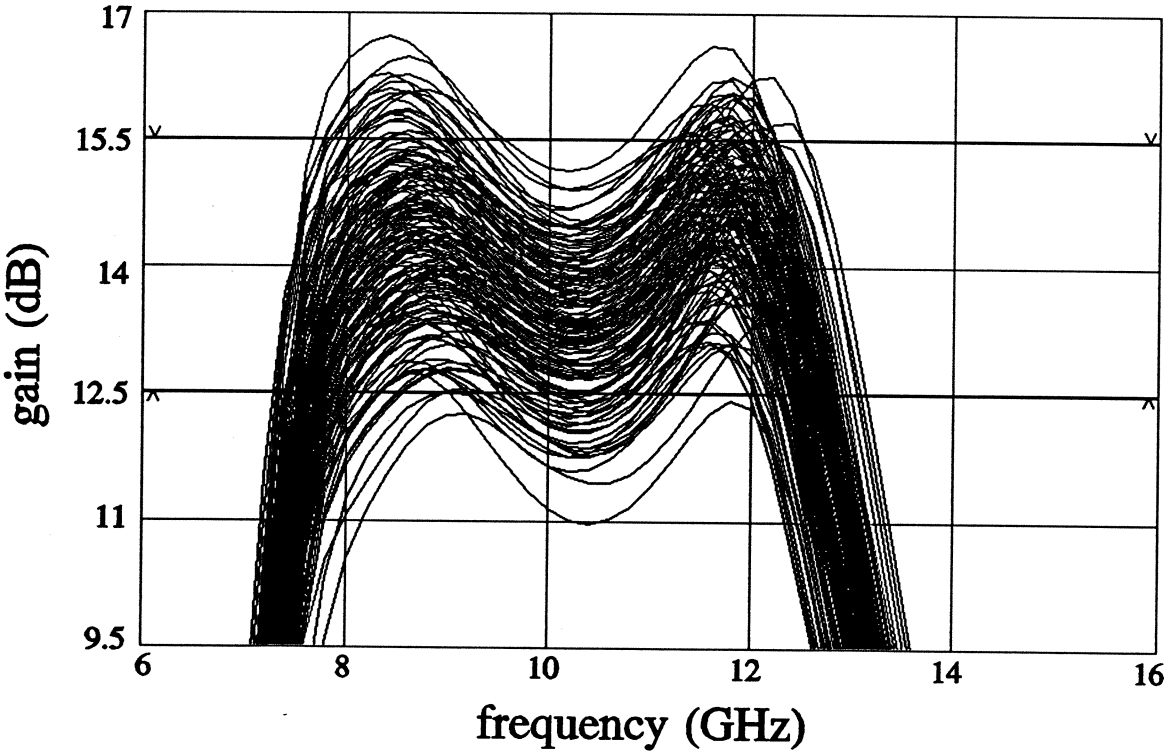

Fig. 18 (b)

Authors: John W. Bandler *et al.*

Title: Physics-Oriented Statistical Modeling, Simulation and Optimization

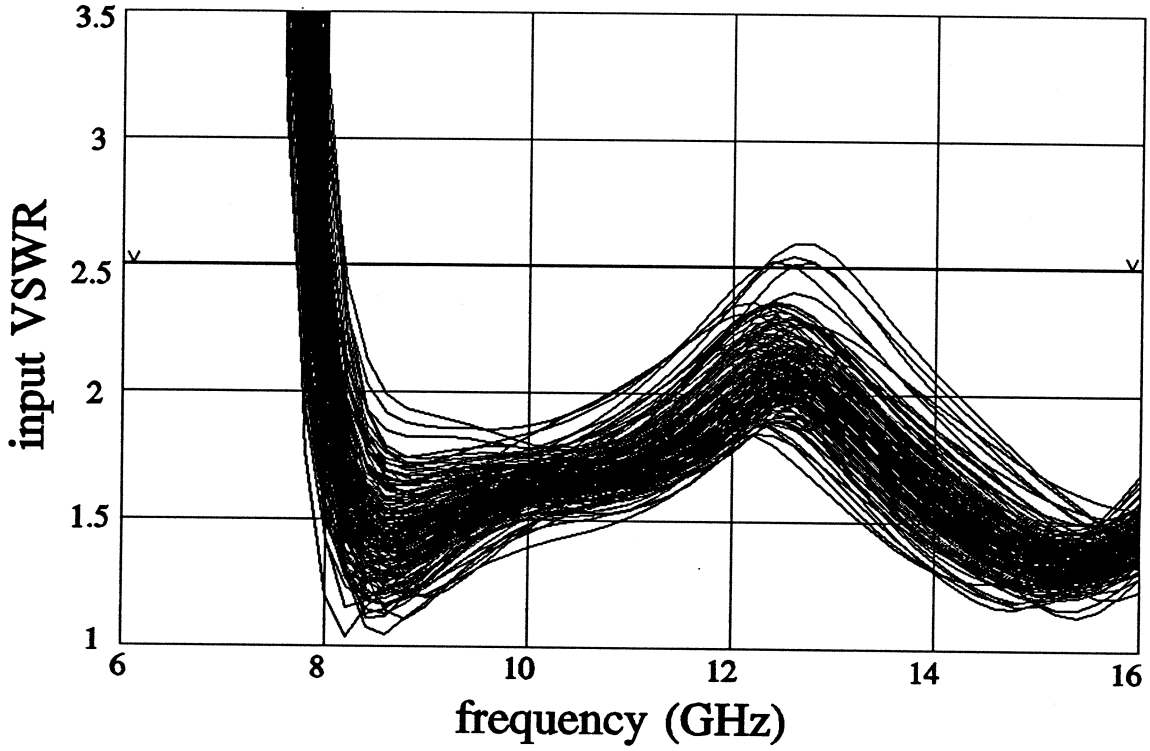

Fig. 19 (a)

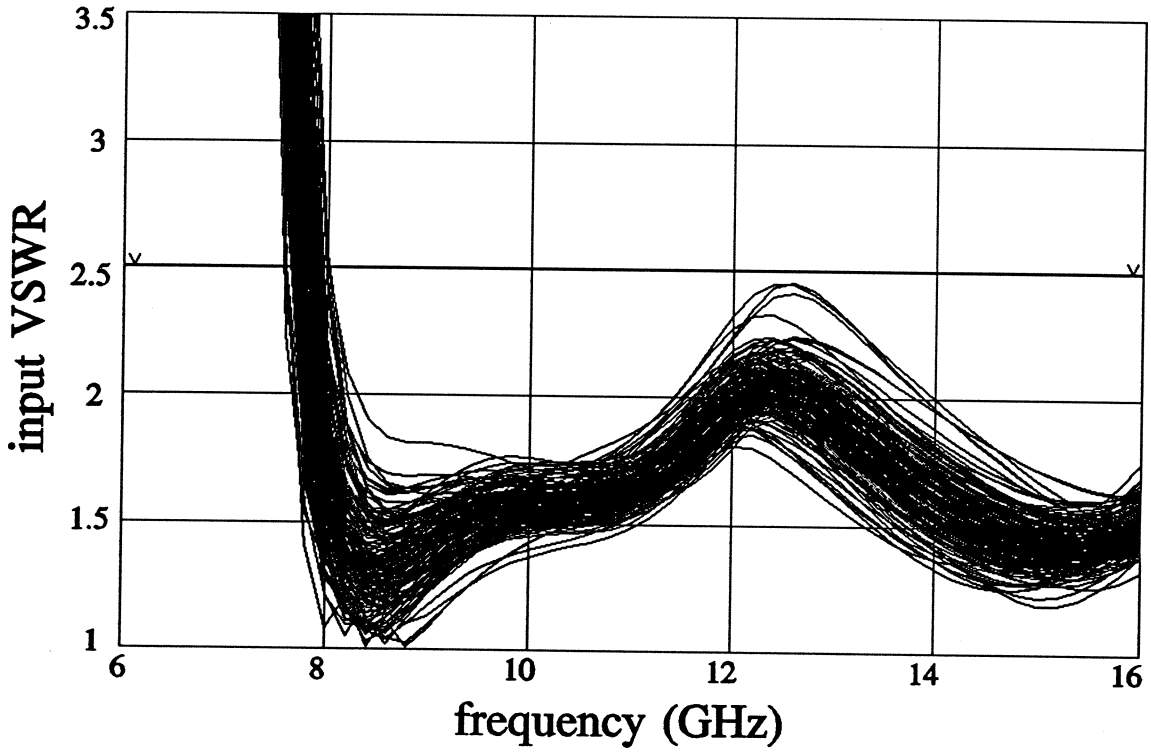

Fig. 19 (b)

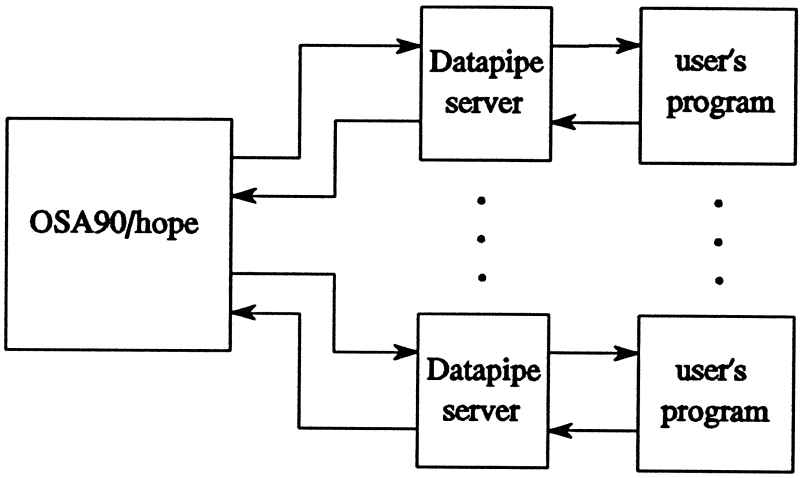
Datapipe server
user's program
OSA90/hope
Datapipe server
user's program

Fig. 20

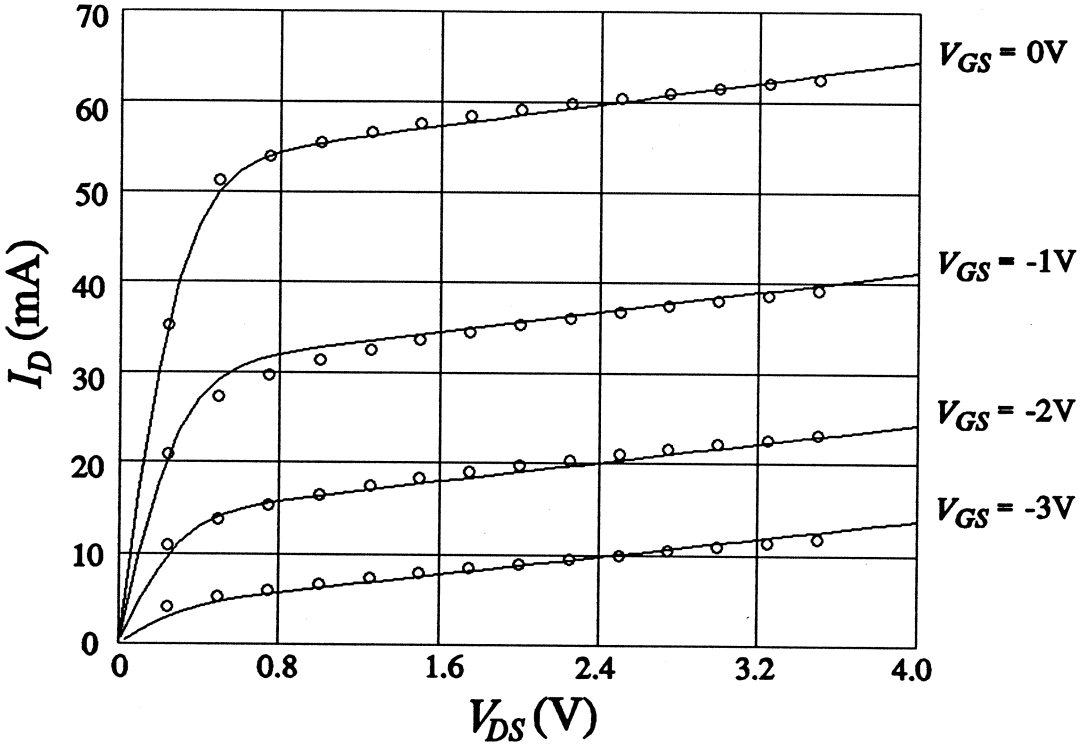

Fig. 21

Authors: John W. Bandler *et al.*

Title: Physics-Oriented Statistical Modeling, Simulation and Optimization